UNIVERSIDADE DE LISBOA

FACULDADE DE CIÊNCIAS

DEPARTAMENTO DE ENGENHARIA GEOGRÁFICA, GEOFÍSICA E ENERGIA

Meteotsunami events in the instrumental records of Iberian coasts

Daniela Alexandra de Vasconcelos Maxial

Mestrado em Ciências Geofísicas

Especialização em Meteorologia e Oceanografia

Dissertação orientada por:

Prof. Dr. Maria Ana Viana-Baptista

Dr. Rachid Omira

2020

Acknowledgements

Durante estes vários meses, foram várias as pessoas que da alguma forma contribuíram para o resultado final desta dissertação.

Primeiramente, um agradecimento especial aos meus orientadores: Prof. Dra. Maria Ana Viana Baptista e Dr. Rachid Omira. Pela paciência, palavras de estímulo e por acreditarem no meu trabalho. Não esquecendo dos importantes contributos que me transmitiram ao longo deste percurso.

O meu sincero agradecimento ao Prof. Alexander Rabinovich, pela disponibilidade e por me dar a conhecer o mundo dos meteotsunamis, e a sua valiosa ajuda para um melhor caminho.

À Inês e à Dina pela companhia e por me mostrarem Viena. À Dra. Maria José Monteiro pelo tempo despendido e o apoio que me demonstrou. Ao Filipe Lisboa pela disponibilidade do programa essencial na análise feita nesta tese.

Não posso deixar de referir e agradecer: à FCT, que através do projeto FAST me deu a incrível possibilidade de realizar esta dissertação de mestrado; ao IDL e ao IPMA cujo apoio foi decisivo para a desenvolvimento do estudo.

Aos meus pais, pela paciência e pelo interesse que sempre mostraram e por deixarem me seguir os meus sonhos. À minha querida irmã, pelo entusiasmo que tem por tudo, por eu poder presenciar a sua boa ética de trabalho e o perfecionismo que tem em tudo. Ao meu cunhado por me aturar, à minha Ângela por distrair a 'titi' quando ela mais precisava e à Ema que tornou 2020 um ano ainda melhor.

À Xibby, melhor amiga, que é um exemplo de persistência, que me mostra todos os dias que se se quisermos conseguimos realizar tudo o que desejamos. Obrigada por me aturares há tanto tempo.

Quando digo que não ultrapassava a vida académica sem a Liliana, é dizer pouco. Pela companhia nos últimos 7 anos, nos bons e menos bons momentos, pela força e por acreditar mais em mim do que eu própria. Que me inspira a trabalhar mais e melhor, sempre. Pela amizade que é para vida.

Não posso esquecer nunca da Raquel, da Catarina e da Solange, pela irmandade, pelo apoio e motivação de sempre. Do Ricardo, Bruno e Daniel pela amizade.

A todos os que não menciono, mas de uma maneira ou outra fizeram parte deste longo caminho.

Obrigada.

“Sunshine is delicious, rain is refreshing, wind braces us up, snow is exhilarating; There is really no such thing as bad weather, only different kinds of good weather.”

John Ruskin

Resumo

Ao longo da costa da Ibérica, pelo menos dois meteotsunamis foram registados/observados nos últimos dez anos. Nesta região, meteotsunamis permanecem menos estudados, apesar das evidências da sua ocorrência. Este trabalho analisa em detalhe os meteotsunamis instrumentais registados nas costas da Península Ibérica, tendo como principal objetivo fornecer uma visão sobre a perigosidade de meteotsunami. Dois dos eventos estudados foram observados na costa ocidental da Península Ibérica e os outros dois eventos nas Ilhas Baleares (Espanha), no Mar Mediterrâneo. Os registos do nível do mar, correspondentes aos eventos de junho de 2006, julho de 2010, junho de 2011 e julho de 2018, realiza-se a remoção do sinal da maré para isolar o sinal correspondente ao meteotsunami. A utilização de ferramentas de análise espectral permitiu avaliar as características do sinal do meteotsunami isolado. Neste trabalho, todos os registos disponíveis no nível do mar foram analisados e apenas os registos relevantes (ou seja, aqueles cuja mediana da altura da crista-vale excedia 30 centímetros) foram selecionados e apresentados como principais resultados. Em seguida, as observações de pressão atmosférica, velocidade, intensidade e direção do vento, foram examinadas para extração das condições meteorológicas que levaram à formação dos meteotsunami registados. Neste estudo, é possível verificar que existem correlações entre os saltos na pressão atmosférica e as mudanças nas direções, velocidades e intensidades do vento, revelando a ocorrência de condições meteorológicas precursoras específicas no momento da geração dos meteotsunami. Os resultados deste estudo em termos de características de meteotsunami (hora de chegada, altura das ondas, períodos, duração) e processos atmosféricos associados (salto da pressão do ar, velocidade do vento, direção do vento) foram compilados num catálogo preliminar. Este produto constitui o primeiro passo para o desenvolvimento de uma avaliação abrangente deste tipo de riscos nesta região, fornecendo informações importantes para desenvolvimento de modelos numéricos de meteotsunami. Este trabalho foi apoiado pelo projeto FAST- Development of new forecast skills for meteotsunamis on the Iberian shelf, financiado pela FCT (PTDC/CTA-MET/32004/2017).

Palavras-chave: meteotsunamis; costa Ibérica; perigo natural; medições do nível do mar; interação ar-mar; análise espectral; forçamento atmosférico; catálogo de meteotsunami.

Abstract

Along the Iberian coast, at least two meteotsunamis have been recorded/observed in the last ten years. In this region, meteotsunamis remain less studied, despite evidence of their occurrence. This work analyses, with unprecedented details, the instrumental meteotsunamis recorded along the coast of the Iberian Peninsula, with the main objective of providing an insight into the meteotsunami hazard. Two of the studied events were observed on the western coast of the Iberian Peninsula (Portugal, Spain and France) and the other two on the Balearic Islands (Spain) in the Mediterranean Sea. Sea-level records corresponding to the events of June 2006, July 2010, June 2011 and July 2018 are de-tided to isolate the signal of the meteotsunami. The use of spectral analysis tools on the recorded signals allowed evaluating the characteristics of the isolated meteotsunami signal. In this work, all available sea-level records were analysed, and only relevant records (i.e. those with median crest-to-trough wave height exceeding 30 centimetres) were selected and presented as main results. Then, the observations of atmospheric pressure, wind speed, intensity and direction are examined to extract the meteorological conditions leading to the formation of the recorded meteotsunami events. In this study, correlations between "jumps" in atmospheric pressure and changes in directions, speeds and intensities of the wind are found, revealing the occurrence of specific precursor meteorological conditions at the time of the generation of meteotsunami. The results of this study in terms of meteotsunami characteristics (arrival time, wave heights, periods, duration) and associated atmospheric processes (air pressure "jump", wind speed, wind

direction) are gathered in a preliminary catalogue. This product is a first step towards developing a comprehensive meteotsunami hazard assessment in the region, providing important information for the development of numerical models of meteotsunami. This work was supported by the FCT funded project FAST- Development of new forecast skills for meteotsunamis on the Iberian shelf (PTDC/CTA-MET/32004/2017).

Key words: meteotsunamis; Iberian coast; natural hazard; sea-level measurements; air-sea interaction; spectral analysis; atmospheric forcing; meteotsunami catalogue.

Resumo Alargado

Os meteotsunamis são ondas longas induzidas por perturbações da pressão atmosférica com períodos que variam entre alguns minutos e as dezenas de minutos. A designação de meteotsunamis surge pela comparação com as ondas de grande comprimento de onda geradas por sismos submarinos. Nomitsu (1935) e Defant (1961) propuseram o termo geral de "tsunamis meteorológicos". Os seus efeitos, por vezes destrutivos, foram observados em diversas partes do mundo tendo sido reconhecidos como um risco natural. Este fenómeno é gerado por forçamento direto da pressão atmosférica; ou seja, os meteotsunamis ocorrem quando se verifica um salto repentino da pressão atmosférica que gera pequenas oscilações no nível do mar. Estas podem depois entrar em ressonância através de mecanismos específicos, amplificando a onda perto da costa.

Rabinovich e Monserrat (1996, 1998) e Monserrat et al. (2006) mostraram a correspondência entre ondas induzidas por estas variações da pressão atmosférica e os tsunamis de origem sísmica e introduziram o termo "meteotsunami". Os meteotsunamis têm designações diferentes nas regiões onde ocorrem com maior frequência tais como: "rissaga" nas Ilhas Baleares (Espanha, Mar Mediterrâneo), "marrubio" em Sicília (Itália, Mar Mediterrâneo)," abiki" na Baía de Nagasaki (Japão)," šćiga" na Croácia," seebär " no mar Báltico," zeebeer" no sul do Mar do Norte," milghuba" em Malta ou "seiches extremos" nos Grandes Lagos (Estados Unidos da América). Os meteotsunamis foram também reportados no Mar Negro, Austrália Ocidental, Nova Zelândia, China, África do Sul, Reino Unido, no Canal da Mancha, Costa Leste e Golfo do México nos Estados Unidos da América e América do Sul (Pattiaratchi & Wijeratne, 2015; Rabinovich, 2019).

Os tipos comuns de ressonância que levam à formação de meteotsunamis são a ressonância de Proudman (Proudman, 1929; Vilibić et al., 2008) e a ressonância de Greenspan (Greenspan, 1956), para além da ressonância fundamental do porto. Devido à natureza complexa do fenómeno, que envolve condições atmosféricas precursoras, efeitos multi-ressonantes atmosfera-oceano e ainda da costa oceânica, a capacidade de previsão dos meteotsunamis não está ainda operacional nos sistemas de alerta de tsunami. A ocorrência de meteotsunamis na Península Ibérica tem sido até agora um fenómeno pouco estudado. No entanto, nos últimos dez anos foram registados dois meteotsunamis. Assim, a integração do alerta de meteotsunamis no sistema operacional de alerta de tsunamis instalado no IPMA constitui um desafio científico e operacional. Para tal importa aprofundar o conhecimento científico sobre este fenómeno através da compreensão das condições atmosféricas e de ressonância específicas que levam à forte amplificação das ondas em mar aberto bem como o seu impacto costeiro.

No sentido de contribuir para o avanço deste conhecimento é objetivo desta dissertação o estudo de quatro meteotsunamis registados na rede maregráfica bem como a análise dos dados atmosféricos e oceânicos disponíveis. Deste modo é possível avaliar não só o efeito forçador atmosférico como a resposta oceânica. Dois destes eventos foram observados na costa ocidental da Península Ibérica (2010, 2011) e outros dois nas Ilhas Baleares (Espanha), no Mar Mediterrâneo (2006, 2018). Os registos do nível do mar correspondentes aos eventos de junho de 2006, julho de 2010, junho de 2011 e julho de 2018 são examinados usando os registos maregráficos após remoção do sinal da maré, isolando deste modo o sinal correspondente ao meteotsunami. De seguida efetua-se análise espectral para avaliar as características do sinal. As observações de pressão atmosférica, velocidade, intensidade e direção do vento, são examinadas para extrair as condições meteorológicas que levaram à formação dos eventos registados.

A análise destes fenómenos contribuirá para a elaboração de um catálogo de meteotsunamis que até aqui não tem sido possível devido à falta de definição clara deste tipo de fenómeno e por dificuldade em

distinguir estes fenómenos de outros tipos de oscilações perigosas no nível do mar (Gusiakov 2019). Este trabalho constitui o primeiro passo para a criação de um catálogo de eventos exclusivamente instrumentais registados ao longo da costa da Península Ibérica, tendo como principal objetivo fornecer uma visão sobre a perigosidade de meteotsunami.

Esta dissertação de mestrado faz parte do projeto FAST, financiado pela FCT (PTDC/CTA-MET/32004/2017). Os principais objetivos são : 1) identificar e analisar os eventos de meteotsunami observados/registrados ao longo da costa ibérica; 2) investigar as condições atmosféricas precursoras que levam à formação dos meteotsunamis identificados; e 3) construir o primeiro catálogo de meteotsunami para a costa ibérica, que incorpora apenas tsunamis de origem atmosférica instrumentais, com informações sobre a data de ocorrência, o tempo de chegada do meteotsunami, a maré na estação, a altura de onda máxima e a amplitude de vale a crista, o período dominante de oscilação, a duração do fenómeno e as perturbações atmosféricas, como a taxa de mudança da pressão do ar e a intensidade e direção do vento.

O trabalho agora apresentado foi estruturado do seguinte modo: um capítulo introdutório, o primeiro capítulo apresenta uma visão geral sobre os meteotsunamis e a motivação para a realização desta tese, expondo os objetivos desta. De seguida, o segundo capítulo conta com o enquadramento teórico e uma breve história sobre meteotsunamis e a sua física. Na terceira secção são apresentados todos os dados usados e as metodologias usadas para cada um: dados maregráficos de nível no mar e dados de informação atmosférica tais como dados de pressão atmosférica, intensidade e direção do vento (à altura da estação e em altitude). No capítulo 4 são exibidos os resultados obtidos nas análises realizadas e a sua discussão. Foram analisados no total, 30 registos maregráficos embora para o trabalho aqui apresentado consiste na análise dos registos das seguintes estações: Cascais e Peniche para o evento de 2010; estações de Peniche, Leixões, Marin e La Corunã para 2011; e para ambos os eventos de 2006 e 2018, as estações de Palma de Mallorca e Ciutadella de Menorca. A análise dos registos maregráficos permitiu a identificação clara de meteotsunami em todos os 30 sinais dos marégrafos examinados, para os quatro eventos em estudo. Foram considerados registos relevantes aqueles em que a altura da crista-vale excedia 30 centímetros ou os que o seu sinal fosse mais notório. Foram identificadas correlações, por comparação visual, entre os saltos na pressão atmosférica e as mudanças nas direções, velocidades e intensidades do vento, revelando a ocorrência de condições atmosféricas precursoras específicas no momento da geração de eventos de meteotsunami. O estudo do conteúdo em frequência dos sinais foi feito recorrendo ao cálculo das onduletas (*wavelets*), mostrando que os períodos dominantes do meteotsunami variam significativamente, de estação para estação. Essa análise também define claramente que o fenómeno amplificou os períodos ressonantes (períodos próprios) de quase todos os portos. O espectro de potência de wavelets confirma que todos os eventos de meteotsunami coincidem com oscilações energéticas na pressão do ar e/ou velocidade do vento (Šepić & Vilibić, 2011; Šepić et al., 2015a, 2015b; Thomson et al., 2009; Vilibić et al., 2014; Linares et al., 2016). De evidenciar que os eventos na costa portuguesa (2010 e 2011), ambos ocorreram durante a maré baixa, sem impactos destruidores. Ao contrário do evento de 2018 nas Ilhas Baleares, que ocorreu em condições de maré alta, provocando estragos de muito maior magnitude. Os resultados deste estudo em termos de características de meteotsunami (hora de chegada, altura das ondas, períodos, duração) e condições climáticas forçadoras (salto da pressão do ar, velocidade do vento, direção do vento) são compilados num catálogo preliminar. Conclusões gerais e perspetivas futuras estão presentes na seção final. A necessidade de altas resoluções espaciais e temporais, é uma conclusão importante de enfatizar. Nos registos de nível médio do mar é na maior parte conseguido (1 minuto). Mas, na pressão atmosférica as resoluções temporais da maioria das estações são de 10 minutos. Esta resolução é relativamente baixa para o que é desejado, uma vez que os saltos de pressão atmosféricas nestes fenómenos são repentinos e da ordem de até 3hPa em 30 minutos. Assim, é necessária uma melhor resolução temporal (de 1 minuto) para dados de pressão

atmosférica. Importante também será a resolução espacial da batimetria, devido à rápida diferença de profundidade nas áreas costeiras, para cálculos posteriores em modelos numéricos de meteotsunami.

Este produto é o primeiro passo para o desenvolvimento de uma avaliação abrangente de riscos de meteotsunami na região. Este catálogo irá fornecer informações cruciais para tese de modelos numéricos de meteotsunami, podendo ser usado no desenvolvimento das habilidades de previsão de meteotsunami para a costa ibérica. Contribuindo assim para aumentar a consciencialização do público ao impacto de meteotsunamis e, consequentemente, aumentar o nível de segurança da população costeira e diminuir o potencial dano em infraestruturas nas costas portuguesa.

Index

List of Figures

List of Tables

1. Introduction

1.1. Overview

In the aftermath of the devastating tsunamis that struck the Indian Ocean in 2004 and the Pacific Ocean in 2011, tsunami science has known a significant progress, opening new fields of research and reaching regions where the tsunami hazard was previously underestimated. Meteotsunamis are among these events that called a particular scientific attention due to their meteorological origin possibly influenced by the increasing climate changes (Bechle et al., 2016). Consequently, the conditions of the meteotsunami formation has been intensively studied during the last two decades, but its evolution involving multi-resonant atmosphere-ocean and ocean-coast effects still need more in-depth investigation.

Meteotsunamis are atmospherically induced high-energy ocean waves in the tsunami frequency band with destructive coastal effects (Monserrat et al., 2006). They occur when sudden atmospheric pressure "jump" forces the ocean to response through the generation of small sea-level oscillations that enter in resonance with the atmospheric forcing. Common types of resonance leading to meteotsunamis generation are the Proudman resonance (Proudman 1929) and the Greenspan resonance (Greenspan, 1956). During the resonance process, the atmospheric disturbances moving above the ocean surface give raise to significant long ocean waves by continuously pumping additional energy into these waves (Rabinovich, 2009). The energetic ocean waves arriving at the coast (bay, inlet, or harbour) can become destructive due to the combination of other amplification mechanisms, including shoaling and resonance local effects (also applicable to tsunamis of other origins). Meteotsunamis differ from tsunamis in one key aspect: their generation mechanism; they are shallow water waves created by sudden air pressure disturbances moving over the sea, rather than by underwater earthquakes, landslides or volcanic eruptions. According to Monserrat et al. (2006), tsunamis and meteotsunamis have the same period, same spectral scales, similar physical properties and affect the coastal areas in a comparably damaging way. 99% of the energy of background oscillations is related to the meteorological forcing, so although damaging, meteotsunamis waves are much less energetic than tsunamis-waves of other more well know origins.

In historical tsunami catalogues, the meteotsunami events are scarce (2% of all documented tsunamis), but it is possible that some of the 'tsunami-like' events of 'unknown origin' which appear in these catalogues are meteotsunamis (Monserrat et al., 2006), showing that there are problems in cataloguing this kind of phenomenon (Gusiakov 2019). Although, meteotsunamis were considered as a global threat only in the early 21st century. Conventionally, this phenomenon was thought to be generated only at a few of meteotsunami "hot spots": in the Mediterranean, especially in Ciutadella in Balearic Islands and Vela Luka in Croatia, or Nagasaki Bay in Japan. All of them, elongated narrow harbours of high resonance properties. Recently, meteotsunamis have been documented in several coasts around the world, causing destructive impacts in some cases while being difficult to forecast (Jansá et al., 2007; Vilibić et al., 2009; Orlić, 2015, Šepić et al., 2015a; Vilibić et al., 2016; Šepić et al., 2016; Carvajal et al., 2017; Lin & Liang, 2017; O'Brien et al., 2018, Kim et al., 2019, Rabinovich, 2019).

The recent worldwide growing interest in studying the meteotsunamis has led to numerous published works. Vilibić et al. (2018) assessed the strength and frequency of meteotsunamis in the future climate and found that the total number of days expected with meteotsunamis in the RCP8.5 scenario is projected to increase consistently over time (by 34% for the Balearic Islands). On the other hand, and in a changing climate, Weisse & Hünicke (2019) show the difficulty to predict how the frequency or intensity of meteotsunamis may change, particularly when dealing with weather conditions such as changing wind patterns. The development of meteotsunami forecast capability, still lacking in most

operating tsunami warning systems, has also been addressed following the hazardous meteotsunamis occurring worldwide. In this sense, several research works investigated the feasibility of forecasting meteotsunami in hazard prone coasts. Renault et al. (2011) used a coupled atmosphere–ocean modelling system to reproduce the whole process, from the source in atmosphere to the meteotsunami dynamics in the ocean for an eventual use in the forecasting of a meteotsunami event with necessary further improvements. More recently, the study by Vilibić et al. (2016) investigated the meteotsunamis in the Mediterranean Sea with the intension to forecast the destructive events and support early warning systems. They show that due to their close correlation with atmospheric processes and in particular with air pressure disturbances, meteotsunamis could presumably be forecasted more easily and at a lower cost than tsunamis of earthquake origin. Meteotsunamis are generated by intense, low-dispersive and sharp air pressure disturbances that can be tracked on the ground (Monserrat & Thorpe 1992; Vilibić et al., 2008; Thomson et al., 2009; Šepić et al., 2009; Tanaka 2010). Such an approach has been used for creation of pilot Adriatic meteotsunami observing network, found to successfully capture meteotsunami events (Šepić & Vilibić 2011). Another feasible approach has been used by the Balearic Meteorological Service (Jansà et al., 2007), which raises a 'rissaga' alert if the synoptic conditions are following the patterns observed during the meteotsunami events. Similar systems are under development in some other countries, including the United States and Japan (Rabinovich, 2019). Sea level stations can be used for detection of a meteotsunami (e.g., on the Balearic Islands, Marcos et al., 2009). Also, vertical sounding profiles (Vilibić & Šepić 2009) and satellite images (Belušić & Strelec-Mahović 2009; Vilibić et al., 2010) can be used for detecting favorable conditions for a meteotsunami event.

Along the coast of Iberia, at least 2 meteotsunamis were recorded/observed in the last 10 years: the July 7, 2010 (Antunes et al., 2011) and the June 27, 2011 (Tappin et al., 2013). The 2010 event was recorded along the Portuguese coast, causing alarm among fishermen and getting some attention of the media. On June 2011, a meteotsunami was formed in the English Channel and travelled towards the Atlantic coasts of Portugal, Spain, France and Britain (Tappin et al., 2013; Frère et al., 2014). In addition to these events, the meteotsunamis on the Mediterranean Sea on June 15, 2006 (Monserrat et al., 2006) and July 17, 2018 are also analysed due to their particular interest and level of damage. The June 2006 meteotsunami damaged more than 40 boats and caused an economic loss of several tens millions of euros in the region of the Balearic Islands (Western Mediterranean) (Monserrat et al., 2006). The most recent event occurred in the same place as the Balearic Islands, where a 1.5 m wave flooded coastal cities in Mallorca and Menorca and caused the death of one person[1].

1.2. Motivation

Along the Iberian coast, the tsunami hazard is mainly associated to large earthquakes occurring within the Azores-Gibraltar fracture zone. Here, the hazard from tsunamis of tectonic origin has been intensively investigated (Baptista et al., 2011; 2017; Omira et al., 2009; 2015). However, the tsunami hazard induced by non-seismic sources (i.e. landslides, volcano eruptions and meteorological conditions) remains not well understood to the same extent as the corresponding hazard from earthquakes. Up to date, despite observations of meteotsunamis along the Iberian coast in some occasions, the studies by Antunes (2011), Antunes et al. (2011) and Frère et al. (2014) remain the only works that addressed the meteotsunamis along the Portuguese coast. Extensive work remains to be done to identify past meteotsunami events that impact/reach the coast of Iberia, to properly determine their physical characteristics, to accurately constrain the atmospheric precursor conditions leading to their formation, and to enable the elaboration of predictive numerical models and hazard assessment.

[1] https://www.thesun.co.uk/news/6795390/majorca-menorca-mini-tsunami-wave-beach-tourists/

Forecasting meteotsunamis remains challenging of any operational tsunami early warning system. The Portuguese Institute for Ocean and Atmosphere (IPMA, Portugal) as authority responsible of forecasting weather and tsunamis in the North East Atlantic faces the challenge of integrating the meteotsunami in its operational system. The IPMA observing and forecasting facilities in both atmosphere and ocean fields may insure a flexible feasibility of this complex task. In this sense, *FAST - Development of new forecast skills for meteotsunamis in the Iberian Shelf-* project leaded by IPMA and funded by Foundation for Science and Technology (FCT) aims at initiating the meteotsunami research in Portugal with the goal of developing forecast skills for this natural hazard phenomenon.

1.3. Objectives and thesis organization

This master thesis is a part of the ongoing FAST project funded by FCT. Its main objective is threefold: 1) to identify and analyse the meteotsunami events observed/recorded along the Iberian coast; 2) to search for the precursor atmospheric conditions leading to the formation of the identified meteotsunamis; and 3) to build the first meteotsunami catalogue for the Iberian coast that incorporates the event source-to-coast information, including both sea-level recorders and atmospheric pressure gauge information. This cataloguing will help to better understand the origin of these types of events, providing crucial information for meteotsunamis science.

To ensure a proper presentation of the working-plan and to reach the objectives mentioned above, this dissertation consists of four main sections. It begins with chapter 1 devoted to a general introduction to meteotsunamis with a focus on the scientific progress made and the remaining challenges. Motivation, objectives and thesis organization are also present in the Introduction section. The next section presents a brief history of meteotsunamis, giving a theoretical framework of the phenomenon. Chapter 3 presents a detailed description of the data used and the methods adopted in this work. Chapter 4 focuses on the presentation and discussion of the dissertation results. General conclusions and future perspectives are present in the final section.

2. Theoretical framework

2.1. Meteotsunami: history

Nomitsu (1935) and Defant (1961) initially proposed the general term of "meteorological tsunamis" to describe the tsunami-like ocean oscillations caused by meteorological phenomena. A few years after the Daytona event, Rabinovich and Monserrat (1996, 1998) and then Monserrat et al. (2006), showed the visible correspondence between these anomalous atmospherically induced waves and seismically generated tsunamis and introduced the term "meteotsunami" to the tsunami community. Worldwide, in regions like Ciutadella de Menorca, where meteotsunamis are observed and considered more frequent ("hot spots"), this type of dangerous event have specific local names like: "*rissaga*" in Balearic Islands (Spain, Mediterranean Sea), "*marrubio*" in Sicily (Italy, Mediterranean Sea), "abiki" in Nagasaki Bay (Japan), "*šćiga"* in Croatia, "*seebär*" in the Baltic Sea, "*zeebeer*" in the southern North Sea, "*milghuba*" in Malta or "*extreme seiches"* in the Great Lakes. Meteotsunamis currently are also reported in the Black Sea, West Australia, New Zealand, China, South Africa, United Kingdom, in the English Channel, East Coast and the Gulf of Mexico in the United States of America and South America (Pattiaratchi &

Wijeratne 2015; Rabinovich 2019). In his latest meteotsunami overview, Rabinovich (2019) demonstrated that such waves can occur anywhere in the world's oceans and not only in a few "hot spots".

However, in historical tsunami catalogues, the meteotsunami events are uncommon (2% of all documented tsunamis) and with well-known cases of meteotsunamis still absent in the database (Gusiakov 2019). In the Global Historical Tsunami Database (GHTD) maintained and updated by the NCEI/NOAA, meteotsunamis constitute a slightly higher fraction (2.4%) of all tsunamis. But still, likely, that some of the events of 'unknown origin' which appear in these catalogues may be meteotsunamis (Monserrat et al., 2006). During the period 1992-2016, there were 290 tsunami events around the world, 63 of which were potentially damaging (i.e. maximum wave heights higher than 1 meter). In Ciutadella Harbour, Menorca Island, alone (one of the meteotsunami hottest spots) between 1992 and 2018, there were 71 meteotsunamis with maximum wave heights larger than 1 meter. Thus, the total number of damaging meteotsunamis in Ciutadella alone was higher than the total number of potentially hazardous seismic tsunamis all over the world (Rabinovich, 2019). Hence, in Spain (Marcos et al., 2009; Renault et al., 2011) and Croatia (Vilibić et al., 2016; Denamiel et al., 2018), regions frequently affected by meteotsunamis, preliminary meteotsunami warning systems have already been developed. Similar systems are under development in some other countries, including the United States, Japan, and Portugal.

2.2. Meteotsunami: physics

The generation mechanism and the multi-resonant waves evolution are the key aspects turning the physics of meteotsunamis different from common tsunamis. Although meteotsunamis are also long waves, often governed by the shallow water equations (Equations 2.1-2.3), they occur under a specific weather condition when sudden atmospheric pressure "jump" forces the ocean to response through small sea-level oscillations (Figure 2.1). The evolution of these oscillations is then conditioned by a set of resonance phenomena, such as the Proudman resonance (Proudman 1929) and the Greenspan resonance (Greenspan, 1956) (Figure 2.1). Proudman resonance is produced when the speed of the atmospheric disturbance, U, matches the phase speed of the ocean long waves c (Equation 2.4).

$$h_t + (hu)_x + (hv)_y = 0, \tag{2.1}$$

$$(hu)_t + \left(hu^2 + \frac{g}{2}h^2\right)_x + (huv)_y = -ghb_x - \frac{h}{\rho}(P_A)_x, \tag{2.2}$$

$$(hv)_t + (huv)_x + \left(hv^2 + \frac{g}{2}h^2\right)_y = -ghb_y - \frac{h}{\rho}(P_A)_y, \tag{2.3}$$

where $h(x,y,t)$ is the depth of the water, $u(x,y,t)$ and $v(x,y,t)$ are velocity in x and y direction, g is the gravitational constant, ρ is the density of water, $P_A(x,y,t)$is the air pressure in Pascal, and $b(x,y)$ is the bottom bathymetry.

$$U = c = \sqrt{gH} \tag{2.4}$$

where g is the gravity acceleration and H is the depth (m) of the water column beneath the traveling pressure perturbation.

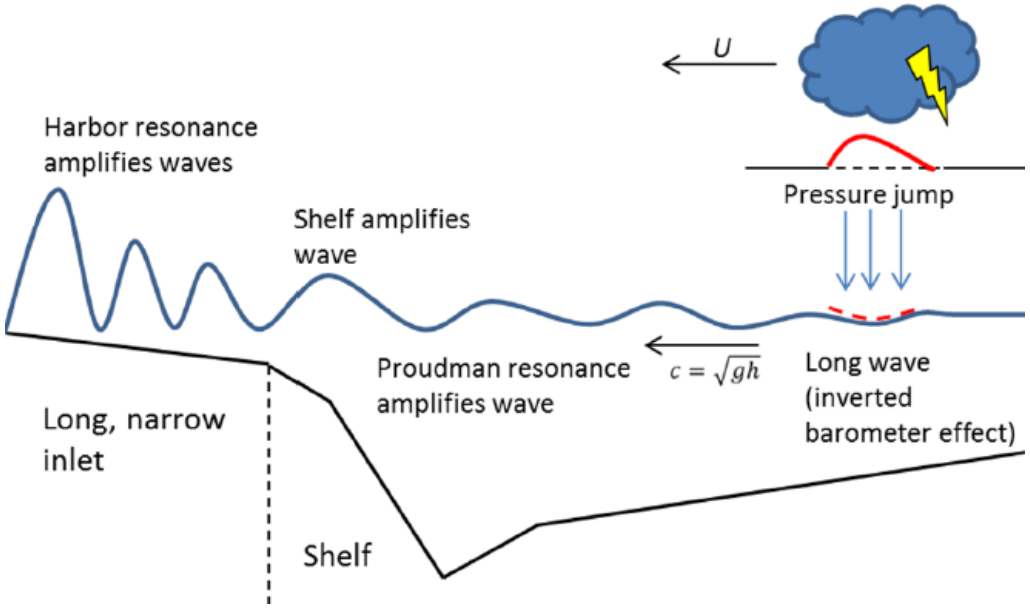

Figure 2.1. Simple illustration of the generation and evolution of a meteotsunami, adapted from NOAA (Technical Report NOS CO-OPS 079), 2014.

At their arrival at the coastal area, meteotsunamis can undergo additional amplification mechanisms, shoaling and local resonance (also applicable to tsunamis of other origins), becoming more destructive. In general, hazardous meteotsunamis are caused by pronounced and sharp air pressure disturbances. The strength of the atmospheric disturbance and the air pressure gradient are the essential mechanism in the generation of meteotsunamis and its intensity depends on the amplification potential of the harbours or bays where they mostly occur (Rabinovich 2009, 2019).

Meteotsunamis are often confused with storm surge associated with tropical storms and other large coastal storms. Storm surge is a wind-driven effect that occurs when strong winds push water onto land, causing water levels to increasingly over the course of several hours. Meteotsunamis differ from storm surge and rogue waves not only because they have different spatial and temporal scales, but also because they have considerably distinct generation mechanisms and affect different oceanic regions (Rabinovich 2019). Table 2.1 summarizes the meteotsunami physical characteristics in comparison to seismic tsunamis and storm surges.

Likewise, as illustrated by Figure 2.2, it is possible to understand what differs meteotsunamis from other marine hazardous long waves by the spectrum of surface gravity waves in the ocean. Storm surge are a low frequency process, with typical periods from several hours to approximately 1 week. They occupy the red band of the ocean wave spectrum. In contrast, rogue waves, are high-frequency phenomena with typical periods from a few seconds to 30 s, corresponding to the blue part of the wave spectrum.1 Meteotsunamis have the same periods as ordinary tsunami waves, ranging from 1 to 2 min to about 3 h. In the ocean wave spectrum, meteotsunamis are located between storm surge and rogue waves.

Table 2.1. Contrasting characteristics of seismic tsunamis, meteotsunamis and storm surges (modified from Pattiaratchi CB, Wijeratne EMS. 2015).

	Seismic tsunamis	**Meteotsunamis**	Storm surges
Source location	Below the sea surface, by sudden displacements of the sea floor	**Above the sea surface, by the inverse barometer effect coupled with resonance effects**	Above the sea surface, by the inverse barometer effect and a strong wind field
Source duration	Impulsive motions of the sea floor which last O(minutes)	**Driven by resonance effects which take effect O(hours)**	Driven by atmospheric pressure and wind field O(hours-days)
Source extent	Fixed to the region of uplift	**Propagate over the region**	Propagate over the region
Water depth	Occur in the deep or shallow water, but higher waves are generated in depths greater than the continental shelf	**Relatively shallow where Proudman resonance can occur**	Shallower and wider continental shelves have a greater influence
Water-level change and currents	Periods of O(minutes) with rapid oscillatory change	**Periods of O(minutes) with rapid oscillatory change**	Gradual change in of O(hours)
Region of impact	Can influence an entire ocean basin and beyond	**Local to regional**	Local to regional in nature

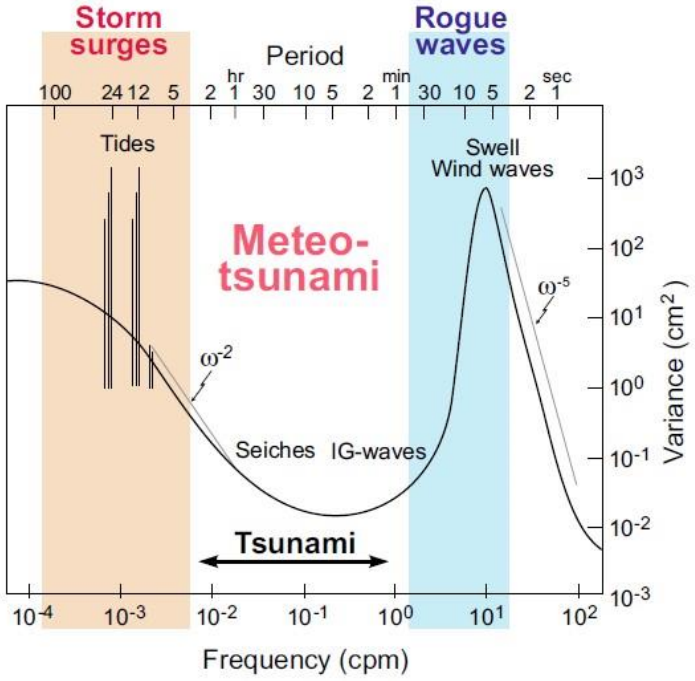

Figure 2.2. Spectrum of surface gravity waves in the ocean (Rabinovich, 2019). The frequency bands of storm surge, tsunami/meteotsunami and rogue waves are indicated. The solid thin black lines denote the theoretical spectral limits of $\omega^{-2}$and ω^{-5} (ω = wave frequency = 2π/T) for open-ocean background spectra.

2.2.1. Physical parameters of meteotsunamis – proposal for a catalogue

Bibliographic research on meteotsunamis was performed, searching for information in national and foreign articles, academic theses and electronic resources. Several studies have been found, and the topic has been thoroughly debated in recent years, for example in countries bordering the Adriatic Sea and the Mediterranean Sea, where this type of event occurs most regularly. Therefore, it was necessary to update the found elements and make a large selection of existing references. This research allowed the identification of the physical processes involved in the meteotsunami event.

This thesis is the first step towards the creation of a catalogue of exclusively instrumental meteotsunami events. The catalogue will have specific information, based on the knowledge of the generation and evolution of the phenomenon. The essential parameters will then be information regarding the date of occurrence, the tsunami arrival time, tide level, the maximum wave height and the crest-to-trough amplitude, the dominant period of oscillation, duration of the phenomenon, and the atmospheric disturbances, like the rate of air pressure change and wind intensity and direction.

3. Data and Methodology

3.1. Sea Level Data

A total of 27 tide-gauge records (Table 3.1 and Figure 3.1) from three different countries: 10 from Portugal, 7 from Spain and 10 from France, were analysed. The sea level data were obtained from operating tide-gauge stations available through the: Intergovernmental Oceanographic Commission Sea Level Monitoring Facility (IOC) (http://www.ioc-sealevelmonitoring.org/); Hydrographic Institute (HI) (www.hidrografico.pt); Directorate-General for Territory (DGT) (ftp://ftp.dgterritorio.pt/Maregrafos) and Network of Mareographs of Puertos del Estado (REDMAR); by their online website or by direct request. Table 3.1 presents the data providers and the sampling interval for each tide-gauge stations. The Cascais tide-gauge has a precision in the sampling interval of 2.499999 seconds. For the analysis of the meteotsunami signal record, an approximation for 2 seconds was necessary.

Usually, tide-gauge stations present records with noise and contain resonance effects, because they are located near the coast or within ports. The tide-gauge stations from IOC, provides sea level data from relative levels, i.e. signal minus average over the selected period (period of approximately 7 days). This site is a data provider from tide-gauge stations all around the world. The HI, an institute of the Portuguese Navy, is recognized as a State Laboratory with the fundamental mission to ensure activities related to the sciences and techniques of the sea[2]. Sea level data consist of data from radar tide-gauge records and some data acquired by HI correspond to the reading of the equipment and are not referred to the Hydrographic Zero (HZ). To refer to data at the HZ level, the following quotas must be applied to the subsequent tide gauges records (y)[3]:

$$Lisboa_{HZ} = y - 0.361 \tag{3.1}$$

[2] http://www.hidrografico.pt1
[3] https://www.hidrografico.pt/tabelamares

$$Peniche_{HZ} = 5.433 - y \tag{3.2}$$

$$Sesimbra_{ZH} = 4.996 - y \tag{3.3}$$

$$Sines_{ZH} = 6.318 - y \tag{3.4}$$

Also, to the Portuguese coast, the tide network managed by DGT consists of two tide-gauges located in Cascais, operating since 1882, and in Lagos, since 1908. In both tide-gauges, were recorded variations in mean sea level off the coast of mainland Portugal. The tide-gauge of Cascais, due to its geographical situation and long-time series of records, is of great importance not only at a national level but also for the entire scientific community, being integrated into the international tide-gauge networks[4]. In its turn, the mareograph network REDMAR has developed and maintains systems for the measurement and forecasting of the marine environment of Spanish coasts, with the main objective of providing ocean and meteorological data. In addition to other services, the system consists of measurement networks (buoys, tidal gauges, and high-frequency radars).

Figure 3.1 depicts the location of all tide-gauge stations that recorded the signals analysed in this work. They are distinguished by different markers referring to the meteotsunami event: black dot for the 2006 event that was recorded only at an atmospheric pressure station); red dots for the 2010 event recorded along the Portuguese coast; blue asterisk for the 2011 event, at the Spanish and French tide-gauge stations; and finally pink crosses corresponding to the meteotsunami of 2018 in the Balearic Islands, Mediterranean Sea. Although the analysis is performed for all the records, this thesis will focus only on the most relevant meteotsunami signals of each event. These concerns the tide-gauges signals of Sines, Cascais, and Peniche for the 2010 event; the records at tide-gauges of Peniche, Leixões, Marin and La Coruña for the 2011 event. For the 2006 and 2018 events, only the available signals at Palma de Mallorca and Ciutadella de Menorca are analysed.

[4] http://www.dgterritorio.pt/cartografia_e_geodesia/geodesia/redes_geodesicas/rede_maregrafica/

Table 3.1. Presentation of the providers of the sea level data from each event and their sampling interval. For Cascais tide-gauge, an approximation of 2 seconds was necessary, because of the precision in the sampling interval of 2.499999 seconds.

DATE	AVAILABLE ON	SAMPLING INTERVAL	TIDE-GAUGE
2010	HI	6 min	Aveiro
			Figueira da Foz
			Leixões
			Viana do Castelo
		1 min	Lisboa
			Peniche
			Sesimbra
			Sines
	DGT	~2 s	Cascais
		3 min	Lagos
2011	IOC-SLMF	1 min	Bilbao
			Boucau-Bayonne
			Brest
			Concarneau
			Ferrol
			Huelva
			Ile d'Aix
			La Rochelle
			Le Conquet
			Le Crouesty
			Les Sables d'Olonne
			Port Bloc
			SOCOA
		5 min	La Coruña
	HI	6 min	Leixões
			Sines
		1 min	Peniche
	DGT	3 min	Lagos
	REDMAR	5 min	Marin
2018	IOC-SLMF	1 min	Palma de Mallorca
			Ciutadella de Menorca

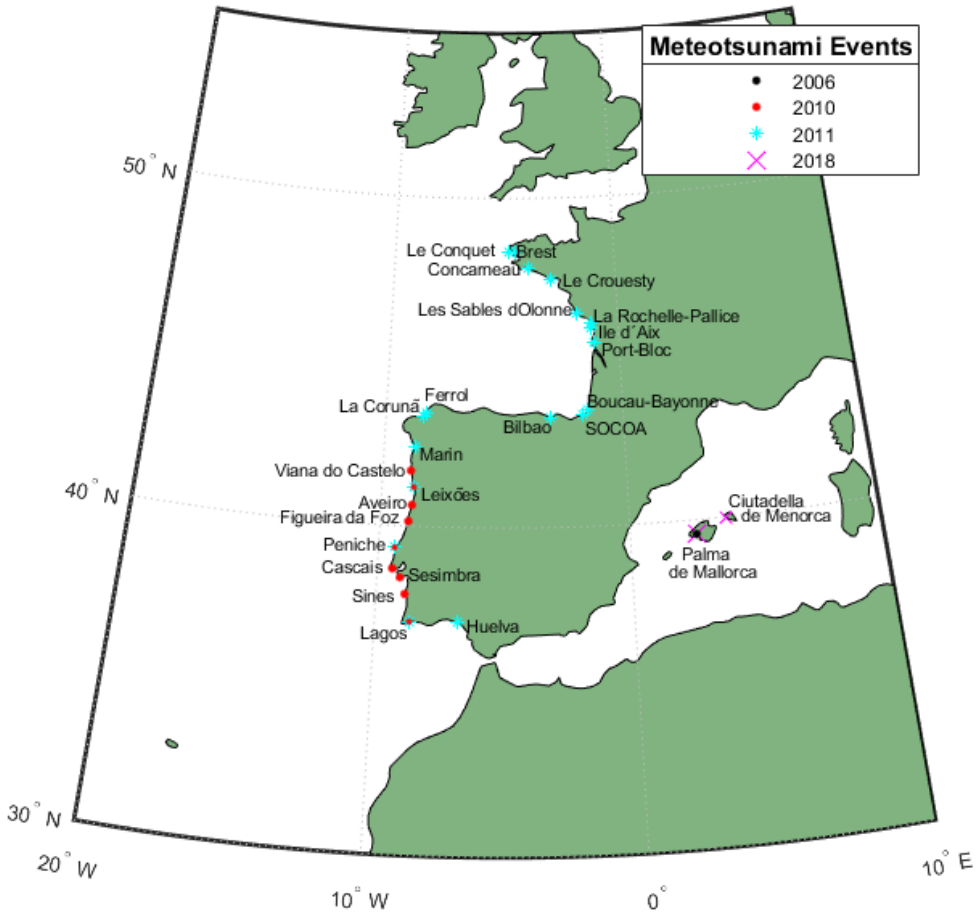

Figure 3.1. Representative map of the location of all tide-gauge stations where the meteotsunamis under study were recorded: with a black point the 2006 event in Palma de Mallorca and a red ball the 2010 even along the Portuguese coast; with a blue asterisk the 2011 event along the Iberian Peninsula and French Atlantic coast and finally with a pink cross the 2018 event in the Balearic Islands.

3.2. Atmospheric Data

Records of sea level and atmospheric pressure in the same site are rare, except for the tide-gauge stations of Balearic Islands. The atmospheric pressure data for this study were obtained from the Portuguese Geographic Institute's online site[5] and by direct request to HI and Spanish State Meteorological Agency (AEMET). For the 2006 event in the Balearic Islands, the atmospheric pressure value was taken from a 2006 article study of Rabinovich. A total of 16 stations were evaluated; most of them are Portuguese (Table 3.2.). The sampling interval is 10 min for all stations except for Sines in Portugal, which has a smaller sampling interval of 1 min.

[5] ftp://ftp.dgterritorio.pt/Maregrafos

Table 3.2. Presentation of the providers of atmospheric pressure data from the stations used in this study and their sampling interval.

DATE	AVAILABLE ON	SAMPLING INTERVAL	STATIONS
2006	*Rabinovich*, 2006	--	Palma de Mallorca
2010	HI	10 min	Cantareira Lisboa Peniche Santa Maria Sesimbra
		1 min	Sines
	DGT	10 min	Cascais Lagos
	AWS I	10 min	Coimbra Faro Lisboa / Gago Coutinho Lisboa / Geofísico Peniche Porto Sagres Sines Viana do Castelo
2011	AWS I	10 min	Coimbra Faro Lisboa / Gago Coutinho Lisboa / Geofísico Peniche Porto Sagres Sines Viana do Castelo
	DGT	10 min	Lagos
2018	AEMET	10 min	Ciutadella de Menorca

To better understand the meteotsunami, it is also important to examine the precursor weather conditions that led to their formation. This will involve the retrieve and analysis of atmospheric high-resolution observations during the period of occurrence of the events under study. Different sources of data will be considered, including: wind speed and direction for the 2010 and 2011 event for the Portugal coast, from the network of surface automatic weather stations from Portugal (Automatic Weather Station (AWS I)) (Table 3.3.); analysis fields and vertical profiles from the European Centre for Medium-range Weather Forecasts (ECMWF). It was also required from ECMWF the atmospheric situation from different layers to the 2010 event and radio-sonde (tefigram)[6] to complement the analysis. In this analysis, it is important to be aware of the presence of a strong vertical wind shear and the presence of

[6] http://weather.uwyo.edu/upperair/europe.html

warmer air around 850 hPa (and cold air at mid-tropospheric levels) that induces an abrupt change of stability in the vertical as stated by Romero et al, 2019.

Table 3.3. Presentation of the providers of wind intensity and direction from the stations data used in this study and their sampling interval and altitude.

DATE	PROVIDED BY	SAMPLING INTERVAL (MIN)	STATION	ALTITUDE (M)
2010 & 2011	AWS I	10	Coimbra	171
			Faro	8
			Lisboa / Geofísico	77
			Lisboa / Gago Coutinho	103.884
			Peniche	32
			Porto	69
			Sagres	25
			Sines	103
			Viana do Castelo	48

3.3. Methodology

This thesis uses a two-step methodology. The first step concerns the analysis of the sea level signal to isolate the meteotsunami and determine its characteristics. While in the second step obtained meteotsunami signals are compared alongside with the atmospheric data to observe possible correlations.

The collected sea-level data are analysed to distinguish the meteotsunami signal and determine its characteristics. This analysis process concerns the de-tiding to isolate the meteotsunami signal from the tidal signal. This process is done by means of the least squares algorithm to fit the interpolated data into polynomials of best fit degree and further improved by applying a band-pass filter. Once the filtered signal is obtained, this work undertakes the spectral analysis by applying the Wavelet algorithm to calculate the distribution of the meteotsunami energy in different frequency bands over the time of its propagation. For both de-tiding and spectral analyses, this work uses the ASAT tool (Lisboa, 2015), developed in the framework of ASTARTE[7] project and was successively applied to study a number of tsunami events (Baptista et al., 2017; Omira et la., 2016).

Wavelet analysis is a common tool for analysing localized variations of power within a time series (Torrence & Compo, 1998). The Wavelet algorithm is used to determinate "when" in time the frequencies of interest happen, information that is lost in Fourier analysis. So, this function can represent another function originally described in the time domain, so that be to analyse the function at a different frequency and time scales. The mathematical formulation of continuous Wavelet uses the integral of the signal function $f(t)$ at a scale $a \in R^n$ and a translational value $b \in R^n$ expressed in the following manner:

$$W_{\Psi|f}(a,b) = \int_{-\infty}^{+\infty} \frac{1}{\sqrt{a}} \Psi^* \left(\frac{t-b}{a}\right) f(t)\, dt \;\; a,b \in R, a > 0 \qquad (3.5)$$

[7] ASTARTE - Assessment, STrategy And Risk Reduction for Tsunamis in Europe, Grant 603839, 7th FP (ENV.2013.6.4-3)

$$\Psi_0(t) = \pi^{-1/4} e^{i\omega_0 t} e^{-t^2/2} \quad (3.6)$$

where a is positive and defines the scale and b is any real number and defines the shift. The $f(t)$ is a continuous function in both time and frequency domains. $\Psi(t)$ is called the mother function wavelet, in this case the Morlet wavelet. The asterisk represents the operation of complex conjugate. The purpose of this mother wavelet is to provide a source function to generate the daughter wavelets, which are the translated and scaled versions of the mother wavelet. In this way, unlike Fourier transforms, Wavelet transforms have the power to construct a time-frequency of a signal. The wavelet transform decomposes a function defined in the time domain into another function, described in the time domain and the frequency domain.

The results of the wavelet algorithm can be presented in amplitude, energy density (ED) or logarithmic energy density classes. While the amplitude generally leads to the interpretation of maximal wave heights (both positive and negative) the Energy Density (ED) represents the squared version:

$$ED(f,t) = \left\| W_{\Psi|f}(f,t) \right\|^2 \quad (3.7)$$

The results of this work are given in terms of energy density, which represents the squared version of the amplitude. That is, replacing in equation 3.5, where a is the frequency and b is the time. Thus, the meteotsunami signal of background noise is better distinguished. These results best illustrate how meteotsunami wave energy varies as a function of frequency and time.

Once the meteotsunami signals is isolated, this work proceeds with comparing observed sea disturbances alongside with the collected precursor weather conditions (air pressure and wind direction and intensity). The objective of this comparison, mainly conducted through observation of data variation side by side, is to infer the correlation between the formation of meteotsunami and the weather conditions.

4. Results

Although a total of 27 tide-gauges records were analysed, the results presented here only focus on the signals that show more relevant perturbation for each event. That is, only those that have a crest-to-through height superior to 0.30 m were selected. For the 2010 event, the signals from tide-gauges of Sines, Cascais, and Peniche are selected; records from the tide-gauges of Peniche, Leixões, Marin and La Coruña for the 2011 event; Palma de Mallorca station signals for both 2006 and 2018 events, and this last event also includes records from Ciutadella de Menorca. (Figure 4.1). To understand the correlation between what happened at sea and the atmosphere, a brief analysis if local atmospheric conditions is made for events with available data. This applies to the analysis of atmospheric pressure and wind at the closest meteorological stations to the location of the tide-gauges. The results of this thesis are presented below in chronological order of meteotsunamis events at the Iberian coast.

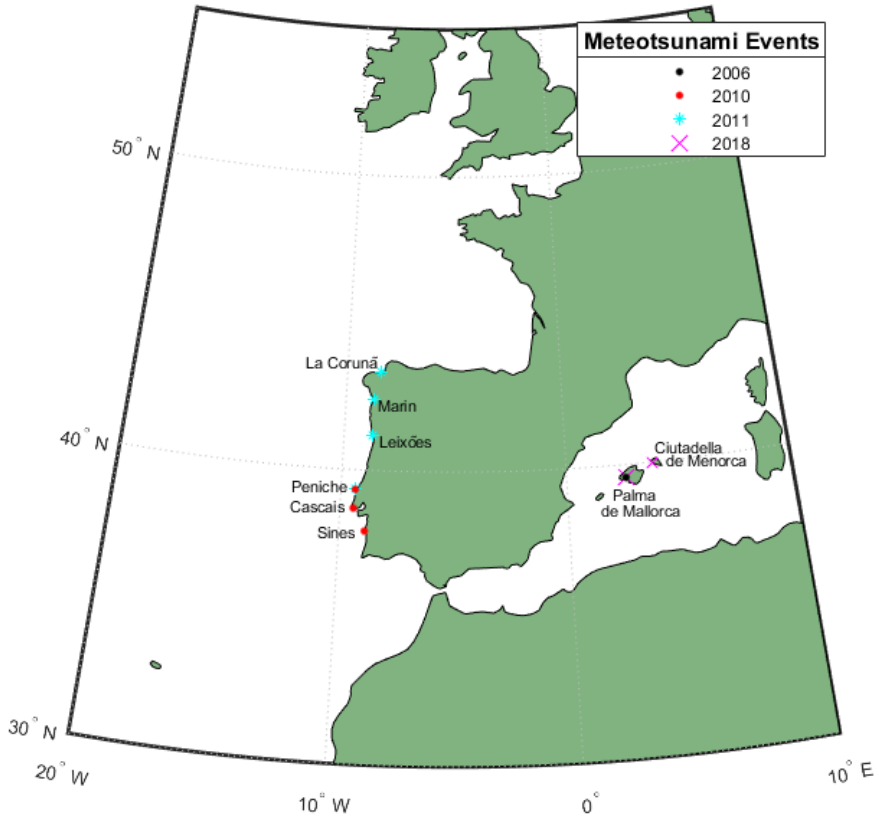

Figure 4.1. Map of the locations of the selected tide-gauge stations where recorded signals analysis is presented in the results section: black point in Palma de Mallorca (for 2006 event);red dots along the Portuguese coast (for 2010 event); blue asterisk along the northwestern Iberian coast (for the 2011 event) and finally pink cross in the Balearic Islands (for the 2018 event).

4.1. The 15 June 2006 event in the Balearic Islands, Mediterranean Sea

Rabinovich and Monserrat (1998) designated as "*rissagas*" in Ciutadella inlet, all sea-level oscillations in which the wave height, in the tide record, exceeds 30 centimetres and with a period ~10 min. Although *rissaga* events with wave heights 1.0–1.5 meters are usually observed in this harbour 1–2 times a year, destructive oscillations with crest-to-through heights of more than 3 meters occur just once every few years. This particular harbour has already suffered the impact of these type of phenomena in both 1984, 2003 and 2006, causing millions of pounds of damage to the harbour and boats[8]. The 2006 event in Ciutadella Harbour, being one of the most dramatic *rissaga,* has been widely studied (Monserrat et al., 2006; Jansá et al., 2007; Vilibić et al., 2008; Renault et al., 2011).

An illustration of the method of generation and propagation of meteotsunamis at this location is shown in Figure 4.2, where it is possible to observe the prominent resonant properties providing significant amplification of incoming waves. Unfortunately, in 2006 no tide-gauges was operational in the inlet; therefore, no records of sea-level variation are available for the 2006 event. From this event, only observed data of atmospheric pressure variation are available to analyse. Figure 4.3 shows the atmospheric pressure records from Palma de Mallorca (Mallorca island) for June 15, 2006. Red dots indicate the beginning and the end of an intense pressure "jump" of approximately 3hPa in 5 min, that occurred at approximately 17:50 UTC. This pressure "jumps" supposedly travelled from SW to NE, with an estimated speed of 25 m/s (Monserrat et al., 2006).

[8] https://www.noonsite.com/news/spain-balearics-meteotsunami-rissaga-floods-islands-of-mallorca-and-menorca/

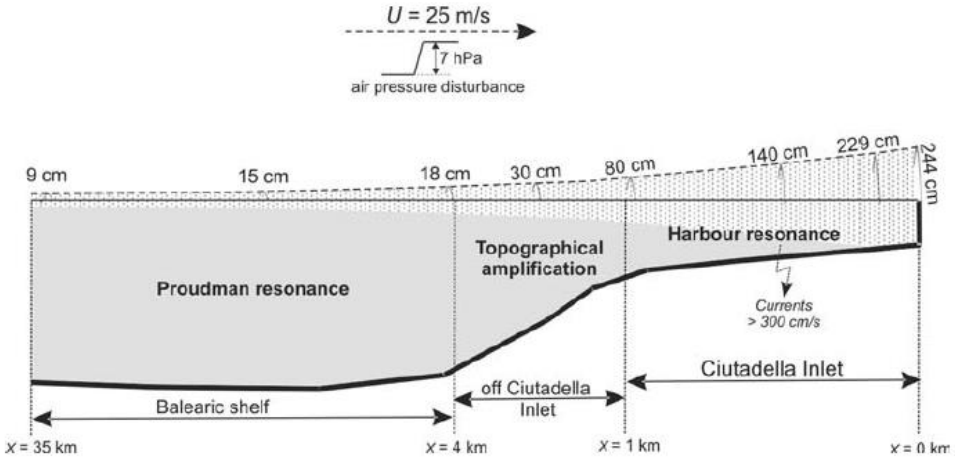

Figure 4.2. A sketch by Vilibić et al.,2008 illustrating the physical mechanisms responsible for the formation of the destructive rissaga on 15 June 2006 in Ciutadella Harbour (Menorca Island).

Figure 4.3. Atmospheric pressure records from Palma de Mallorca on June 15, 2006. Red dots indicate the strong "jump" in atmospheric pressure.

It is also possible to verify and confirm the general synoptic pattern associated with *rissagas* described by Jansá et al. (2007), quite apparent in the vertical profile of the Palma de Mallorca radio sounding (Figure 4.4). The pattern is characterized by a three-layer structures described by Jansá et al. (2007) as follow: "(1) low level Mediterranean air, with a weak surface depression, (2) warmer African air blowing above, around 850 hPa, with an inversion layer separating (1) and (2); and (3) a poorly stable or even a conditionally unstable layer between the African air and colder air in the upper levels, with a marked vertical wind shear across this layer (usually with strong south-westerly wind blowing at upper levels)". In Figure 4.4, it is possible to identify the vertical shear and the temperature variation between 850 hPa and the average levels of the troposphere. This consists of an abrupt change in vertical stability. The atmosphere is conditionally unstable, constituting an important condition for the occurrence of convection (Miranda, 2013).

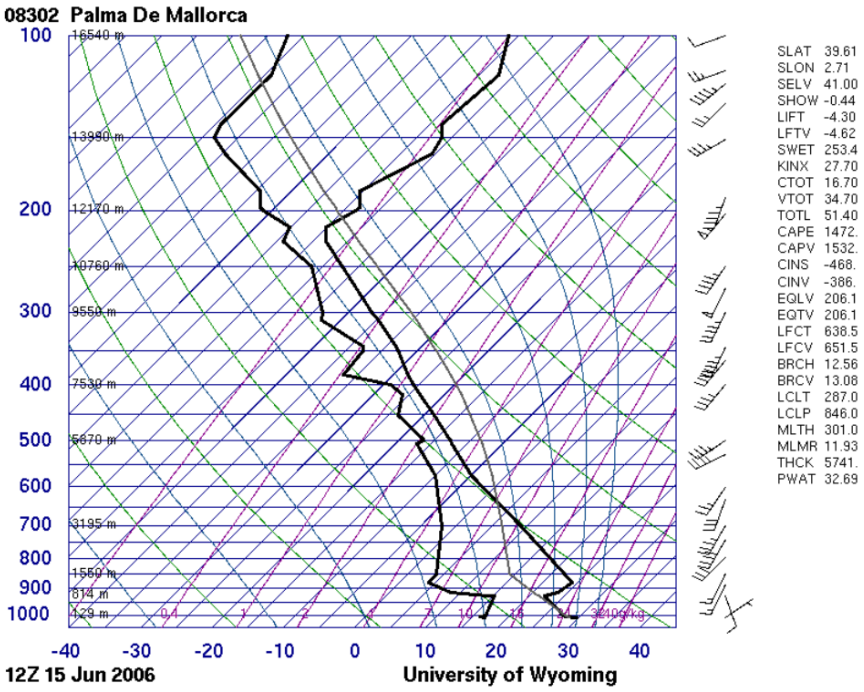

Figure 4.4. Vertical profile for Palma de Mallorca at 1200 UTC on 15 June 2006.

Regarding sea-level disturbances caused by the 2006 event, several simulations have been performed to better understand this specific event and to approximate the meteotsunami wave heights reported in this channel (e.g. Rabinovich et al., 1999, Jansá et al., 2007, Vilibić et al., 2008, Renault et al., 2011, Ličer et al., 2017). Both Vilibić et al. (2008) and Renault et al. (2011) applied models for this region of the Balearic Islands.

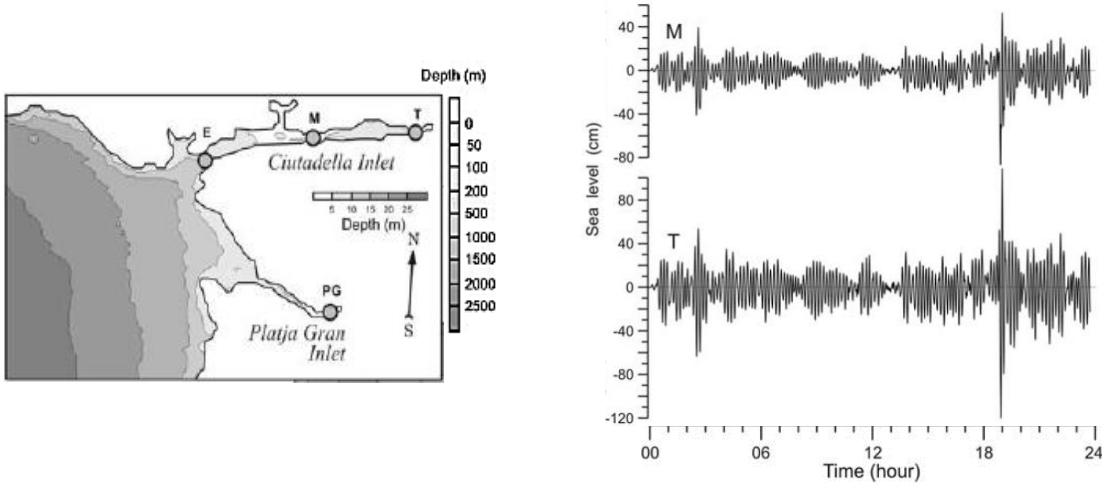

Figure 4.5. A map of the computational domain and topography used by Vilibić et al.,2008 in Menorca Island with the position of select grid points used in the analyses, and the simulated sea-level disturbances at sites M and T during the rissaga event of 15 June 2006.

Vilibić et al. (2008) simulated the 2006 meteotsunami using a 2-D nonlinear shallow-water model. This model is forced by a travelling atmospheric disturbance, with constant speed (25 m/s) and direction (225º), reconstructed from microbarograph measurements. The model was verified based on two weaker

meteotsunami events of 1997. In the left panel of Figure 4.5, the domain under Vilibić et al. (2008) study is shown, with the position of select grid points used in the analyses. In the right panel, the figure depicts the simulated sea-level disturbances at sites M (Ciutadella inlet-centre) and T (Ciutadella inlet-head) during the "*rissaga*" event of 15 June 2006. It is clear from these results that the incident wave underwent a significant amplification due to the harbour resonance, reaching the trough-to-crest wave height of about 2 meters at grid point T.

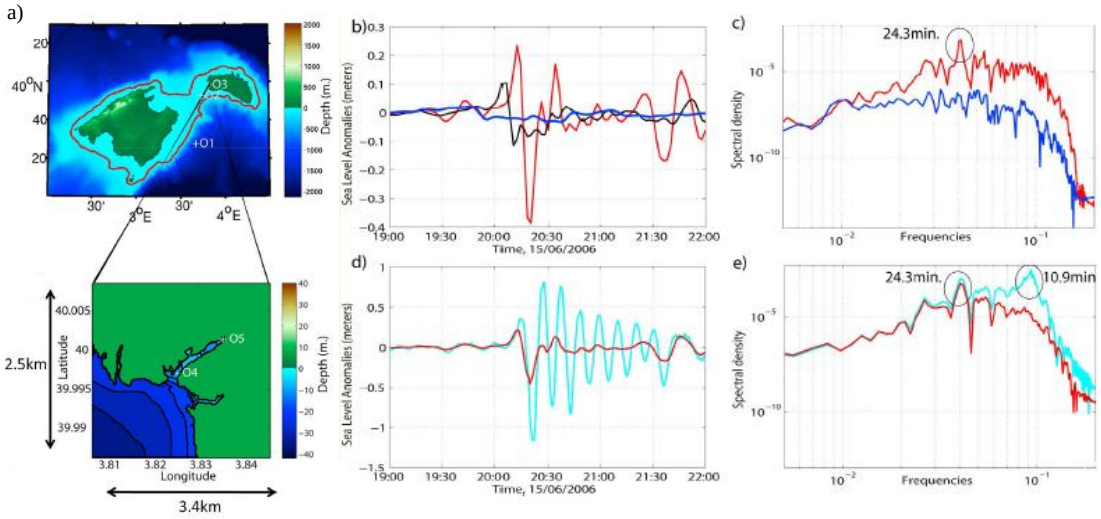

Figure 4.6. a) Model domains and topography used by Renault et al. (2011), in the Ciutadella Harbour. (b) Simulated sea level anomalies at selected points O1 (blue), O2 (black) and O3 (red). (c) Spectrum of the sea level anomaly timeseries at selected the point O3 (red) and O1(blue). (d) The same as Figure 4b but for the points O4 (red line) and O5 (cyan line). (e) The same as Figure 4c but for the points O4 (red line) and O5 (cyan line).

Figure 4.6 presents the results of the 2006 meteotsunami simulations performed by Renault et al. (2011). Their simulations applied a coupled atmospheric (Weather Research Forecast (WRF) atmospheric model) oceanic (Regional Ocean Modeling System (ROMS) forced by the WRF pressure field) model to compute the meteotsunami waveforms at the points of interest. The point O4 near the entrance of Ciutadella inlet and the point O5 at the Ciutadella inlet-head (Figure 4.6.a). At this grid point, the trough-to-crest wave also reaches 2 meters (Figure 4.6.d)). Due to the Proudman resonance, the spectrum of the sea-level anomalies time series increases, and the dominant period is around 24.3 min (Figure 4.6.e)), which characterizes the shelf eigenfrequencies. Inside the harbour, as the main harbour eigenfrequency is 10.5 min and the main period simulated is about 10.9 min. In both simulations, the estimated maximum trough-to-crest wave height (~2 meters) is approximately one half of that reported by witnesses who claimed 4.5 meters waves in the harbour.

4.2. The 6-7 July 2010 event in the Atlantic coast of the Iberian Peninsula

4.2.1. Sea level and air pressure analyses for the July 2010 event

At the end of July 6, 2010, between 21:00 and 22:00 local time, a convective cell of atmospheric instability developed SW of the Iberian Peninsula, characterized by strong downstream currents associated with surface gusts travelling in the NNW direction (Antunes et al., 2011). These led to

uncommon ocean waves that were observed south of Portugal and propagated all over the coast. Here, analyses of the sea-level records of three Portuguese stations: Sines, Cascais and Peniche are presented.

For Sines, the analysis of the recorded signal is depicted in Figure 4.7. Figure 4.7 allows identifying the arrival of the meteotsunami at Sines at around 00:20 on July 7 (red line through the figure). After de-tiding and filtering of the signal (Figure 4.7 middle panel), the maximum crest-to-through meteotsunami height is estimated at 0.32 meters. This maximum occurs between 05:24 and 05:34. During this time interval, it is possible to observe more significant anomalies at sea with a dominant period window of [13.6-46.1] min (Figure 4.7 bottom panel). The meteotsunami event at Sines station ended approximately 12 hours later.

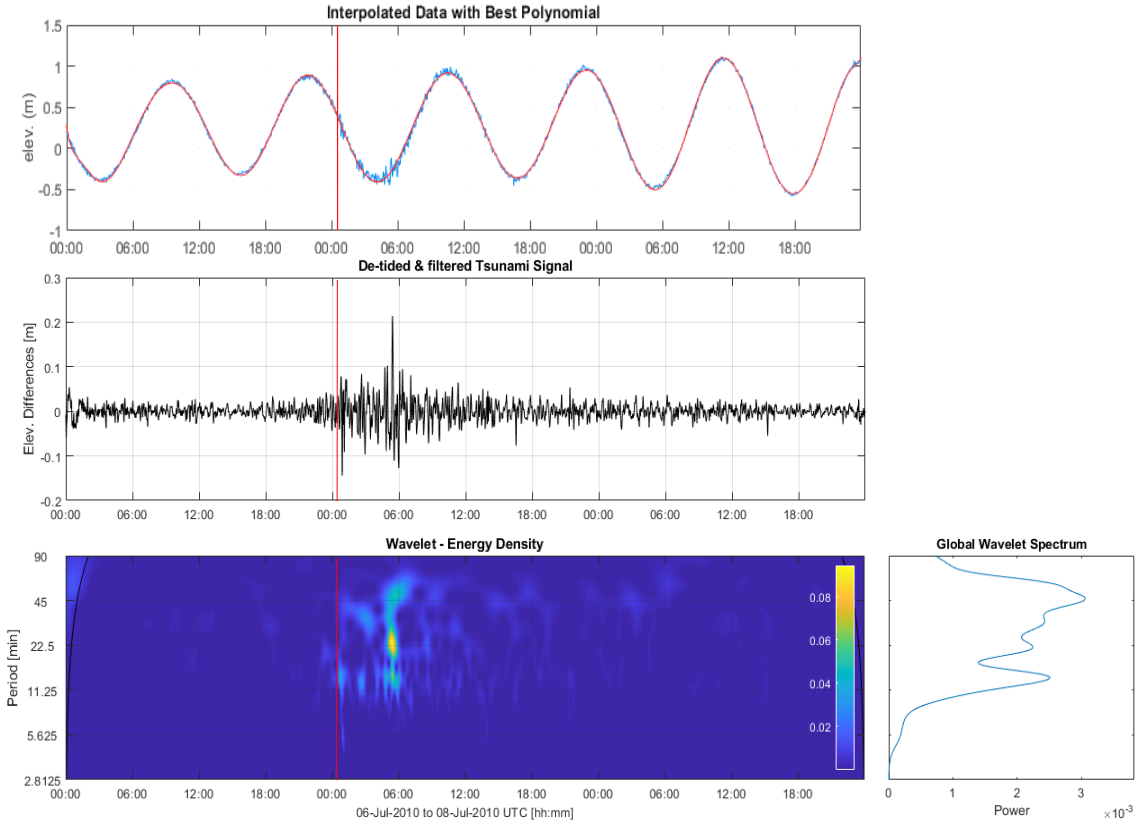

Figure 4.7. Signal of meteotsunami in Sines tide-gauge station (sample interval is 1 minute) and its spectral analysis. Top panel represents sea level variation, the middle panel depicts the de-tided and filtered meteotsunami signal, and the bottom panel presents the wavelet analysis results. The red line represents the estimated arrival of the phenomenon recorded in the tide-gauge.

Atmospheric pressure variation at Sines during the time of meteotsunami observation is depicted in Figure 4.8. From this figure, it is possible to observe four significant sudden jumps in atmospheric pressure. The most significant "jump" of 4.3 hPa occurred between 00:45 and 00:51, the time that almost corresponds to the estimated arrival of the maximum meteotsunami wave at Sines coast. The other three air pressure "jumps" occurred between 05:00 and 06:00, with values of 2.5 hPa, 1.5 hPa and 2.6 hPa, respectively, which corresponds to the most important activity on the meteotsunami spectrum (Figure 4.7 bottom). It is possible to relate the arrival of meteotsunami with the first abrupt "jump" in atmospheric pressure, and it is also important to note that the period between the most significant "jumps" (~20 min) approximates the meteotsunami waves periods shown in the spectrum.

Figure 4.8. Atmospheric pressure from Sines station. The sample interval is 1 minute. The red dots identify the four more significant "jumps" in pressure.

The signal recorded at Cascais tide-gauge (Figure 4.9), ~95 km further north from Sines station shows the arrival of the meteotsunami at around 02:20 during low tide. The station captures maximum crest-to-through height of about 0.47 meters around 07:00 (Figure 4.9, middle panel). The wavelet analysis results (Figure 4.9, bottom panel) show that the meteotsunami period band is around [7-20] min and between [22.5-45] min, with the dominant period being 32.1 min. In this coastal location, the meteotsunami perturbations ended after about16 hours.

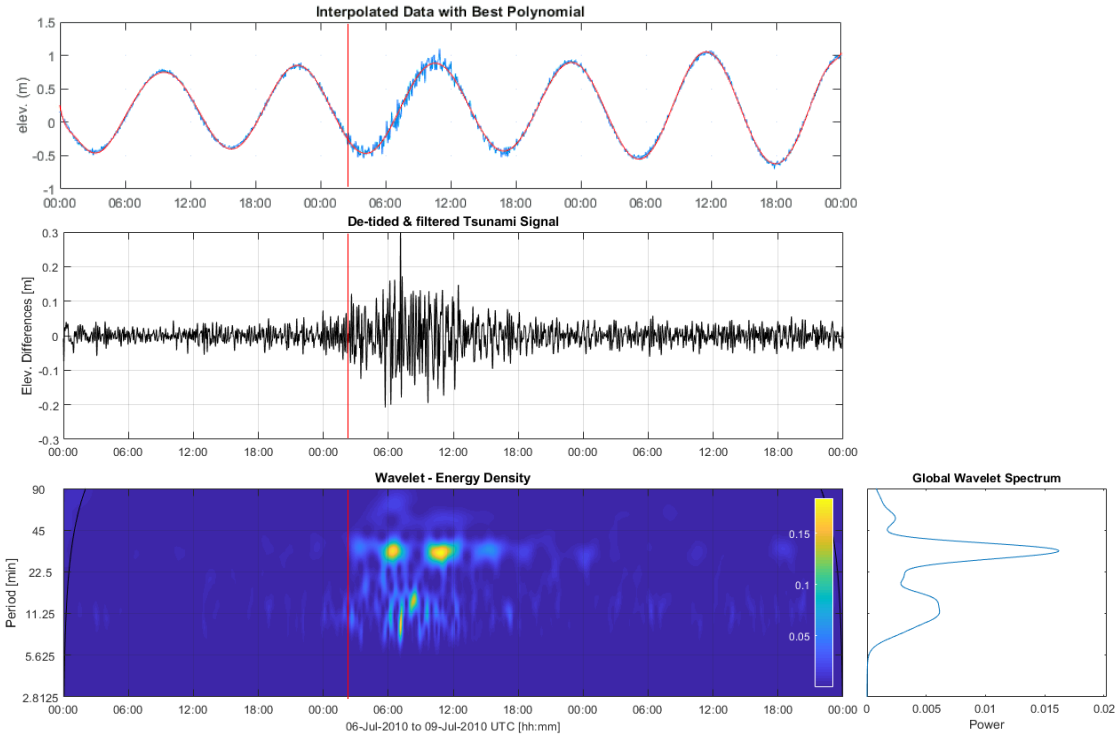

Figure 4.9. Signal of meteotsunami in Cascais tide-gauge station (sample interval is ~2 seconds) and its spectral analysis. Top panel represents sea level variation, the middle panel depicts the de-tided and filtered meteotsunami signal, and the bottom panel presents the wavelet analysis results. The red line represents the estimated arrival of the phenomenon recorded in the tide-gauge.

Air pressure data at Cascais (Figure 4.10) are of low temporal resolution (10 minutes) and low precision in the decimal point of the observed values, which turns any correlation with the observed meteotsunami difficult to make. Still, it is possible to observe a significant "jump" in atmospheric pressure of 3 hPa (1013-1017 hPa) between 06:30 and 07:00 on July 7 (third and fourth red dots in Figure 4.10), corresponding to the same time where the maximum wave height occurred.

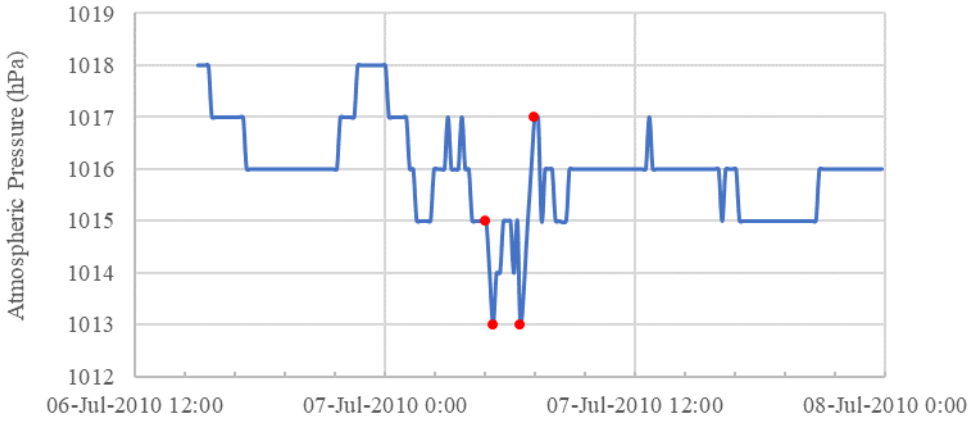

Figure 4.10. Atmospheric pressure from Cascais station. The sample interval is 10 minutes. The red dots identify the four more significant "jumps" in pressure.

Finally, the tide-gauge of Peniche, the northernmost of the three Portuguese stations for which the records were examined for the 2010 event, and where highest wave crest-to-trough height (0.58 meters) occurred. The meteotsunami arrived at approximately 07:00 on July 7, during low tide (Figure 4.11, top panel). The dominant period band is around [12-45] minutes, with a dominant period of 17.3 min (Figure 4.11, middle panel). At this coastal site, having a narrow bay entrance, it is clear that the eigen periods of the bay are between [11.25-22.5] min (Figure 4.11, bottom panel), suggesting this narrow bay as the leading cause of amplifying the meteotsunami signal. The meteotsunami ended at Peniche after about 11 hours of increased activity.

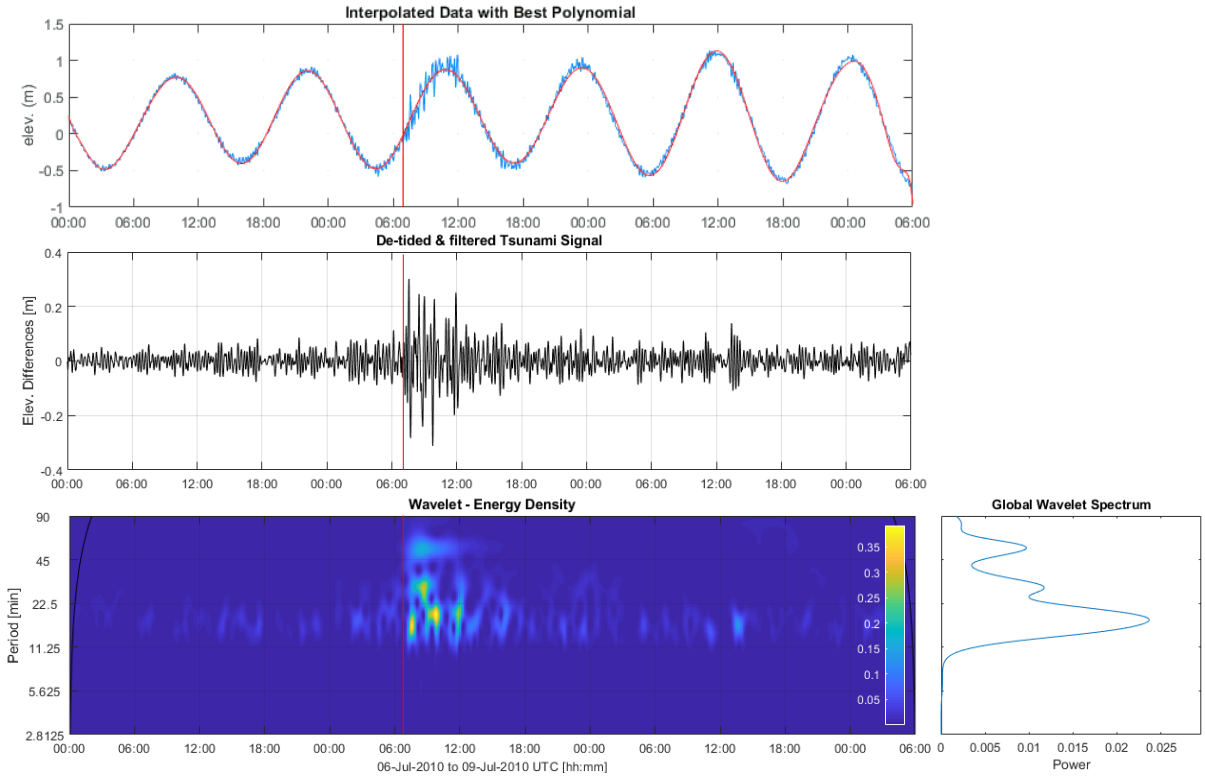

Figure 4.11. Signal of meteotsunami in Peniche tide-gauge station (sample interval is 1 minute) and its spectral analysis. Top panel represents sea level variation, the middle panel depicts the de-tided and filtered meteotsunami signal, and the bottom panel presents the wavelet analysis results. The red line represents the estimated arrival of the phenomenon recorded in the tide-gauge.

In Peniche, it is possible to observe two crucial "jumps" in atmospheric pressure (Figure 4.12). In the early hours of the July 7, between 07:00 and 08:00, perturbations in atmospheric pressure between 07:00 and 07:30 are noticeable as a sudden decrease of 2.7 hPa (1015.2 to 1012.5 hPa), followed by a rise of 3.9 hPa until 08:00. These two perturbations in air pressures show good correlation with the arrival of the meteotsunami at Peniche tide-gauge station at about 07:00, and it is maximum wave heights that occurred at 07:34.

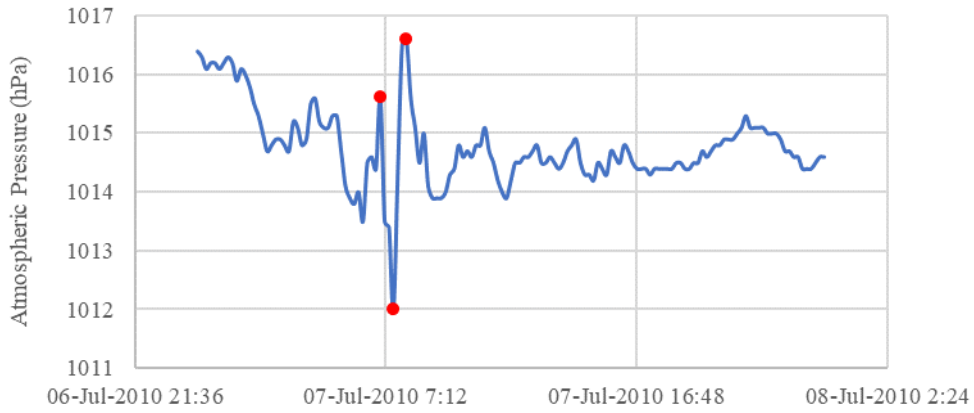

Figure 4.12. Atmospheric pressure from Peniche station. The sample interval is 10 minutes. The red dots identify the more significant jumps in pressure.

Considering these three tide-gauges, the median crest-to-trough height for the 2010 event is 0.47 meters. The spectral analysis shows an average dominant period of approximately 25 minutes.

The speed of the meteotsunami varies as it approaches the coast, due to differences in depth. Nevertheless, given the location of the Sines and Peniche tide-gauge stations (Figure 4.1), it is possible with a simple ratio (speed equals distance over time) to deduce the average speed of the wave generated by the meteotsunami. The distance between Sines and Peniche stations it is roughly 162 kilometres. Based on the time of arrival of the first wave at Sines (00:20) and Peniche (06:40) tide-gauges, the average speed of the meteotsunami wave that travelled between Sines and Peniche is approximately 25 km/h ≈ 7m/s.

4.2.2. Atmospheric conditions for the July 2010 event

For the 2010 event, clear disturbances in the signal records can be observed in all meteorological stations (Figures 4.13, 4.14 and 4.17), both in the atmospheric pressure field and the surface wind intensity. An air mass that affected Portugal Mainland was transported from July 4-7 through a depression valley that stretched from North Africa (Boletim Climatológico Mensal – Julho 2010, IM)[9]. A depression valley is a "configuration defined by isobars extending out of a low-pressure region. It has an associated valley axis (or valley line), which corresponds to a minimum pressure line (compared to adjacent points) on either side of the line)"[10]. Thus, at the end of July 6, an atmospheric instability caused by convective cells was formed SW of the Iberian Peninsula that moved in the NNW direction (Antunes et al., 2011).

In all three stations, upon arrival of the meteotsunami, a drop in atmospheric pressure accompanied by an increase in wind intensity is observed. It is important to emphasize here the well-known fact that the higher the atmospheric pressure difference is for a given point, the more intense the wind acting at that point. For such a reason, the correlation between these measures can easily be observed, and therefore, its temporal concordance with what happens on the sea surface. Overall, there is a higher sea disturbance activity, reflected in greater intensity in the energy density of the spectrum when there are higher amplitude and variation of wind intensity.

It is also worth mentioning that the collected wind values, obtained by the network of surface automatic weather stations in Portugal, are at station level and not at mean sea level. Therefore, the following values refer to this difference. For Sines, it is at 103 meters altitude. For Cascais, the relatively nearest station is used, being Lisbon/Gago Coutinho, which is 103,884 meters. For Peniche, the Cabo Carvoeiro lighthouse station is used which has an elevation of 32 meters.

[9] https://www.ipma.pt/resources.www/docs/im.publicacoes/edicoes.online/20100805/vyJoENHeCqVoSirCTGWm/cli_20100701_20100731_pcl_mm_co_pt.pdf

[10] https://www.ipma.pt/pt/educativa/glossario/meteorologico/index.jsp?page=glossario_uv.xml

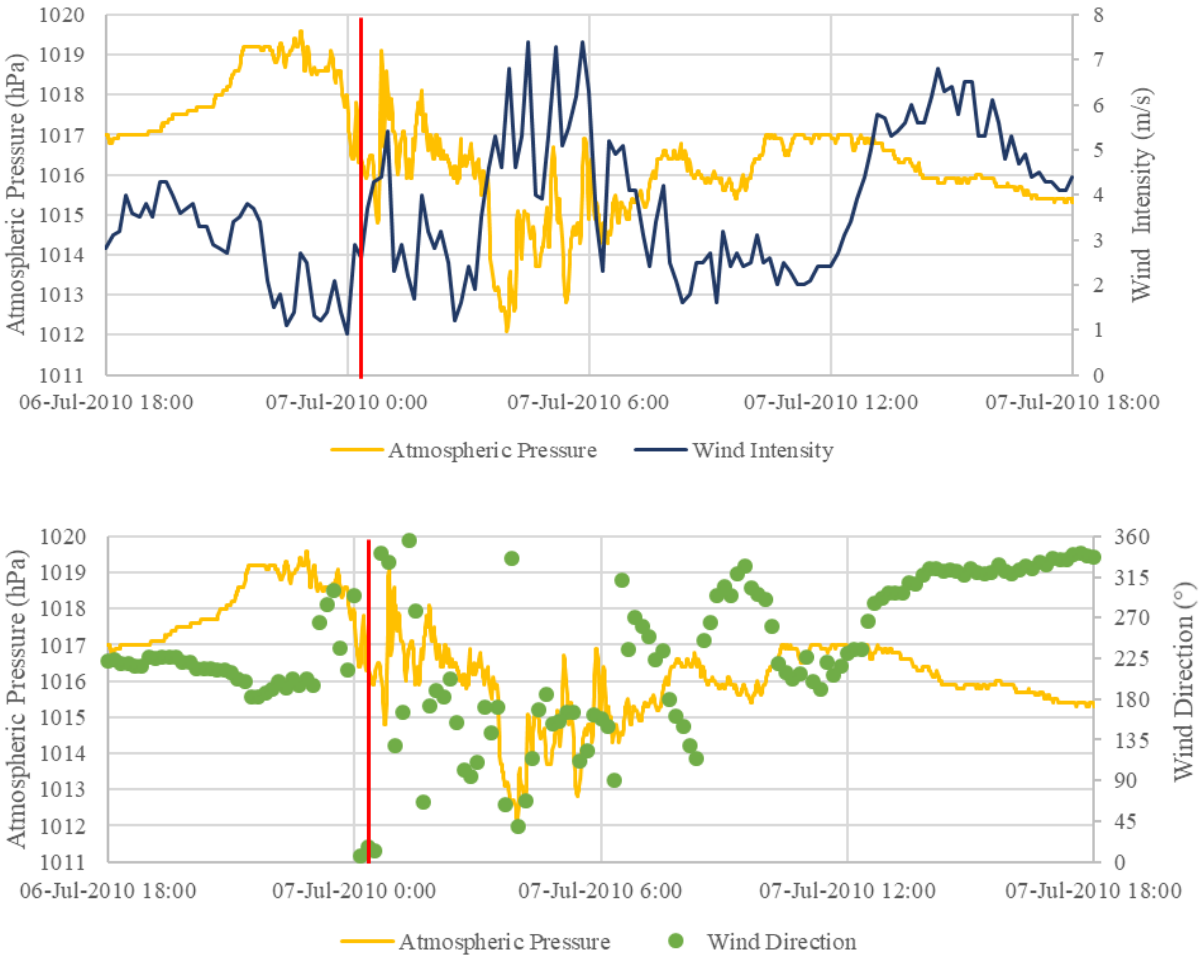

Figure 4.13. Atmospheric conditions of Sines station. Wind intensity (top) and direction (down) and atmospheric pressure at station level. The sample interval is 10 minutes. The red line represents the estimated arrival of the phenomenon recorded in the tide-gauge.

At Sines (Figure 4.13), it is possible to relate the arrival time at 00:20 on July 7 and the drop in atmospheric pressure at that time. It is also possible to observe that the period of highest activity and highest energy occurred around 5:30 on that day. The sharp drop in atmospheric pressure, and the increase in wind intensity, reaching 7 m/s. The same value previously referred to as the supposed average speed of meteotsunami between Sines and Peniche. A considerable variation in wind direction is also observed during this period, from 00:00 on day 7 to approximately 12:00 on the same day. Outside this period, the direction seems to remain constant. Around 225º (SW) before the arrival of the meteotsunami and NW/N after the event.

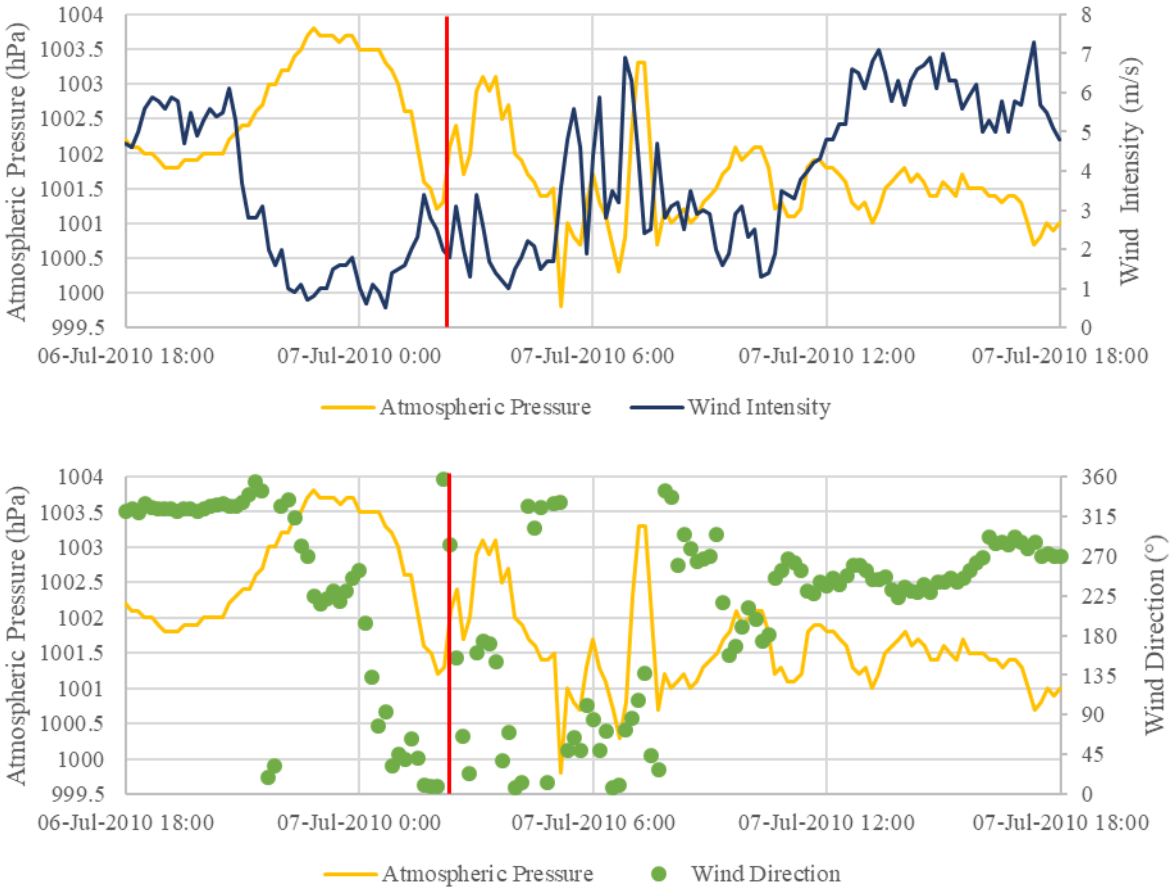

Figure 4.14. Atmospheric conditions of Lisboa / Gago Coutinho station. Wind intensity (top) and direction (down) and atmospheric pressure at station level. The sample interval is 10 minutes. The red line represents the estimated arrival of the phenomenon recorded in the tide-gauge.

As Lisbon station is further east than Cascais, the data show a certain delay in detecting the disturbances. Still, it is possible to observe in the figure above (Figure 4.14) the period of meteotsunami energy focus, corresponding to the interval between 05:00 and 11:00 on July 7. This is noticeable once again in the wind intensity, which reaches 7 m/s during this period, especially at nearly 07:00. Regarding the wind direction, it seems constant N/NW outside the event's duration (between 270º after and 315º before), and quite dispersed during the event.

At this station, it is also possible to observe what happened at altitude (Figure 4.15). Given the general synoptic patterns suggested by Jansá et al. (2007), it is important to highlight the wind shear that occurs at the first levels and the conditionally unstable layer between 850 hPa and upper layers. This is observed due to the approximation of the black segment to the blue segment (air temperature). The black segment is performed to determine the lifted condensation level (i.e. the approximate point where the lowest clouds will be found), based on air at the surface. It takes the dewpoint at the ground (green segment) up the mixing ratio line, and the temperature (blue segment) up to the dry adiabatic simultaneously until they intersect. Above the condensation level, the air is always saturated, describing a curve called saturated adiabatic.

As shown in Figure 4.16 of the geopotential at 500 hPa wind between 00:00 and 12:00, it is possible to evaluate that the disturbances had propagation speeds of 29-46 km/h, with the disturbance at 00:00 having a speed of 12 m/s = 43 km/h toward SW. This disturbance is thus confirmed to be characterized by strong downward currents associated with gusting surface winds (top panel of Figure 4.16). The

average meteotsunami speed calculations, given the waver arrival at each station, leads to values between 15-48 km/h. These velocities are within the expected range to get the Proudman resonance.

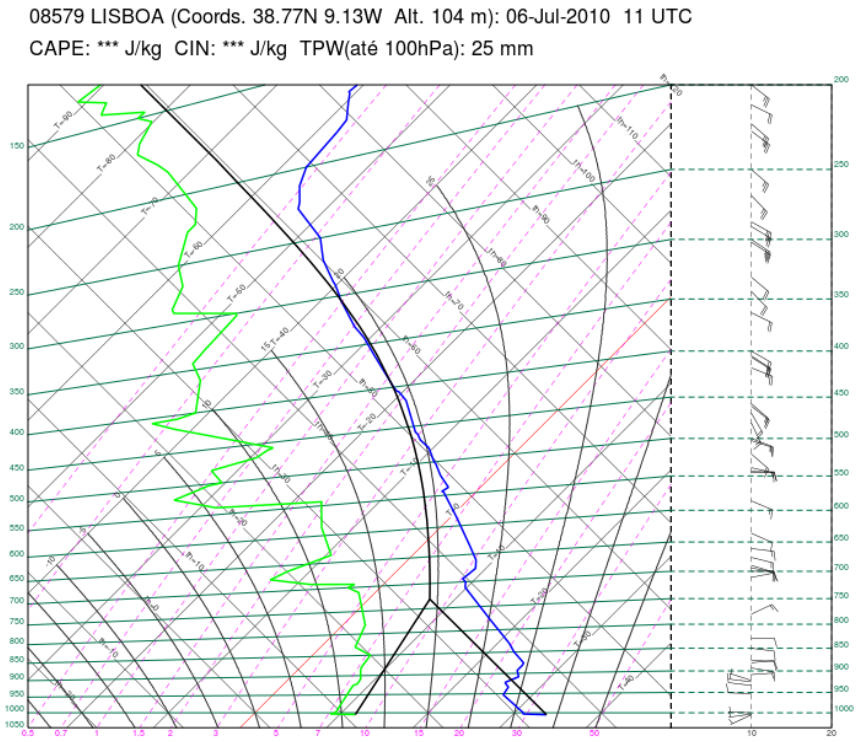

Figure 4.15. Radiosounding data from Lisboa station on 7 June 2010 at 00:00 (local time).

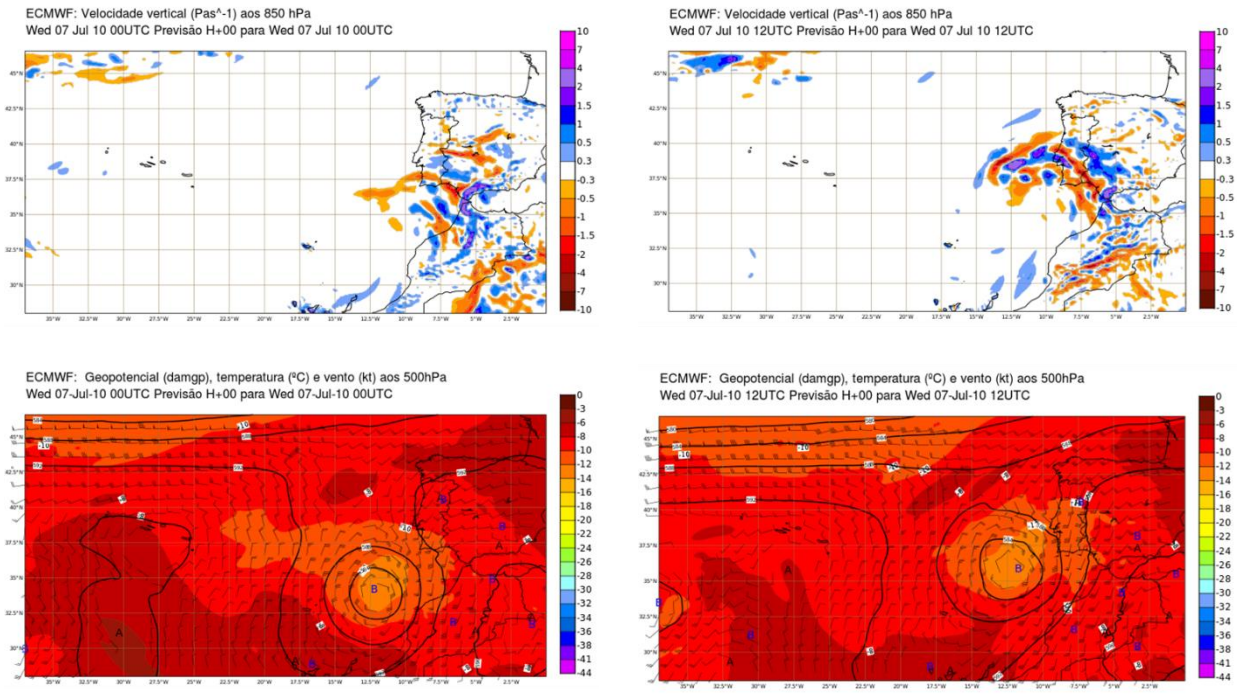

Figure 4.16. Top panel: Vertical speed at 850 hPa for 00 UTC and 12UTC of the 7 July 2010. On the scale, negative values represent descending wind speeds. Bottom panel: Geopotential (damgp), temperature (ºC) and wind (kt) at 500 hPa for the same time.

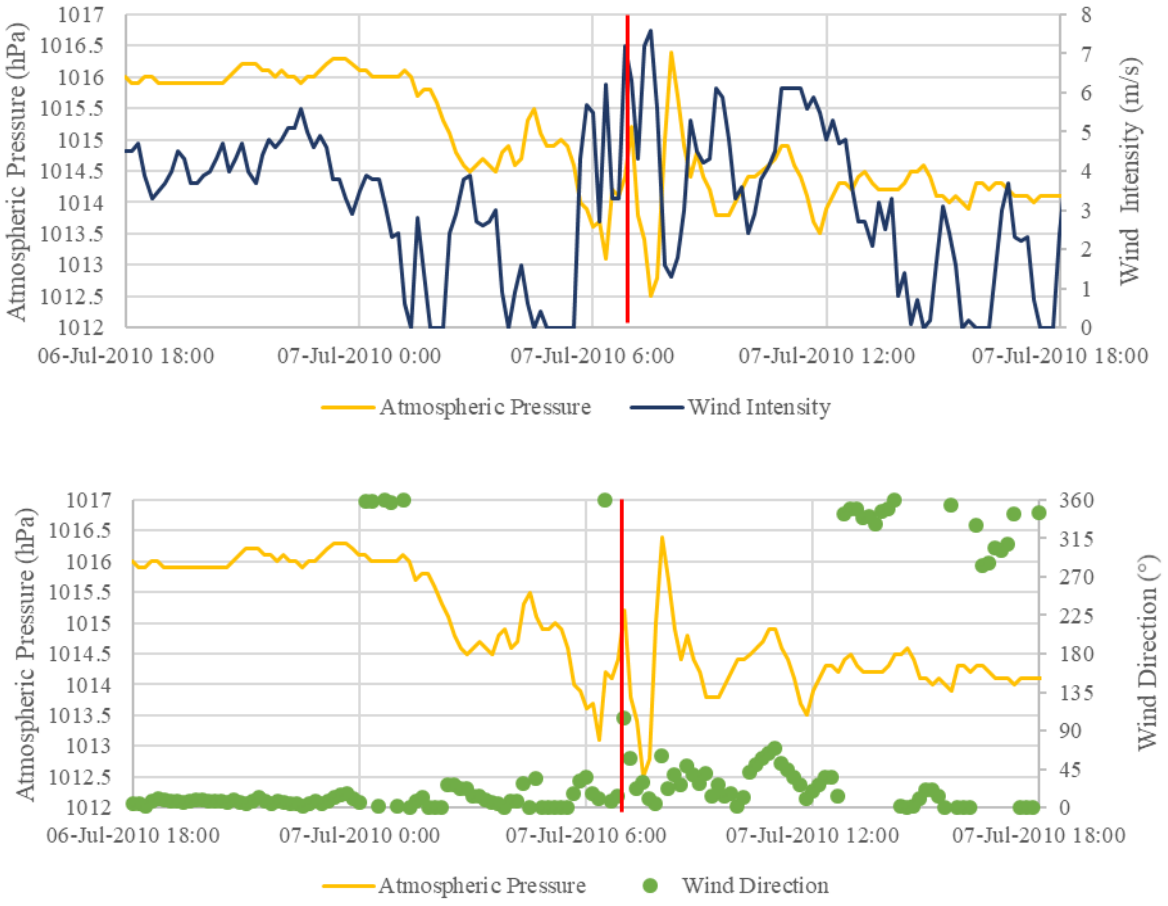

Figure 4.17. Atmospheric conditions of Peniche station. Wind intensity (top) and direction (down) and atmospheric pressure at station level. The sample interval is 10 minutes. The red line represents the estimated arrival of the phenomenon recorded in the tide-gauge.

Figure 4.17 shows that there are significant atmospheric disturbances between 07:30 and 08:00, at the time of the arrival of the meteotsunami estimated at approximately 07: 00. Once again, a wind of 7 m/s is observed during this period, with wind intensity peaks relating to the atmospheric pressure decreases. The wind direction recorded at this station is relatively constant northward, with little variation during the event towards E (90º).

Equilibrium response to surface pressure variations of only a few hPa cannot directly explain significant oscillations of the sea-level. This is because of the inverted barometer principle. This response would account for an equivalent of a couple of centimetres. Since the effect of the inverted barometer is not enough, this is where the Proudman resonance (Equation 2.4) is important, reflecting the matching of the long ocean waves speed and the propagation speed of the precursor atmospheric gravity wave (Romero, 2019). In this specific case of the 2010 event for the Portuguese continental coast, considering a depth (H) between 1 and 10 meters in the harbour, it is possible to observe that c ≈ 3-10 m/s ≈ 11-36 km/h. At station height, only U ≈ 7 m/s ≈ 25 km/h is obtained, but in Figure 4.15 and 4.16, a speed of 15-48 km/h is extracted at the altitude that fit within the range of the resonance. Moreover, in all the three stations, the harbour resonance may contribute to the amplification of the incident meteotsunami.

4.3. The 26-27 June 2011 event in the Iberian Peninsula and the northeast of the English Channel

4.3.1. Sea level and air pressure analyses for the June 2011 event

Meteotsunamis can happen sequentially along the line of the same synoptic system (Šepić et al., 2015b; 2009). The event of 26-27 June 2011 took place on the shores of the NE Atlantic and the English Channel, affecting nearly 300 km of coastline. Driven by convective cells extending from the southern Iberian Peninsula to the northeast of the English Channel, the meteotsunami was observed in about 30 harbours. Tappin et al. (2013) rapidly rejected other 'geological' tsunami sources for the phenomena and Frère et al. (2014), using spectral analysis showed a dominant period of 25 min present on almost all data. This is because the phenomenon highlighted the resonant periods of the harbours (eigen periods). Through comparison with atmospheric data, they also show that the travelling pressure anomaly was probably the origin of these sea level anomalies, having this disturbance travelled to the northeast at 20-25 m/s. Here, the analyses of four sea-level records, two from Portuguese stations (Peniche and Leixões) and two from Spanish stations (Marin and Coruña), are reported. For the rest of the stations that recorded the 2011 event, the analyses are presented in Appendix III.

Peniche station recorded the arrival of the meteotsunami at around 13:00 on June 26 (red line through Figure 4.18, top panel). The maximum crest-to-trough wave is about 0.34 meters (Figure 4.18, middle panel). The meteotsunami energy is concentrated in the period bands [11.25-22.5] min (Figure 4.18 bottom panel). The event lasted ~ 4 hours.

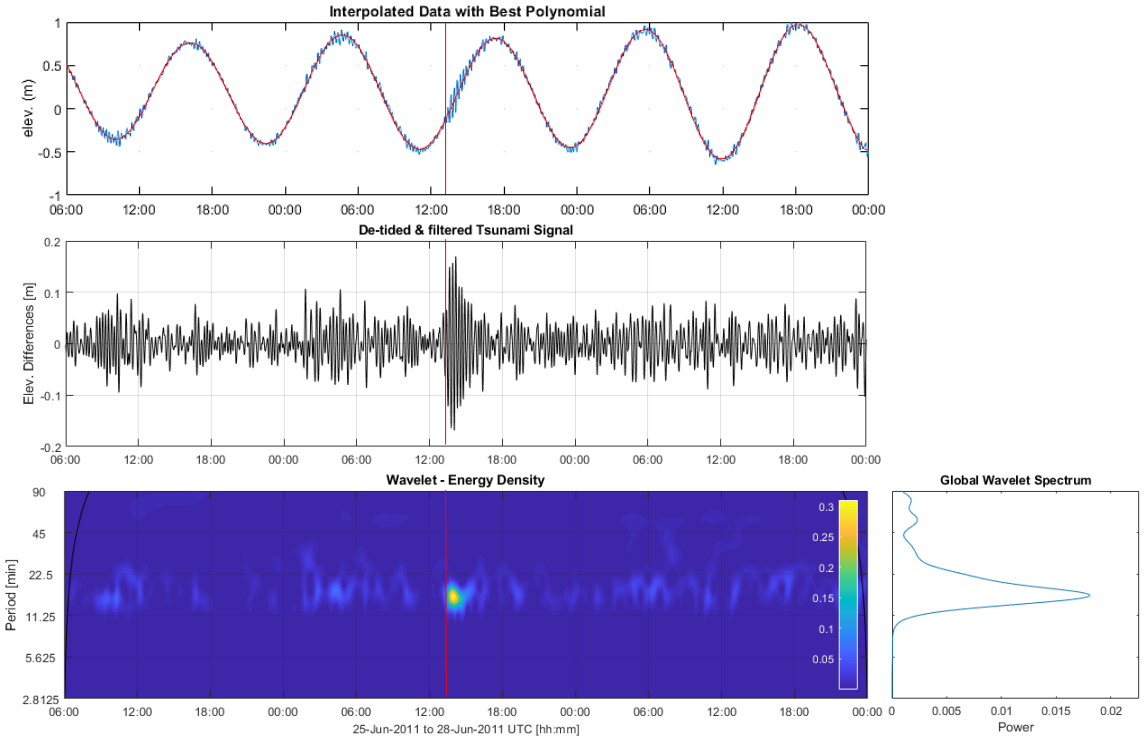

Figure 4.18. Signal of meteotsunami in Peniche tide-gauge station (sample interval is 1 minute) and its spectral analysis. Top panel represents sea level variation, the middle panel depicts the de-tided and filtered meteotsunami signal, and the bottom panel presents the wavelet analysis results. The red line represents the estimated arrival of the phenomenon recorded in the tide-gauge.

In Peniche, it is possible to observe the “jump” of 0.6 hPa in atmospheric pressure (Figure 4.19) between 13:00 and 13:20 on June 26. This disturbance, although small, can be related to the arrival of the meteotsunami at the Peniche station at around 13:00.

Figure 4.19. Atmospheric pressure from Peniche station. The sample interval is 10 minutes. The red dots identify the more significant jumps in pressure.

Another Portuguese tide-gauge is Leixões, ~212 kilometres further north from Peniche, that also recorded the 2011 meteotsunami. In Figure 4.20, it is possible to observe the arrival of the meteotsunami during low tide, around 17:30 on June 26 (red line through the figure). The maximum crest-to-trough wave occurs shortly after the arrival with a height of 0.28 meters. The wavelet analysis results show that the meteotsunami energy focus is in the period’s bands of [18-50] min and the dominants period is of 40 min (Figure 4.19 bottom panel). The event lasted approximately 6 hours.

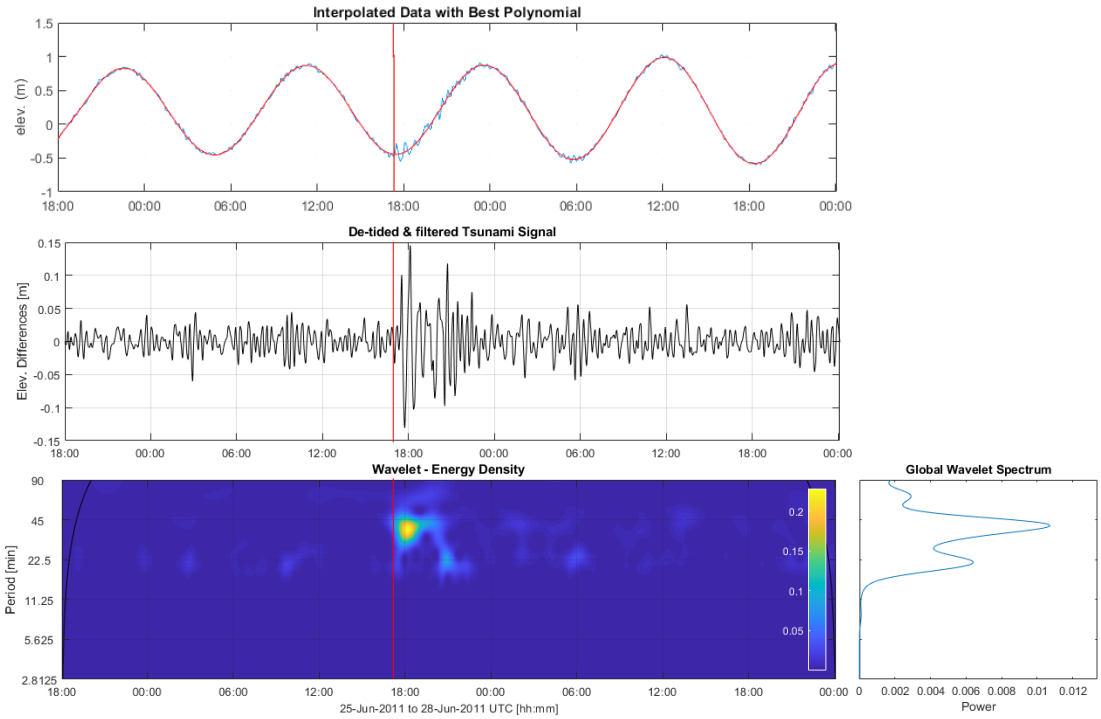

Figure 4.20. Signal of meteotsunami in Leixões tide-gauge station (sample interval is 6 minutes) and its spectral analysis. Top panel represents sea level variation, the middle panel depicts the de-tided and filtered meteotsunami signal, and the bottom panel presents the wavelet analysis results. The red line represents the estimated arrival of the phenomenon recorded in the tide-gauge.

In the atmospheric pressure recorded at the Porto station, the closest station to Leixões (Figure 4.21), it is worth noting the "jump" of 1.1 hPa in atmospheric pressure in 10 min. This jump occurs around 17:30 on June 26.

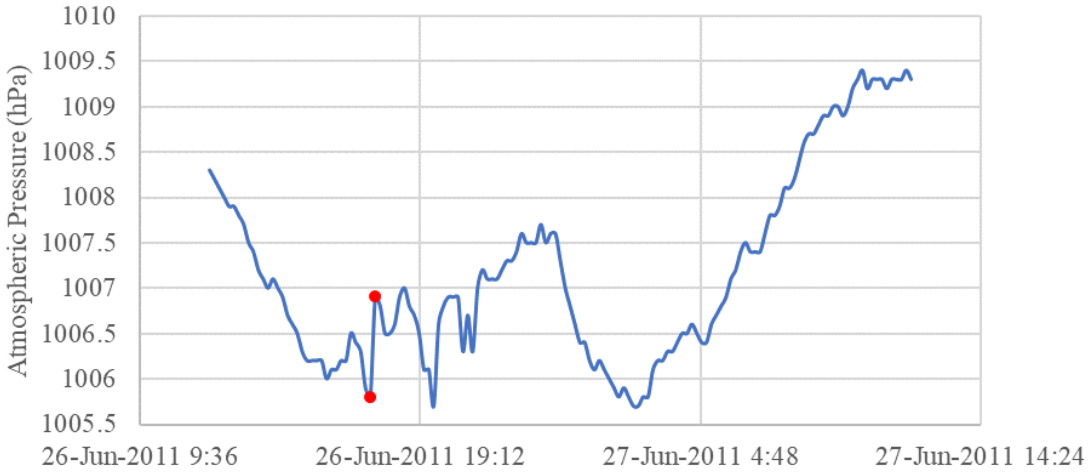

Figure 4.21. Atmospheric pressure from Porto station. The sample interval is 10 minutes. The red dots identify the more significant jumps in pressure.

At Spanish stations, the Marin tide-gauge recorded the arrival of the meteotsunami at around 20:00 on June 26 (red line through Figure 4.22). Although the anomaly at mean sea level is small, the

difference in elevation in the filtered signal is clearly noticeable (Figure 4.22, middle panel). Around 23:30, maximum crest-to-trough wave height of 0.34 meters is observed (Figure 4.22 middle panel). The wavelet analysis results show that the meteotsunami energy is concentrated in the period bands of [50-90] min with a dominant period of 72.4 min. In this location, the event lasted just over 4 hours.

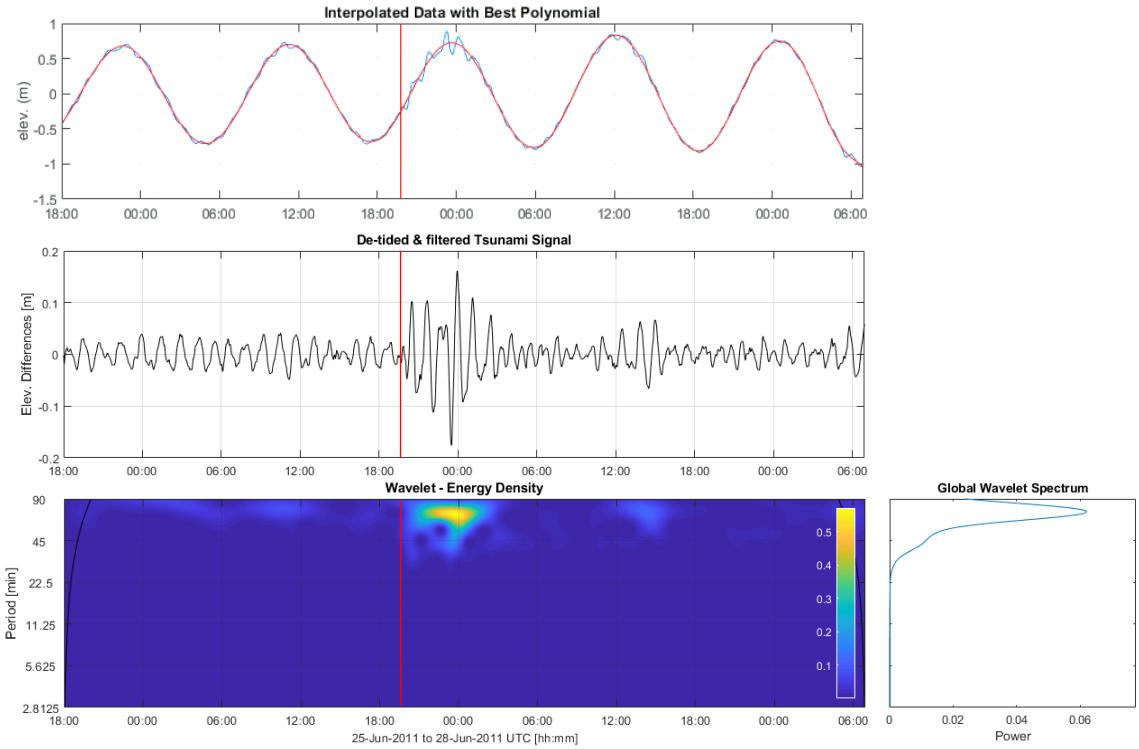

Figure 4.22. Signal of meteotsunami in Marin tide-gauge station (sample interval is 5 minutes) and its spectral analysis. Top panel represents sea level variation, the middle panel depicts the de-tided and filtered meteotsunami signal, and the bottom panel presents the wavelet analysis results. The red line represents the estimated arrival of the phenomenon recorded in the tide-gauge.

At the northernmost station of the Iberian Peninsula, La Coruña tide-gauge presents a clear signal, with meteotsunami arriving at high tide early on June 27, around 00:00 (red line through Figure 4.23). Approximately half an hour after, crest-to-trough wave height of 0.21 meters reached the station (Figure 4.23, middle panel). The dominant period is clearly observed at 34 min. The event lasted approximately 8 hours.

Considering the four tide-gauges the median crest-to-trough height is 0.31 meters. The obtained results are in good agreement with those presented in Tappin et al. (2013) and Frère et al. (2014), that show that the 2011 meteotsunami is explained by atmospheric convective activity in the Bay of Biscay and the English Channel. Frère et al. (2014) assumed the speed of the event in the Iberian coast to be approximated 20m/s ≈ 72 km/h.

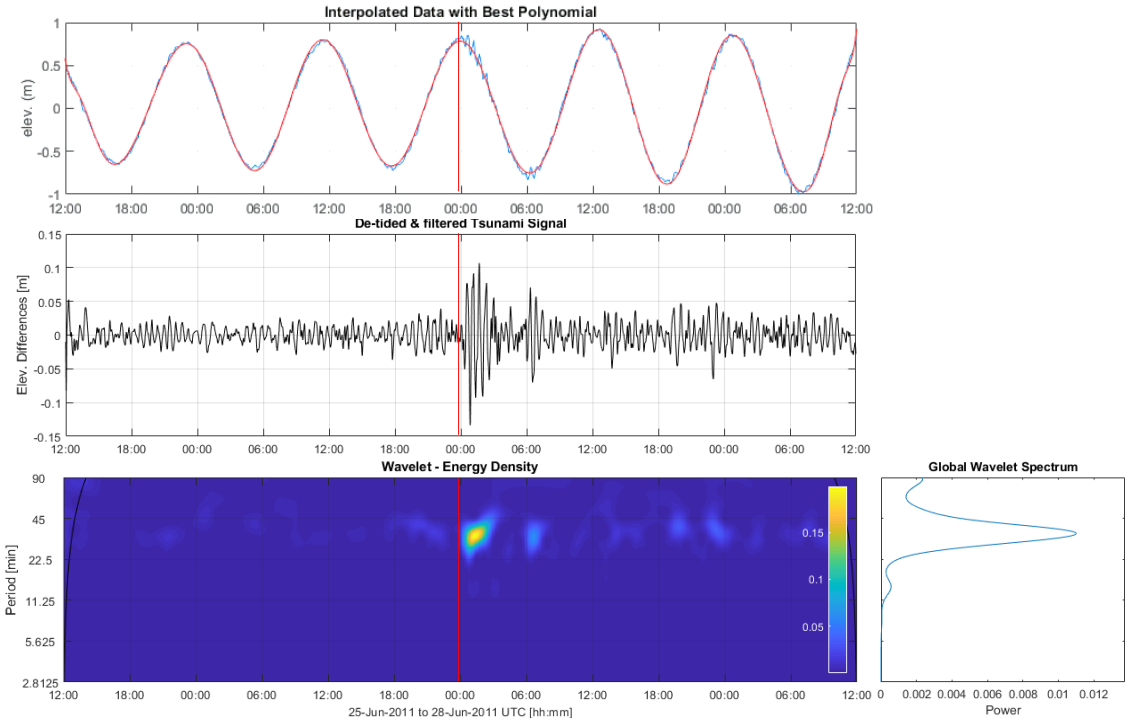

Figure 4.23. Signal of meteotsunami in La Coruña tide-gauge station (sample interval is 5 minutes) and its spectral analysis. Top panel represents sea level variation, the middle panel depicts the de-tided and filtered meteotsunami signal, and the bottom panel presents the wavelet analysis results. The red line represents the estimated arrival of the phenomenon recorded in the tide-gauge.

4.3.2. Atmospheric conditions for the June 2011 event

Williams et al. (2018) combined observations and numerical models to show that convective weather systems generate meteotsunamis that occur in the English Channel. The 2011 meteotsunami, that also affected the coasts on the English Channel is confirmed to have been generated by a travelling pressure anomaly originated over western Iberia, that travelled to the northeast at 20-25 m/s speed.

Less clear than for the previous event, it is possible to observe the correlation of the rate change of atmospheric pressure and the wind intensity and speed, in the Portuguese stations (Figures 4.24 and 4.25). Upon the arrival of the meteotsunami, the drop in atmospheric pressure is observed and consequently a difference in wind intensity. The wind direction, however, does not suffer a significant visible variation.

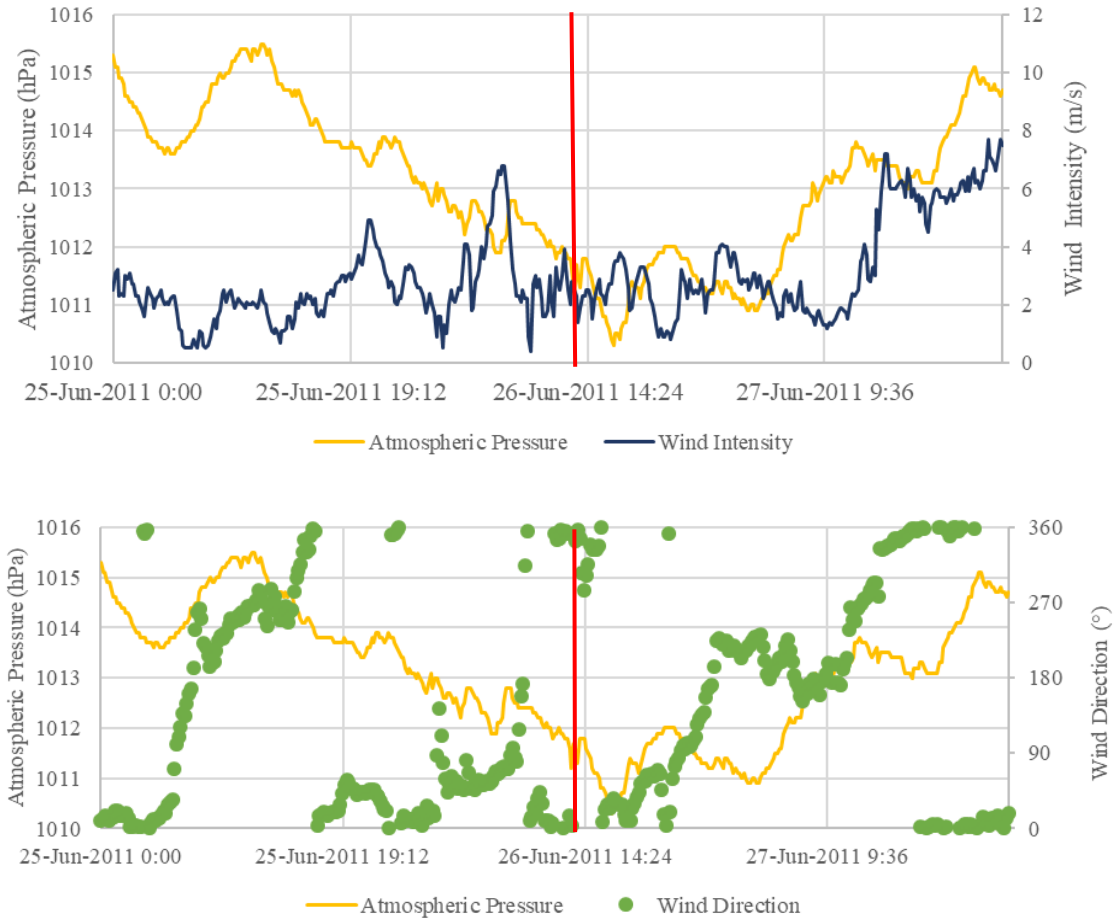

Figure 4.24. Atmospheric conditions of Peniche station. Wind intensity (top) and direction (down) and atmospheric pressure at station level. The sample interval is 10 minutes. The red line represents the estimated arrival of the phenomenon recorded in the tide-gauge.

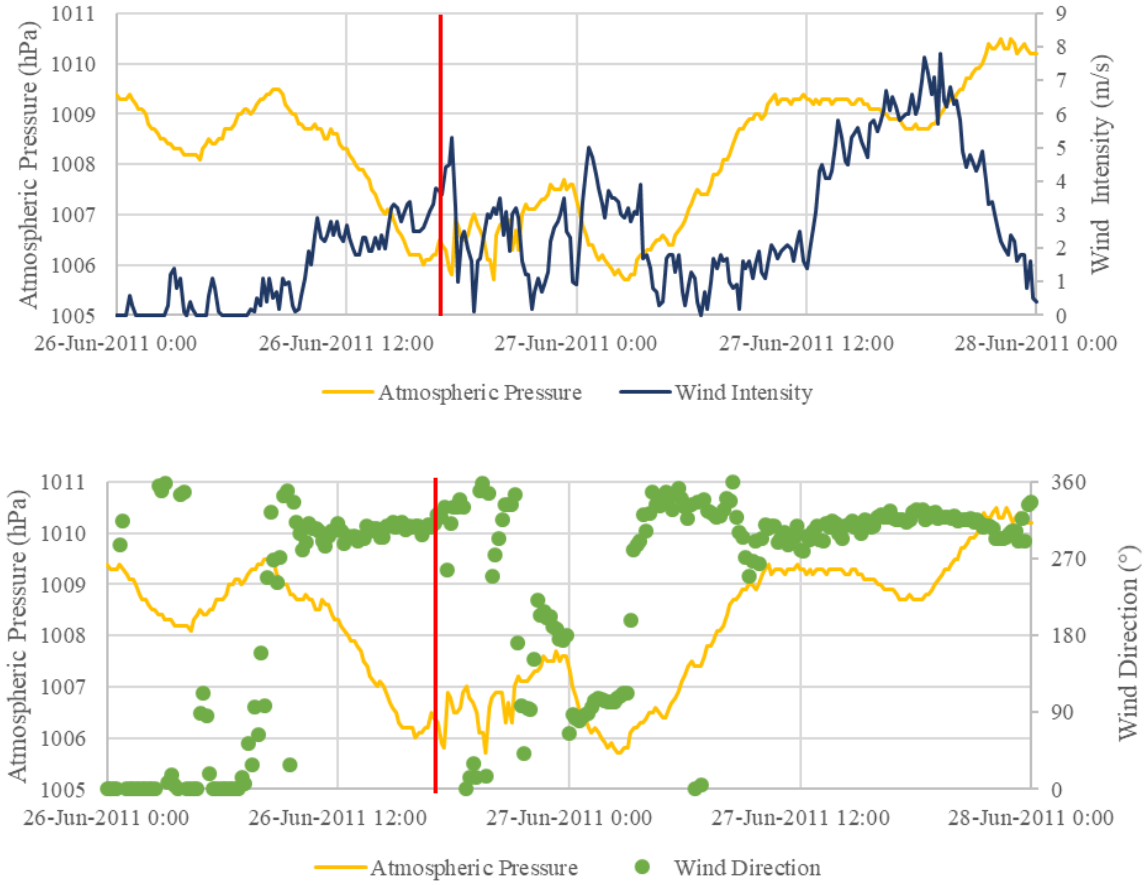

Figure 4.25. Atmospheric conditions of Porto station. Wind intensity (top) and direction (down) and atmospheric pressure at station level. The sample interval is 10 minutes. The red line represents the estimated arrival of the phenomenon recorded in the tide-gauge.

The radiosounding data for La Coruña (Figure 4.26) shows an unstable vertical weather profile. This presents a potentially unstable air mass capable of causing strong downward wind gusts (Tappin et al., 2013). At 500 hPa it is possible to observe wind of approximately 40 knots which are roughly 80 km/h ≈ 22 m/s blowing from the southwest.

From the analysis made by Tappin et al. (2013) for Point du Raz and Penmarche stations, it is possible to identify 2-3 hPa disturbances between 05:30 and 06:30 on June 27. These pressure “jumps” correlate with the first tidal anomaly in the French tide-gauge at Le Conquet at 05:50 (Appendix III.). Therefore, Tappin et al. (2013) support that "the number of pressure falls recorded at the Brittany buoys" are the result "of a series of downdraughts that probably initiated the meteotsunami" in the English Channel.

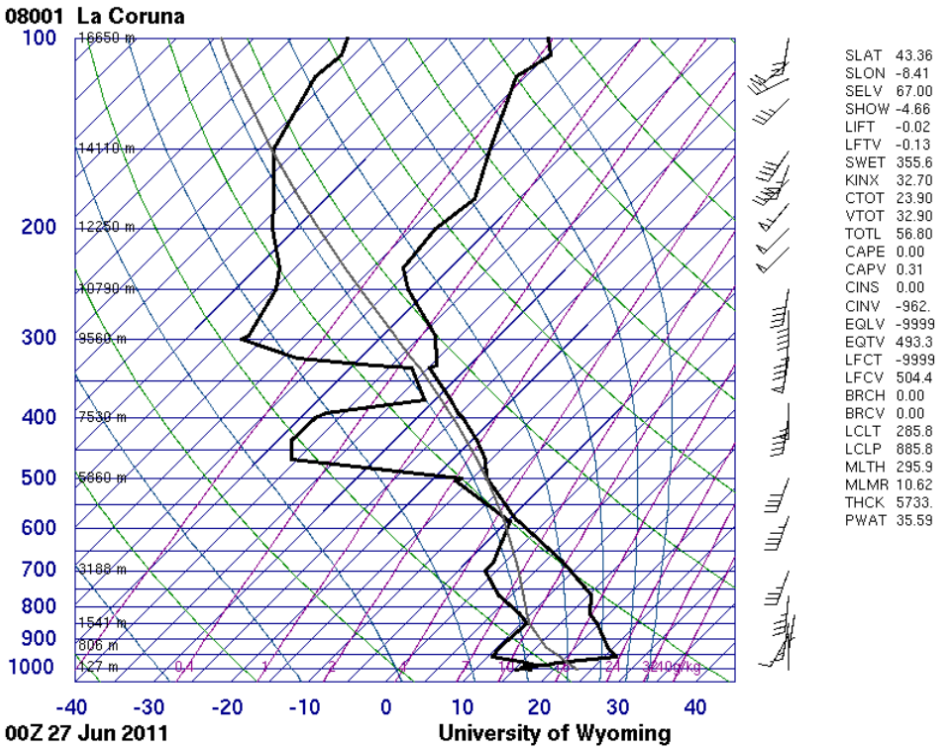

Figure 4.26. Radiosounding data from La Coruña on 27 June 2011 at 00 UTC.

4.4. The 15-17 July 2018 event in the Balearic Islands, Mediterranean Sea

4.4.1. Sea level and air pressure analyses for the July 2018 event

During the early morning of 16 July 2018, a meteotsunami formed in the Mediterranean Sea near the coast of Spain and flooded the coasts of Mallorca and Menorca[11]. For this event, only two tide-gauges are available and analysed: Palma de Mallorca and Ciutadella de Menorca, in the Western Mediterranean.

The first sea-level anomalies begin to be observed in Palma de Mallorca (Figure 4.27), around 17:30 on July 15. Unlike the results so far analysed, this phenomenon has a longer duration in this location, of more than 24 hours. The maximum crest-to-trough height is 0.53 meters (Figure 4.27, middle panel). The wavelet analysis results show that the meteotsunami energy is concentrated in [20-77] min, with a dominant period of 24.1 min and 75 min. The disturbances caused by the event lasted approximately 24 hours.

[11] https://www.mirror.co.uk/news/world-news/majorca-menorca-tourist-beaches-hit-12930997

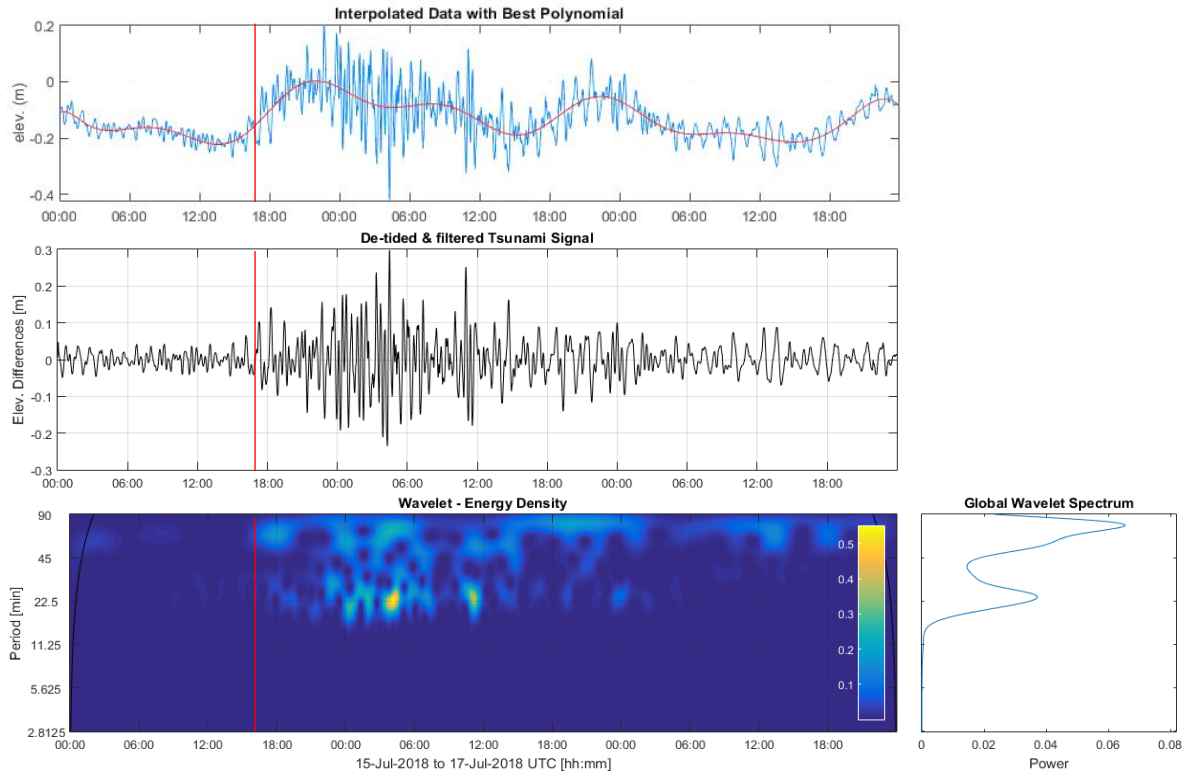

Figure 4.27. Signal of meteotsunami in Palma de Mallorca tide-gauge station (sample interval is 1 minute) and its spectral analysis. Top panel represents sea level variation, the middle panel depicts the de-tided and filtered meteotsunami signal, and the bottom panel presents the wavelet analysis results. The red line represents the estimated arrival of the phenomenon recorded in the tide-gauge.

About 3 hours later, the first anomalies arrived in Ciutadella (Figure 4.28). Estimating 21:00 on 15 July as the time of arrival (red line through the figure), the crest-to-trough wave height is 0.66 meters (Figure 4.28, middle panel). This tide-gauge, being out of the channel, does not have the typical period of 10.5 min. Nevertheless, the dominant period band is approximately between [10-45] min. The meteotsunami energy is higher at 24.3 min. This result meets the simulations made for the 2006 event (Figure 6.6.). The disturbances caused by the event lasted approximately 24 hours.

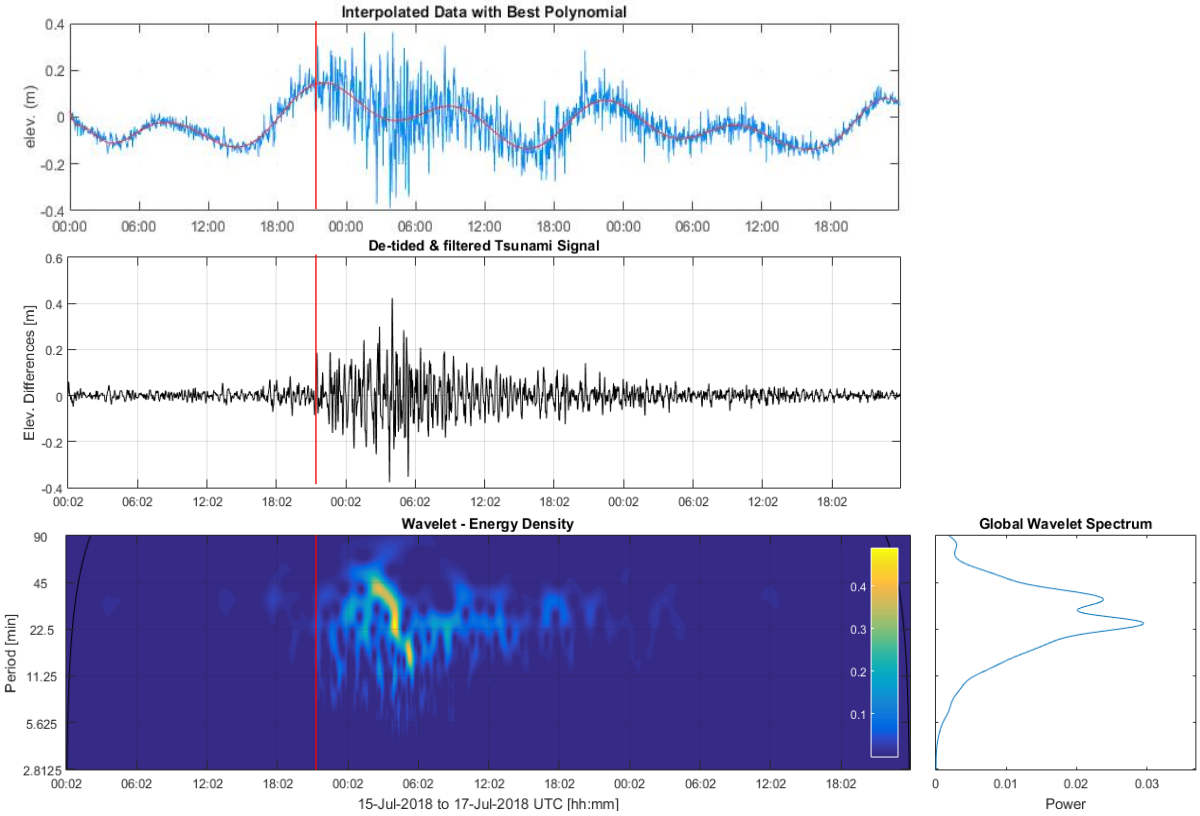

Figure 4.28. Signal of meteotsunami in Ciutadella de Menorca tide-gauge station (sample interval is 1 minute) and its spectral analysis. Top panel represents sea level variation, the middle panel depicts the de-tided and filtered meteotsunami signal, and the bottom panel presents the wavelet analysis results. The red line represents the estimated arrival of the phenomenon recorded in the tide-gauge.

Observing the rate of atmospheric pressure change of this event, several significant disturbances in the atmospheric pressure corresponds to the highest intensity period of meteotsunami observed in the Balearic Islands (Figure 4.29), approximately between 00:00 and 05:00 on July 16. The most relevant being 3.9 hPa in 30 minutes, between 01:50 and 02:20.

Figure 4.29. Atmospheric pressure from Ciutadella de Menorca station. The sample interval is 10 minutes. The red dots identify the time interval with more significant "jumps" in pressure.

4.5. First Catalogue of Meteotsunamis along the Iberian Coastline

The ultimate product of this research project concerns the compilation of a meteotsunami catalogue. The parameters characterizing meteotsunami phenomenon are first defined. This includes parameters at sea level and the atmospheric precursor conditions of meteotsunami events. These parameters are extracted from the performed analyses and compiled in Table 4.1, on the next page.

The first column of the table shows the date of the meteotsunami. Then, the tide gauges where the event was recorded. In the third and fourth columns, the day and time (local) of the estimated arrival of the meteotsunami. These parameters, plus the state of the tide when the first wave arrives, from the next column, and the maximum wave height in the sixth column, are all estimated visually. The first recorded oscillations of the tide gauge signal are taken into account. In the results obtained after de-tiding and filtering the sea level record, we can estimate the height of the maximum wave (6th column) and the peak-to-peak height recorded for the tide gauge (7th column). Column 8 shows the dominant periods of oscillation obtained by the spectrograms, referring to the maximum energy recorded. For the duration of the event (column 9), the period of most significant activity recorded in the tide gauge is observed, between the estimated arrival of the first wave of the meteotsunami and the end of the oscillations observed in the filtered data. The last two columns show atmospheric data. The rate of atmospheric pressure change is calculated from the largest "jumps" observed in the atmospheric pressure graphs throughout the event. The intensity and direction of the wind, estimated in the data of the surface automatic weather stations, radiosounding and/or weather charts.

Table 4.1. Preliminary catalogue of the meteotsunamis studied in this dissertation along the Iberian Coastline.

Date	Tide-Gauge	Day and Time of Arrival (local time)		Tidal Stage	Max. Wave Height (m)	Crest-to-trough (m)	Period of Oscillation (min)	Duration (h)	Rate of Atm. Pre. Change hPa(/min)	Wind (m/s)
15 June 2006	Ciutadella de Menorca	15	~20:50	High	--	--	~ 10.5	--	~3 (/5)	25 SW
6-7 July 2010	Lagos	6	~20:30	High	0.18	0.33	56.6	~22	2 (/30)	SW
	Sines	7	~00:20	Low	0.21	0.32	21.8 [13.5-46.1]	~8	4.1 (/5)	
	Sesimbra	7	~00:40	High	0.14	0.26	[10.1-58.3]	~12	2.8 (/30)	
	Cascais	7	~02:20	Low	0.30	0.47	32.1	~16	3 (/30)	
	Lisboa	7	~03:00	Low	0.05	0.13	53.4	~14	2.5 (/30)	
	Leixões	7	~05:00	Low	0.11	0.22	38.7 [35-45]	~14	1.2 (/30)	
	Viana	7	~06:50	Low	0.08	0.16	29.7 [22-50]	~14	1.2 (/30)	
	Peniche	7	~07:00	Low	0.30	0.58	17.3 [12-60]	~11	3.9 (/30)	
	Figueira	7	~09:20	High	0.09	0.14	46.4 [32-55]	~12	1.2 (/30)	
	Aveiro	7	~10:00	High	0.06	0.14	40.4 [39-57]	~8	1 (/30)	
26-27 June 2011	Huelva	26	~06:45	Low	0.04	0.07	29.7 [22-50]	~4	--	20-30 S/SW
	Peniche	26	~13:00	Low	0.17	0.34	15.8 [12.2-22]	~4	0.6 (/20)	
	Leixões	26	~17:30	Low	0.15	0.28	21.4; 41 [18-50]	~6	1.1 (/10)	
	Marin	26	~20:00	Low	0.16	0.34	72.4 [50-90]	~4	--	
	La Coruña	27	~00:10	High	0.11	0.21	34.4 [21-54]	~8	--	
	Ferrol	27	~00:20	High	0.06	0.12	24.9 [16-34]	~3	--	
	Brest	27	~05:30	Low	0.11	0.15	21.5; 74.4 [14-92]	~12	--	
	Le Conquet	27	~05:55	Low	0.07	0.19	44.3 [41-70]	~20	--	
	Les Sables d'Olonne	27	~06:30	Low	0.25	0.38	37 [22.5-45]	~22	--	
	Concarneau	27	~06:30	Low	0.18	0.32	21.8; 72.2 [14-90]	~14	--	
	Le Crouesty	27	~06:45	Low	0.12	0.28	41.6 [22.5-44]	~12	--	
	Port-Bloc	27	~07:00	Low	0.07	0.12	74.4 [30.5-97]	~17	--	
	La Rochelle-Pallice	27	~07:40	Low	0.11	0.05	74.9 [15-90]	~8	--	
	Ile d'Aix	27	~11:00	Low	0.06	0.13	47.5 [37-60]	~8	--	
	Boucau-Bayonne	27	~14:00	Low	0.05	0.07	55 [45-90]	~14	--	
	SOCOA	27	~14:35	High	0.07	0.14	15.8 [12-70]	~14	--	
	Bilbao	27	~15:30	High	0.08	0.16	46.1 [36-63]	~6	--	
15 - 16 July 2018	Palma de Mallorca	15	~18:00	High	0.30	0.53	22.7 [24.1-76]	~24	3.9 (/30)	--
	Ciutadella de Menorca	15	~21:00	High	0.42	0.66	24.6 [24.1-34.9]	~24	3.9 (/30)	--

5. Discussion and Conclusions

This dissertation investigates the instrumental meteotsunamis occurred in the Iberian coasts intending to improve our understanding of the phenomena in the region. It focusses on the analysis of both oceanic and atmospheric data. It attempts to identify a correlation between the meteotsunami generation and propagation and the precursor atmospheric conditions of the Iberian coast. The analysis allows determining the characteristics of the meteotsunami events together with the atmospheric conditions leading to their formations. These characteristics are then compiled in a preliminary catalogue of instrumental meteotsunamis in the region. The compiled catalogue forms a first step towards performing a comprehensive meteotsunami hazard assessment.

A total of 30 tide-gauges records, corresponding to two meteotsunamis that occurred along the Iberian Peninsula coast (2010 and 2011 events) and two others of particular interest in the Balearic Islands (2006 and 2018 events), were analysed. Instrumental records of tide-gauges from Portugal, Spain and France were first collected and then examined to isolate the meteotsunamis signals and determine their metrics. The observed sea-level anomalies were quantified by spectral analysis of the records. Montserrat et al. (1998) showed that a spectral ratio is a useful tool for identifying tsunami signals. The spectral analysis divides the variance of a time series as a function of frequency (Thomson, 2014), enhancing amplifications at periods belonging to the tsunami. The same can be said about meteotsunamis. This time-frequency analysis (or wavelet analysis) is a powerful tool for studying the temporal variations of time-dependent phenomena, showing where the meteotsunami energy is concentrated in time bands at different times (Heidarzadeh & Satake, 2013).

Among the 10 tide-gauge records examined for the 2010 event, the maximum crest-to-trough wave height was observed in Peniche tide-gauge with a value of 0.58 meters. Off Peniche, a wide continental shelf with depth between [50-150] meters spreads toward SW direction. At this continental shelf, the Proudman resonance condition (Equation 2.4), corresponds to a speed of 22-38 m/s, favouring the amplification of small meteotsunamis approaching from SW with a speed 22-38 m/s (Kim & Omira, 2020). The 2010 event lasted approximately 13 hours, along the Portuguese coast. For the 2011 meteotsunami, the results presented in this dissertation show that the maximum crest-to-trough wave height was registered in Marin tide-gauge with a value of 0.34 meters. Although taking into consideration the 17 sea-level signals examined for 2011 meteotsunami event, Les Sables d'Olonne tide-gauge (Appendix III.) in France recorded a maximum crest-to-trough wave height of 0.38 meters. This event lasted approximately 11 hours along the affected coast. For the 2018 event, the maximum crest-to-trough wave height was in Ciutadella de Menorca station with 0.66 meters. This event had the longest duration, with 24 hours of activity. Regarding the oscillation periods, there is a dominant period in the range of [20-50] min, for all events. This period is directly related to resonant (eigen) periods. These periods are determined by the location of the tide-gauge, geometry and depth (Rabinovich, 2009). For all the records analysed, the natural frequencies (eigen periods) of the harbour can be clearly identified from the background noise.

Observations of atmospheric pressure and wind speed, intensity and direction are examined to extract the meteorological conditions that lead to the formation of the recorded meteotsunami events. For all the events studied, on average, the rate of change in atmospheric pressure was distinguished between the values of 2-4 hPa in 30 min. Correlations were found between “jumps” in atmospheric pressure and changes in directions, speeds and intensities of the wind, revealing the occurrence of specific precursor climatic conditions at the time of the generation of meteotsunami events. For all the events, it is important to note that the dominant wind velocity was in the range of the 20-30 m/s wind. On the other hand, it is noticeable that the wind direction varies widely for each event and differs from

a station to another, but, in general, there is a prominent wind direction from S/SE for 2010 and S/SW for 2011 (Appendix III.). The atmospheric conditions from the 2010 and 2011 events evidence that the wind velocities were within the expected range to favour the occurrence of Proudman resonance.

This work compiled the parameters determined by meteotsunamis in a preliminary catalogue (Table 4.1). Parameters such as arrival time, tide stage at the arrival of the meteotsunami, maximum wave height, crest-to-trough height, dominant periods and duration are quantified. The catalogue also contains quantities of the forcing climatic conditions like "jump" in air pressure, wind speed and direction. This preliminary catalogue could be useful for further meteotsunami hazard and prediction.

Prediction of meteotsunamis is in its early stage (Pattiaratchi, 2015) and is mainly dependent on the availability of high spatial and temporal resolution of atmospheric data allowing a better constrain of the precursor conditions and of the resonances involved (Bubalo et al., 2019). The air pressure "jump" often considered a characteristic of the atmospheric disturbances related to meteotsunamis (Belušić & Strelec-Mahović, 2009). The air pressure "jump" occurs suddenly within some minutes. Such a meteotsunami precursor must be detected/predicted using high-resolution temporal instruments/models, for meteotsunami forecast purpose.

Preliminary results of this work were presented at an international conference, the European Geosciences Union General Assembly 2019 (Appendix I). They were well received by the conference audience, although most of the audience was not aware of the occurrence of meteotsunami on the Iberian coast. This shows the importance of such a work, performed in the frame of FAST project, in contributing, to raise public awareness in coastal areas vulnerable to meteotsunami impact and, therefore, increase safety level of coastal population and decrease potential damage along the Portuguese coastline. Future FAST work will consist of using the results of this dissertation as a starting point to develop meteotsunami prediction models (Kim and Omira, 2020) as well as generating prototype meteotsunami hazard maps and educational material for the Iberian coast. These achievements are expected to impact different groups of end-users including scientists, coastal engineers, coastal management authorities, and civil protection.

6. References

Antunes et al., 2011: Antunes C., Luís J., Matias L. (2011). Meteo-Tsunami - Sul de Portugal (06 e 07 de Julho de 2010). http://webpages.fc.ul.pt/~cmantunes/MeteoTsunami-7Julho2010.pdf

Antunes, 2011: Antunes, C. (2011). Monitoring sea level change at Cascais tide gauge. Journal of Coastal Research, 64: 870.

Baptista et al., 2011: Baptista, M.A., Miranda, J.M., Omira, R., Antunes, C. (2011). Potential inundation of Lisbon downtown by a 1755-like tsunami. Natural Hazards and Earth System Science (Nat. Hazards Earth Syst. Sci., 11, 3319-3326, 2011. http://www.nat-hazards-earth-syst-sci.net/11/3319/2011/nhess-11-3319-2011.pdf

Baptista et al.,2017: Baptista, M.A., Miranda, J. M., Batlló, J., Lisboa, F., Luis, J., Macia, R. (2016). New study on the 1941 Gloria Fault earthquake and tsunami. Nat. Hazards Earth Syst. Sci., 16, 1967-1977, 2016 https://www.nat-hazards-earth-syst-sci.net/16/1967/2016.

Bechle et al., 2016: Bechle, A., C. H. Wu, Kristovich, D., Anderson, E., Schwab, D. & Rabinovich, A.B. (2016). Meteotsunamis in the Laurentian Great Lakes. Scientific Reports. 6. 37832. 10.1038/srep37832.

Belušić & Strelec-Mahović, 2009: Belušić D. & Strelec Mahović, N. (2009). Detecting and following atmospheric disturbances with a potential to generate meteotsunamis in the Adriatic. Physics and Chemistry of the Earth, Parts A/B/C. 34. 918-927. 10.1016/j.pce.2009.08.009.

Bubalo et al., 2019: Bubalo, M., Janeković, I., & Orlić, M. (2019). Simulation of flooding and drying as an essential element of meteotsunami modelling. Continental Shelf Research, 184, 81–90. https://doi.org/10.1016/j.csr.2019.07.003.

Carvajal et al., 2017: Carvajal M., Contreras M., Winckler P., Sepulveda I. (2017). Meteotsunamis Occurring Along the Southwest Coast of South America During an Intense Storm. Pure and Applied Geophysics. 174. 10.1007/s00024-017-1584-0.

Defant, 1961: Defant, A. (1961). Physical oceanography. New York, NY: Pergamon Press.

Denamiel et al., 2018: Denamiel, C, Šepić, J., & Vilibić, I. (2018). Impact of Geomorphological Changes to Harbor Resonance During Meteotsunamis: The Vela Luka Bay Test Case. Pure and Applied Geophysics. doi:10.1007/s00024-018-1862-5.

Frère et al., 2014: Frère A., Daubord C., Gailler A., Hébert H. (2014). Sea level surges of June 2011 in the NE Atlantic Ocean: observations and possible interpretation. Nat Hazards (2014) 74:179–196.

Greenspan, 1956: Greenspan, H. (1956). The generation of edge waves by moving pressure distributions. J. Fluid Mech. 1: 574–592.

Gusiakov, 2019: Gusiakov, V. (2019). Seismically generated tsunamis, meteotsunamis and rogue waves: Problems of identification, parameterization and cataloguing. In the First World Conference on Meteotsunamis, Split, Croatia, 8–11 May 2019, Book of Abstracts, p. 70.

Heidarzadeh & Satake, 2013: Heidarzadeh, M., Satake, K., (2013). The 21 May 2003 Tsunami in the Western Mediterranean Sea: Statistical and Wavelet Analyses. Pure and Applied Geophysics, vol. 170, issue 9-10 (2013) pp. 1449-1462.

IH, 2009: Tabela de Marés (2010) — Volume I — Portugal, PUB (N)-IH-228-O. Instituto Hidrográfico. Lisboa. Portugal.

Jansá et al., 2007: Jansá A., Monserrat S., Gomis Bosch, D. (2007). The rissaga of 15 June 2006 in Ciutadella (Menorca), a meteorological tsunami. Advances in Geosciences. 10.5194/adgeo-12-1-2007.

Kim & Omira, 2020: Kim, J., Omira, R. (2020, submitted). The July 6 - 7, 2010 meteotsunami along the coast of Portugal: insights from data analysis and numerical modelling. Natural Hazards.

Kim et al., 2019: Kim, M.-S.,Kim, H., Eom, H.-M., Yoo, S.-H., and Woo, S.-B. (2019). Occurrence of Hazardous Meteotsunamis Coupled with Pressure Disturbance Traveling in the Yellow Sea, Korea. Journal of Coastal Research 91(sp1), 71-75, (28 August 2019). https://doi.org/10.2112/SI91-015.1

Ličer et al., 2017: Ličer M., Mourre B., Troupin C., Krietemeyer A., Jansá A., Tintoré J., 2017. Numerical study of Balearic meteotsunami generation and propagation under synthetic gravity wave forcing. Ocean Modelling, 111, pp. 38-45.

Lin & Liang, 2017: Lin, L.-C. & M.-C. Liang (2017). Meteotsunamis produced by high frequency atmospheric pressure forcing. Terr. Atmos. Ocean. Sci., 28, 1033-1040, doi: 10.3319/TAO.2017.03.20.01.

Linares et al., 2016: Linares, A., Bechle, A. J. & Wu, C. H. (2016). Characterization and Assessment of the meteotsunami hazard in northern Lake Michigan. Journal of Geophysical Research: Oceans. 121. 10.1002/2016JC011979.

Lisboa, 2015: Lisboa, F. (2015). ASAT - ASATARTE Signal Analysis Tool. User Manual.

Marcos et al., 2009: Marcos M., Monserrat S., Medina R., Orfila A., Olabarrieta M. (2009). External forcing of meteorological tsunamis at the coast of the Balearic Islands. Physics and Chemistry of the Earth, Parts A/B/C. 938-947. 10.1016/j.pce.2009.10.001.

Miranda, 2013: Miranda, P. (2013). Introdução à Meteorologia. IDL, Faculdade de Ciências, Universidade de Lisboa.

Monserrat & Thorpe, 1992: Monserrat S., and Thorpe, A. J. (1992). Gravity-wave observations using an array of microbarographs in the Balearic Islands. Quarterly Journal of the Royal Meteorological Society, 118: 259–282.

Monserrat et al., 1998: Monserrat, S., Rabinovich, A.B., Casas, B. (1998). On the reconstruction of the transfer function for atmospherically generated seiches. Geophysical Research Letters, vol. 25, issue 12 (1998) pp. 2197-2200 Published by American Geophysical Union.

Monserrat et al., 2006: Monserrat, S., Vilibić, I., Rabinovich, A.B. (2006). Meteotsunamis: atmospherically induced destructive ocean waves in the tsunami frequency band. Natural Hazards and Earth System Science, 6: 1035-1051.

NOAA Technical Report, 2014: NOAA Technical Report NOS CO-OPS 079 (2014). An Examination of the June 2013 East Coast Meteotsunami Captured By NOAA Observing Systems. Silver Spring, Maryland.

Nomitsu, 1935: Nomitsu, T. (1935), A theory of tsunamis and seiches produced by wind and barometric gradient, Mem. Coll. Sci. Imp. Univ. Kyoto A,18(4),201–214.

O'Brien et al., 2018: O'Brien, L., Renzi, E., Dudley, J. M., Clancy, C., and Dias, F. (2018). Catalogue of extreme wave events in Ireland: revised and updated for 14 680 BP to 2017, Nat. Hazards Earth Syst. Sci., 18, 729-758, https://doi.org/10.5194/nhess-18-729-2018, 2018.

Omira et al., 2009: Omira, R., Baptista, M.A., Matias, L., Miranda, J.M., Catita, C., Carrilho, F., and Toto, E. (2009). Design of a Sea-level Tsunami Detection Network for the Gulf of Cadiz. Nat. Hazards Earth Syst. Sci., 9, 1327–1338, 2009.http://www.nat-hazards-earth-syst-sci.net/9/1327/2009/nhess-9-1327-2009.pdf

Omira et al., 2015: Omira, R., Baptista, M.A., and Matias, L. (2015). Probabilistic Tsunami Hazard in the Northeast Atlantic from Near-and Far-Field Tectonic Sources. Pure Appl. Geophys., 172(3-4), 901-920. Doi:10.1007/s00024-014-0949-x.

Omira et al., 2016: Omira, R., Baptista, M.A., & Lisboa, F. (2016). Tsunami Characteristics Along the Peru–Chile Trench: Analysis of the 2015 Mw8.3 Illapel, the 2014 Mw8.2 Iquique and the 2010 Mw8.8 Maule Tsunamis in the Near-field. Pure and Applied Geophysics, 173(4), 1063–1077.

Orlić, 2015: Orlić M. (2015). The first attempt at cataloguing tsunami-like waves of meteorological origin in Croatian coastal waters. Acta Adriatica. 56. 83-95.

Pattiaratchi & Wijeratne, 2015: Pattiaratchi, C.B., Wijeratne, E.M.S. (2015). Are meteotsunamis an underrated hazard? Phil. Trans. R. Soc. A 373: 20140377. http://dx.doi.org/10.1098/rsta.2014.0377

Proudman, 1929: Proudman, J. (1929). The effects on the sea of changes in atmospheric pressure. Geophys. Suppl. Mon. Not. R. Astron. Soc. 2: 197–209.

Rabinovich & Thomson, 2007: Rabinovich, A.B. & Thomson, R. (2007). The 26 December 2004 Sumatra tsunami: analysis of tide gauge data from the world ocean part 1. Indian ocean and South Africa. Pure appl. Geophys., 164, 261–308. https://doi.org/10.1007/s00024-006-0164-5.

Rabinovich and Monserrat, 1996: Rabinovich, A.B., Monserrat, S. (1996). Meteorological tsunamis near the Balearic and Kuril Islands: Descriptive and statistical analysis. Natural Hazards, vol. 13, issue 1 (1996) pp. 55-90 Published by Springer Netherlands.

Rabinovich and Monserrat, 1998: Rabinovich, A.B. & Monserrat, S. (1998): Rabinovich A. B., and Monserrat S. (1998). Generation of Meteorological Tsunamis (Large Amplitude Seiches) Near the Balearic and Kuril Islands). Natural Hazards, 18: 27–55.

Rabinovich et al., 1999: Rabinovich, A.B., Monserrat, S., Fain, I. (1999). Numerical modeling of extreme seiche oscillations in the region of the Balearic Islands. Oceanology, vol. 39, issue 1 (1999) pp. 12-19.

Rabinovich, 2009: Rabinovich, A.B. (2009). Seiches and harbour oscillations. In: Handbook of Coastal and Ocean Engineering. Ed. Y.C. Kim, World Scientific Publ., Singapore, 193-236.

Rabinovich, 2019: Rabinovich, A.B. (2019). Twenty-Seven Years of Progress in the Science of Meteorological Tsunamis Following the 1992 Daytona Beach Event. Pure Appl. Geophys. (2019). https://doi.org/10.1007/s00024-019-02349-3.

Renault et al., 2011: Renault, L., Vizoso, G., Jansá, A., Wilkin, J., Tintoré, J. (2011). Toward the predictability of meteotsunamis in the Balearic Sea using regional nested atmosphere and

ocean models. Geophysical Research Letters - GEOPHYS RES LETT. 38. 10.1029/2011GL047361.

Romero et al., 2019: Romero, R., Vich, M., & Ramis, C. (2019). A pragmatic approach for the numerical prediction of meteotsunamis in Ciutadella harbour (Balearic Islands). Ocean Modelling, 142, 101441. https://doi.org/10.1016/j.ocemod.2019.101441.

Šepić & Vilibić, 2011: Šepić, J. & Vilibić, I. (2011). The development and implementation of a real-time meteotsunami warning network for the Adriatic Sea. Natural Hazards and Earth System Sciences. 11. 10.5194/nhess-11-83-2011.

Šepić et al. 2009: Šepić, J., Vilibić, I., and Belušić, D. (2009). Source of the 2007 meteotsunami (Adriatic Sea). J. Geophys. Res. 114, C03016. Doi: 10.1029/2008JC005092.

Šepić et al., 2015a: Šepić, J., Vilibić, I., Rabinovich, A.B., Monserrat, S. (2015). Widespread tsunami-like waves of 23-27 June in the Mediterranean and Black Seas generated by high-Altitude atmospheric forcing. Scientific Reports. 10.1038/srep11682.

Šepić et al., 2015b: Šepić, J., Vilibić, I., and Fine, I. (2015). Northern Adriatic meteorological tsunamis: Assessment of their potential through ocean modelling experiments. J. Geophys. Res. Oceans, 120, 2993–3010, doi:10.1002/ 2015JC010795.

Šepić et al., 2016: Šepić, J., Medugorac, I., Janeković, I., Dunić, N., and Vilibić, I. (2016). Multi Meteotsunami Event in the Adriatic Sea Generated by Atmospheric Disturbances of 25–26 June 2014. Pure Appl. Geophys. 173: 4117–4138.

Tanaka, 2010: Tanaka, K. (2010). Atmospheric pressure-wave bands around a cold front resulted in a meteotsunami in the East China Sea in February 2009. Natural Hazards and Earth System Sciences, 10: 2599-2610.

Tappin et al., 2013: Tappin, D. R., Sibley, A., Horsburgh, K., Daubord, C., Cox, D., and Long, D. (2013). The English Channel 'tsunami' of 27 June 2011–a probable meteorological source. Weather, 68(6):144-152.

Thomson et al. 2009: Thomson, R.E, Rabinovich, A.B., Fine, I., Sinnott, D.C., McCarthy, A., Sutherland, N.A.S., and Neil, L.K. (2009). Meteorological tsunamis on the coasts of British Columbia and Washington. Phys. Chem. Earth. 34: 971–988.

Thomson, 2014: Thomson, R, Emery, W. Data Analysis Methods in Physical Oceanography: Third Edition (2014) pp. 1-716 Published by Elsevier Inc. doi:10.1016/C2010-0-66362-0.

Torrence & Compo, 1998: Torrence, C., & Compo, G.P. (1998). A Practical Guide to Wavelet Analysis. University of Colorado. Boulder, Colorado: Program in Atmospheric and Oceanic Sciences.

Vilibić & Šepić, 2009: Vilibić, I., and Šepić, J. (2009). Destructive meteotsunamis along the eastern Adriatic coast: Overview. Physics and Chemistry of the Earth, 34: 904-917.

Vilibić et al. 2010: Vilibić, I., Šepić, J., Ranguelov, J., Strelec-Mahović, N., and Tinti, S. (2010). Possible atmospheric origin of the 7 May 2007 western Black Sea shelf tsunami event. Journal of Geophysical Research, 115, C07006. Doi: 10.1029/2009JC005904.

Vilibić et al., 2008: Vilibić, I., Monserrat, S., Rabinovich, A.B., and Mihanović, H. (2008). Numerical modelling of the destructive meteotsunami of 15 June 2006 on the coast of the Balearic Islands. Pure and Applied Geophysics, 165: 2169-2195.

Vilibić et al., 2009: Vilibić, I., Monserrat, S., Rabinovich, A.B, Mihanović, H. (2009). Numerical Modelling of the Destructive Meteotsunami of 15 June 2006 on the Coast of the Balearic Islands. 10.1007/978-3-0346-0057-6_10.

Vilibić et al., 2014: Vilibić, I., Horvath, K., Mahović, N.S., Monserrat, S., Marcos, M., Amores, A., and Fine, I. (2014). Atmospheric processes responsible for generation of the 2008 Boothbay meteotsunami. Natural hazards, 74(1): 25-53.

Vilibić et al., 2016: Vilibić, I., Šepić, J., Rabinovich, A.B., and Monserrat, S. (2016). Modern Approaches in Meteotsunami Research and Early Warning. Front. Mar.Sci.3:57. doi: 10.3389/fmars.2016.00057.

Vilibić et al., 2018: Vilibić, I., Šepić, J., Dunić, N., Sevault, F., Monserrat, S., & Jordà, G. (2018). Proxy-Based Assessment of Strength and Frequency of Meteotsunamis in Future Climate. Geophysical Research Letters, 45(19), 10,501-10,508. https://doi.org/10.1029/2018GL079566.

Weisse & Hünicke, 2019: Weisse, R., & Hünicke, B. (2019). Baltic Sea Level: Past, Present, and Future. 10.1093/acrefore/9780190228620.013.693.

Williams et al., 2018: Williams, D. A., Horsburgh, K. J., Schultz, D. M., & Hughes, C. W. (2018). Examination of generation mechanisms for an English Channel meteotsunami: combining observations and modeling. Journal of Physical Oceanography. doi:10.1175/jpo-d-18-0161.1.

This presentation participates in OSPP

Outstanding Student Poster & PICO Contest

POSTER NUMBER: EGU2019-9953

METEOTSUNAMIS IN THE INSTRUMENTAL RECORDS OF THE IBERIAN COAST

Oceanic and atmospheric data analysis towards building a meteotsunami catalogue

Daniela Maxial[1,2], Rachid Omira[1,3], Maria Ana Baptista[3,4], Alexander Rabinovich[5,6], and Pedro Viterbo[1]

[1] Instituto Português do Mar e da Atmosfera, (IPMA), Lisbon, Portugal, [2] Faculdade de Ciências da Universidade de Lisboa, Lisbon, Portugal, [3] Instituto Dom Luiz – IDL, Faculdade de Ciências da Universidade de Lisboa, Lisbon, Portugal, [4] Instituto Superior de Engenharia de Lisboa – ISEL, Instituto Politécnico de Lisboa, Lisbon, Portugal, [5] P.P. Shirshov Institute of Oceanology, Russian Academy of Sciences, Moscow, Russia, [6] Institute of Ocean Sciences, Department of Fisheries and Oceans, Sidney, BC, Canada

Abstract

Meteotsunamis are atmospherically induced high-energy ocean waves in the tsunami frequency band that destructively affect many coasts of the world oceans. However, meteotsunami forecast capabilities are still lacking in most operating tsunami warning systems. The Iberian coast is prone to the meteotsunami threat and the regional tsunami warning center (IPMA, Portugal) faces the challenge of integrating the meteotsunami into the alert strategy. The first step of this approach is building a meteotsunami catalogue that incorporates relevant information on the events' characteristics and their pre-cursor conditions. In this work, past meteotsunamis, including the June 2006, July 2010, June 2011, and July 2018 events, are examined with unprecedented details through analyses of all available oceanic and atmospheric data.

To isolate the tsunami signal and evaluate its characteristics, we perform de-tiding and spectral analysis of recorded signals. We then retrieve and analyse the atmospheric data during the identified events in order to define the pre-cursor weather conditions leading to meteotsunami formation. The results of this study consist of a catalogue incorporating tsunamis of the atmospheric origin with information on the date of occurrence, the tsunami arrival time, the maximum wave height, the number of waves, the wave period, and variation in the atmospheric pressure.

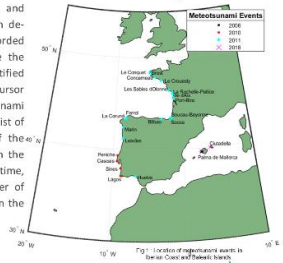

Fig 1: Location of meteotsunami events in the Iberian Coast and Balearic Islands

Meteotsunami

CHARACTERISTICS OF METEOTSUNAMI (modified from [1])

Source location	Source duration	Source extent	Water depth	Water level change	Region of Impact
Above the sea surface	Driven by resonance effects which take effect (O)hours	Propagate over the region	Relatively shallow where Proudman resonance can occur	Periods of O(minutes) with rapid oscillatory change	Local to regional

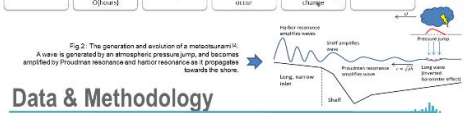

Fig 2: The generation and evolution of a meteotsunami [4]. A wave is generated by an atmospheric pressure jump, and becomes amplified by Proudman resonance and harbor resonance as it propagates towards the shore.

Data & Methodology

Sea level and air pressure data were obtained from operating tide-gauge stations available through the: **Intergovernmental Oceanographic Commission Sea Level Monitoring Facility** (IOC-SLMF) (http://www.ioc-sealevelmonitoring.org/); **Hydrographic Institute** (www.hidrografico.pt); **Portuguese Geographic Institute** (ftp://ftp.dgterritorio.pt/Maregrafos) and **Meteorology Statal Agency** (AEMET) (http://www.aemet.es/es/portada), by their online website or by direct request.

The preliminary analysis of the signals recorded by tide gauges stations includes: **de-tiding** and **filtering of the records** (helps to isolate the meteotsunami signal), and **wavelet analysis** (allows a comprehensive estimate of the dominant meteotsunamis periods). After interpolating the data, the de-tiding process was done by of the least squares algorithm to fit the interpolated data into polynomials of degree 9 and further improved by applying a band-pass filter. Once the filtered signal is obtained, we used the Wavelet algorithm [3] to calculate the distribution of the tsunami energy in different frequency bands over the time of its propagation [4].

Signal analysis of the meteotsunami records for the 3 events

2010 meteotsunami in Portugal

2011 meteotsunami in NE Atlantic

2018 meteotsunami in Spain

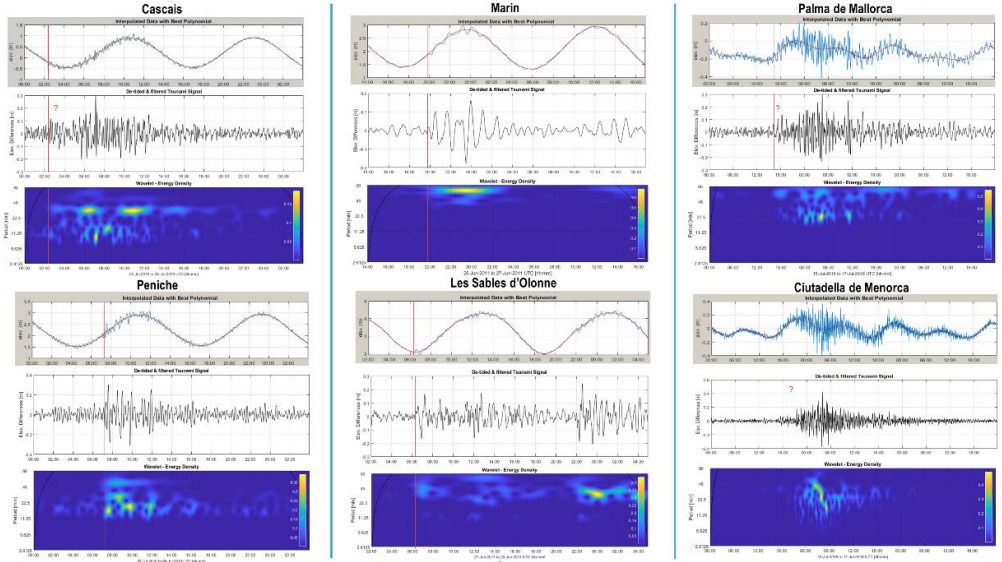

Fig.3 : Analysis of the meteotsunami records for the 3 event (2010: Cascais + Peniche; 2011: Marin + Les Sables d'Olonne; 2018: Ciutadella + Palma). Top panel of each figure depicts the de-tided and filtered tsunami signal, and bottom panel presents the wavelet analysis results.

Catalogue of meteotsunamis in the Iberian coast

Nº	Location		Date	Tide	Max. Wave Height (m)	Time of Arrival (local time)	Period of Oscillation (min)	Duration (h)	Atmospheric Pressure Change (hPa)	Wind Direction	Wind Velocity (ms^{-1})
1	Ciutadella de Menorca	Spain	15 June 2006	High	--	~ 20:50	~ 10.5 [2]	--	~ 3 [2]	SW [2]	25 [2]
2	Sines	Portugal	6 July 2010	Low	0.203	~22:30	21.4	~20	4.1	SSE	--
3	Cascais		7 July 2010	High	0.298	~ 02:30	31.9	~9	3		--
4	Peniche		7 July 2010	High	0.298	~ 07:00	18	~20	3.9		--
5	Marin	Spain	26 June 2011	Low	0.149	~ 19:00	71.7	~20	--	SSW	20-30
6	La Coruñã		27 June 2011	High	0.106	~ 00:10	34.4	~9	--		
7	Les Sables d'Olonne	France	27 June 2011	Low	0.246	~ 06:30	41	~24	--		
8	Palma de Malorca	Spain	15 July 2018	High	0.208	~ 16:00	24.1	~48	2.92	--	--
9	Ciutadella de Menorca			High	0.422	~ 21:00	24.1	~32		--	--

References

[1] Pattiaratchi CB,Wijeratne EMS. (2015) Are meteotsunamis an underrated hazard? *Phil. Trans. R. Soc. A 373: 20140377*. http://dx.doi.org/10.1098/rsta.2014.0377. [2] S. Monserrat, I. Vilibić, and A. B. Rabinovich, (2006) Meteotsunamis: atmospherically induced destructive ocean waves in the tsunami frequency band, [3] Rabinovich, A. B., and Thomson, R. E. (2007). The 26 December 2004 Sumatra tsunami: analysis of tide gauge data from the world ocean part 1. Indian ocean and South Africa. Pure appl. Geophys., 164, 261–308. [4] Omira, R., Baptista, M. A., & Lisboa, F. (2016). *Tsunami Characteristics Along the Peru-Chile Trench: Analysis of the 2015 Mw8.3 Illapel, the 2014 Mw8.2 Iquique and the 2010 Mw8.8 Maule Tsunamis in the Near-field. Pure and Applied Geophysics, 173(4), 1063–1077.* doi:10.1007/s00024-016-1277-0

This work was supported by the FCT funded project FAST- Development of new forecast skills for meteotsunamis on the Iberian shelf (PTDC/CTA-MET/32004/2017).

II. Characteristics of all the tide-gauges under study.

Table II.1 Geographic characteristics (location and coordinates) of the tide-gauges under study.

Tide-Gauge	Country	Coordinates
Lagos	Portugal	37º5'55.774"N 8º40'0.617"W
Sines	Portugal	37º55'59.999"N 8º52'59.999"W
Sesimbra	Portugal	38º25'59.999"N 9º5'60"W
Cascais	Portugal	38º41'35.498"N 9º24'55.102"W
Lisboa / Gago Coutinho	Portugal	38º45'58.23"N 9º 7'39.005" W
Peniche	Portugal	39º19'59.999"N 9º21'59.998"W
Figueira da Foz	Portugal	40º8'53.304"N 8º51'57.24"W
Aveiro	Portugal	40º38'32.28"N 8º45'10.44"W
Leixões	Portugal	41º11'4.999"N 8º42'10.001"W
Viana do Castelo	Portugal	41º41'6"N 8º50'56.4"W
Huelva	Spain	37º7'55.272"N 6º50'1.284"W
Marin	Spain	42º24'22.032"N 8º41'27.888"W
La Coruña	Spain	43º21'59.76"N 8º24'0"W
Ferrol	Spain	43º27'46.26"N 8º19'32.952"W
Bilbao	Spain	43º21'5.508"N 3º2'42.468"W
Ciutadella de Menorca	Spain	39º59'15.317"N 3º49'41.354"E
Palma de Maiorca	Spain	39º33'36.54"N 2º38'14.928"E
St. Jean de Luz (SOCOA)	France	43º23'42.72"N 1º40'53.832"W
Boucau-Bayonne	France	43º31'38.28"N 1º30'53.388"W
Port-Bloc	France	45º34'6.6"N 1º3'41.652"W
Ile d'Aix	France	46º0'26.64"N 1º10'27.264"W
La Rochelle-Pallice	France	46º9'30.6"N 1º13'14.34"W
Les Sables d'Olonne	France	46º29'51"N 1º47'37.428"W
Le Crouesty	France	47º32'33.72"N 2º53'42.54"W
Concarneau	France	47º52'25.32"N 3º54'26.568"W
Le Conquet	France	48º21'36"N 4º46'48"W
Brest	France	48º22'48"N 4º30'0"W

III. Instrumental records of tide-gauges and respective spectral analyses

All other tide-gauges analysed for the 2010 and 2011 events. Top panel of each figure represents sea level variation, the middle the de-tided and filtered meteotsunami signal, and bottom panel presents the wavelet analysis results. The red line represents the estimated arrival of the phenomenon recorded in the tide-gauge.

a) Meteotsunami of 2010 on the Portuguese coast of the Iberian Peninsula

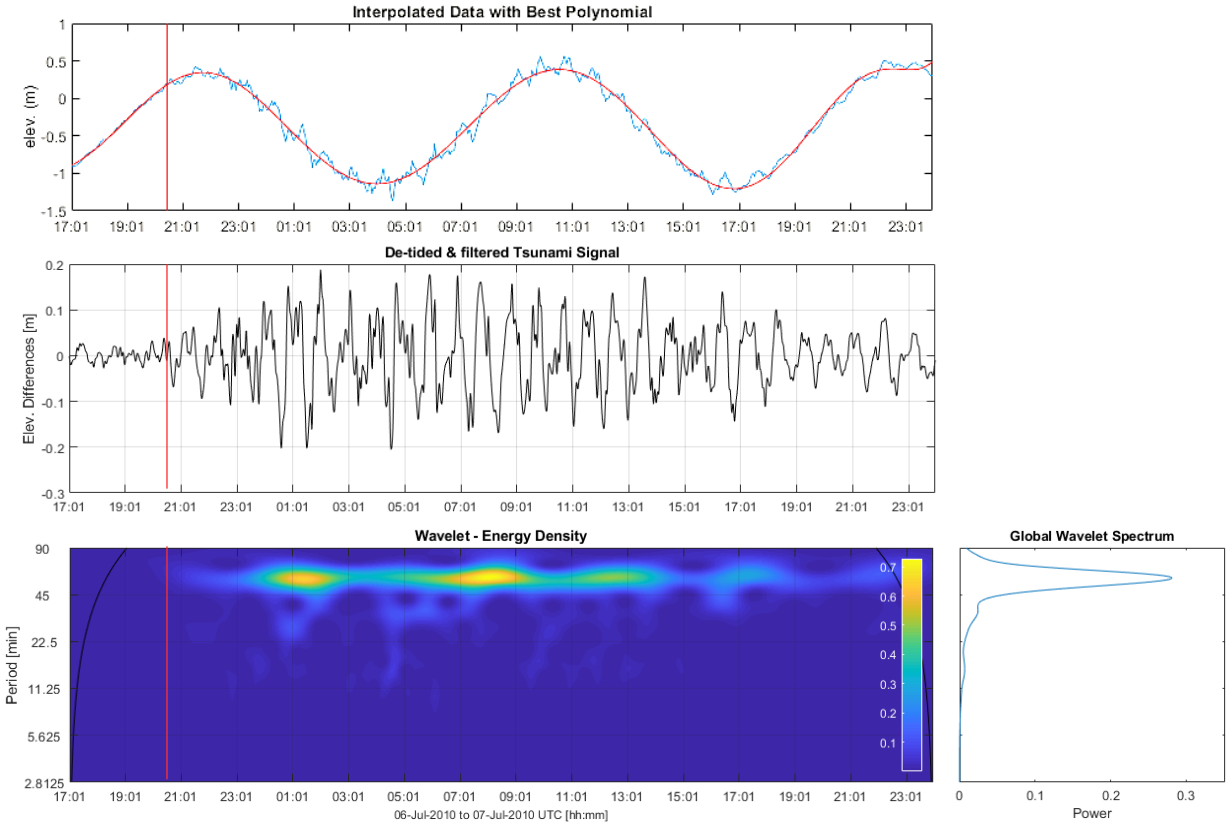

Figure III.1 Signal of meteotsunami in Lagos tide-gauge and spectral analysis of the sea level. The sample interval is 3 minutes.

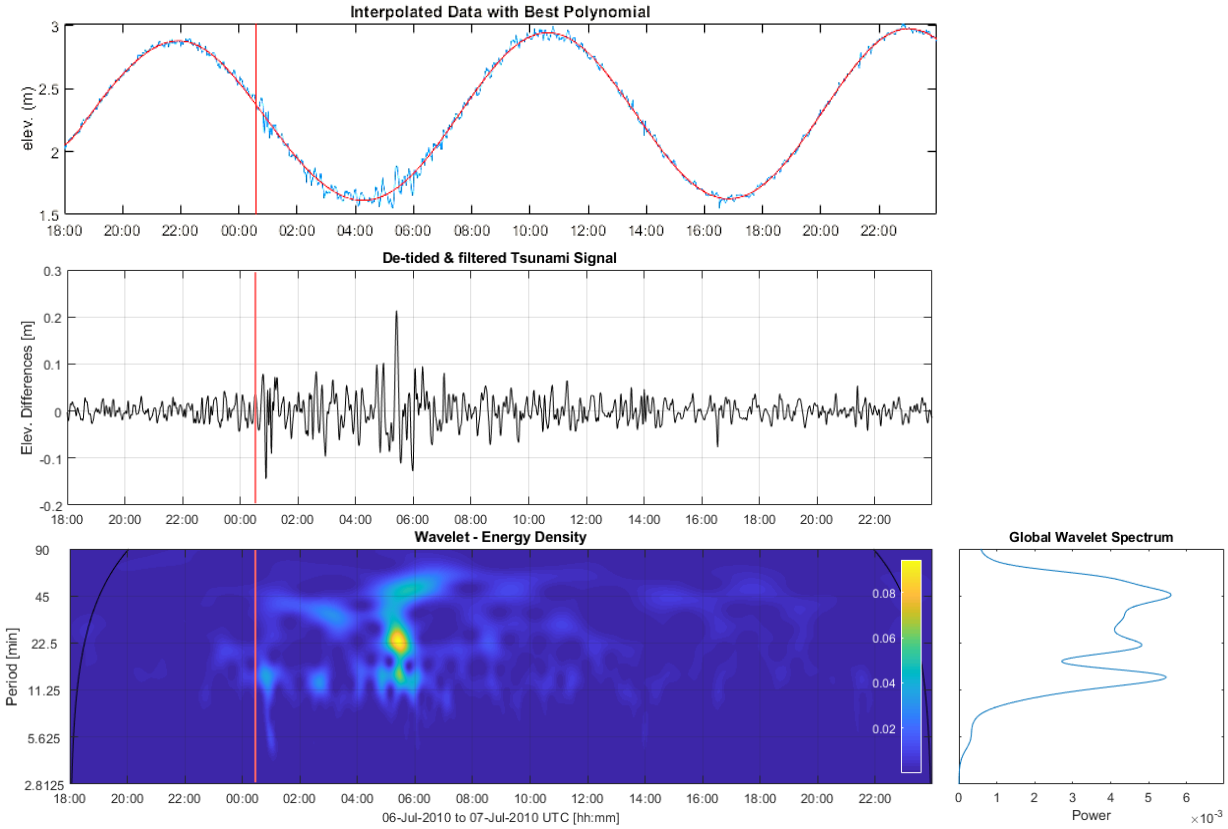

Figure III.2. Signal of meteotsunami in Sines tide-gauge and spectral analysis of the sea level. The sample interval is 1 minute.

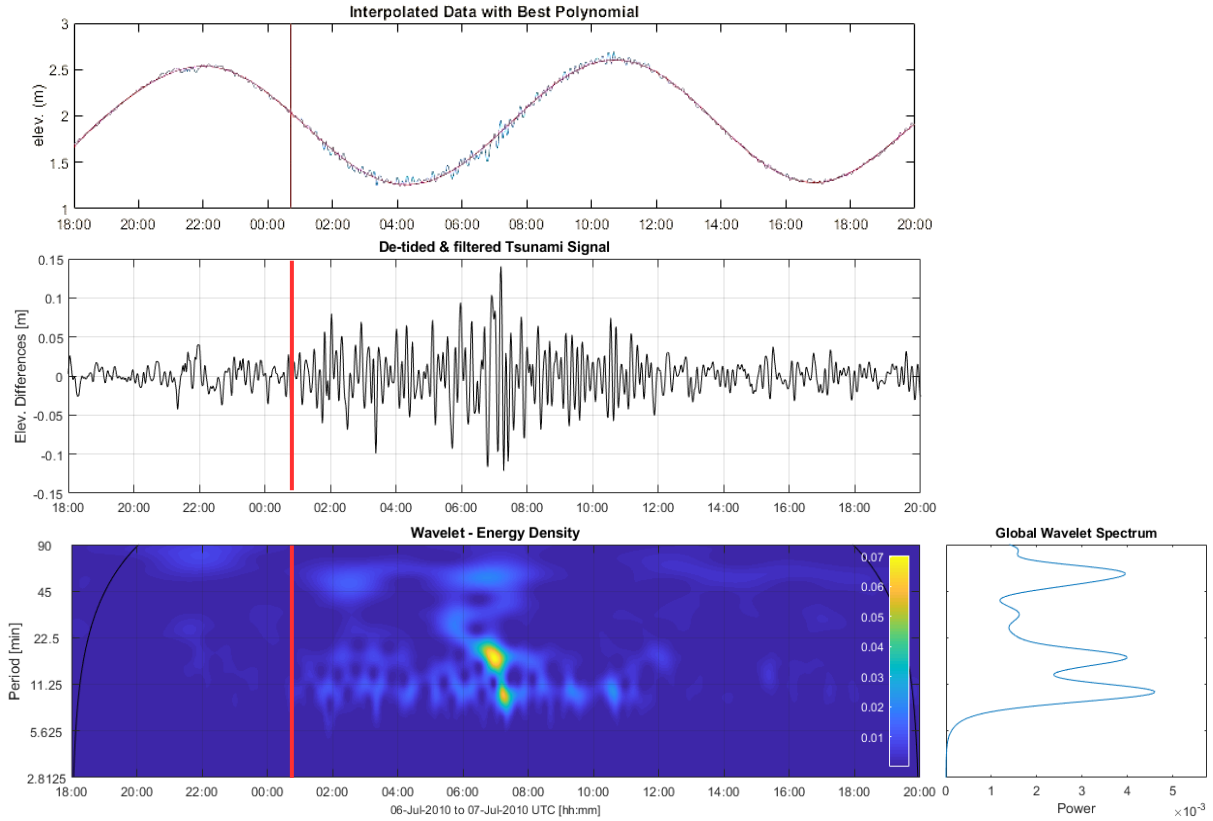

Figure III.3. Signal of meteotsunami in Sesimbra tide-gauge and spectral analysis of the sea level. The sample interval is 1 minute.

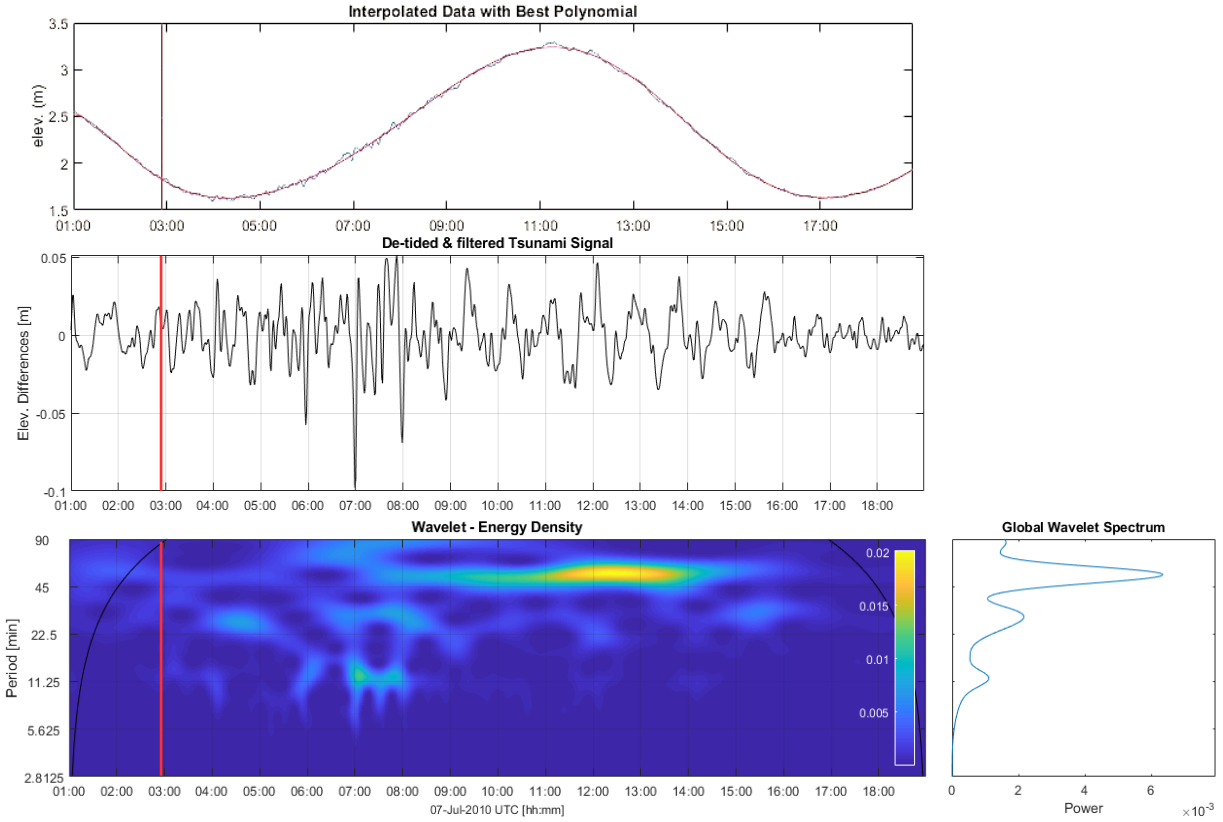

Figure III.4. Signal of meteotsunami in Lisboa tide-gauge and spectral analysis of the sea level. The sample interval is 1 minute.

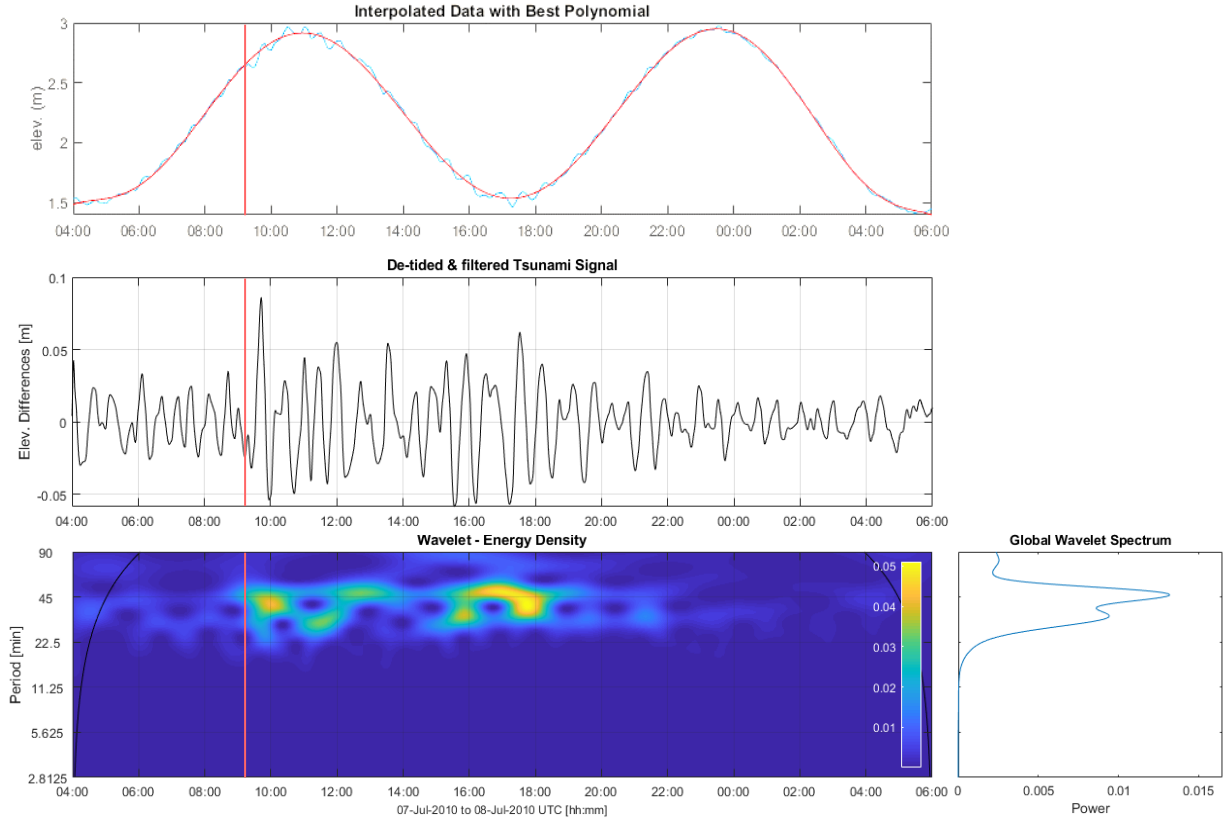

Figure III.5. Signal of meteotsunami in Figueira da Foz tide-gauge and spectral analysis of the sea level. The sample interval is 6 minutes.

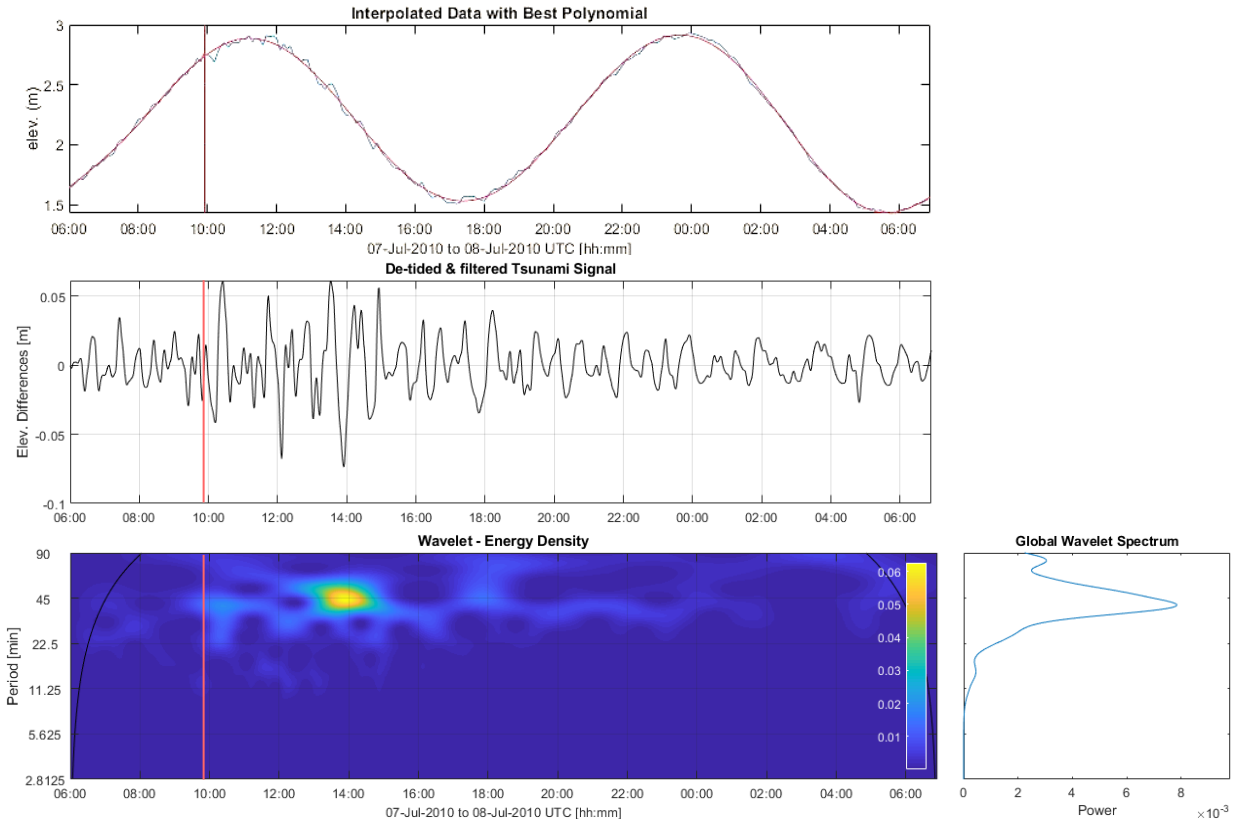

Figure III.6. Signal of meteotsunami in Aveiro tide-gauge and spectral analysis of the sea level. The sample interval is 6 minutes.

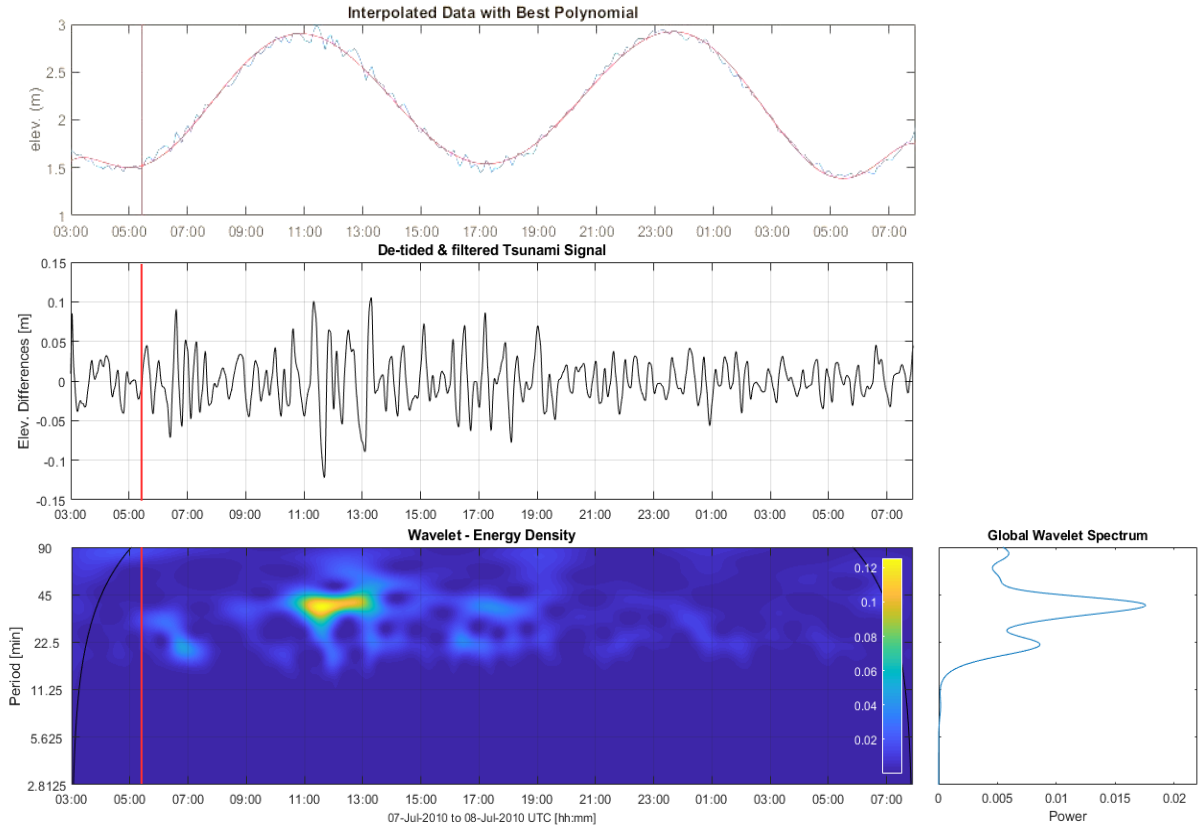

Figure III.7. Signal of meteotsunami in Leixões tide-gauge and spectral analysis of the sea level. The sample interval is 6 minutes.

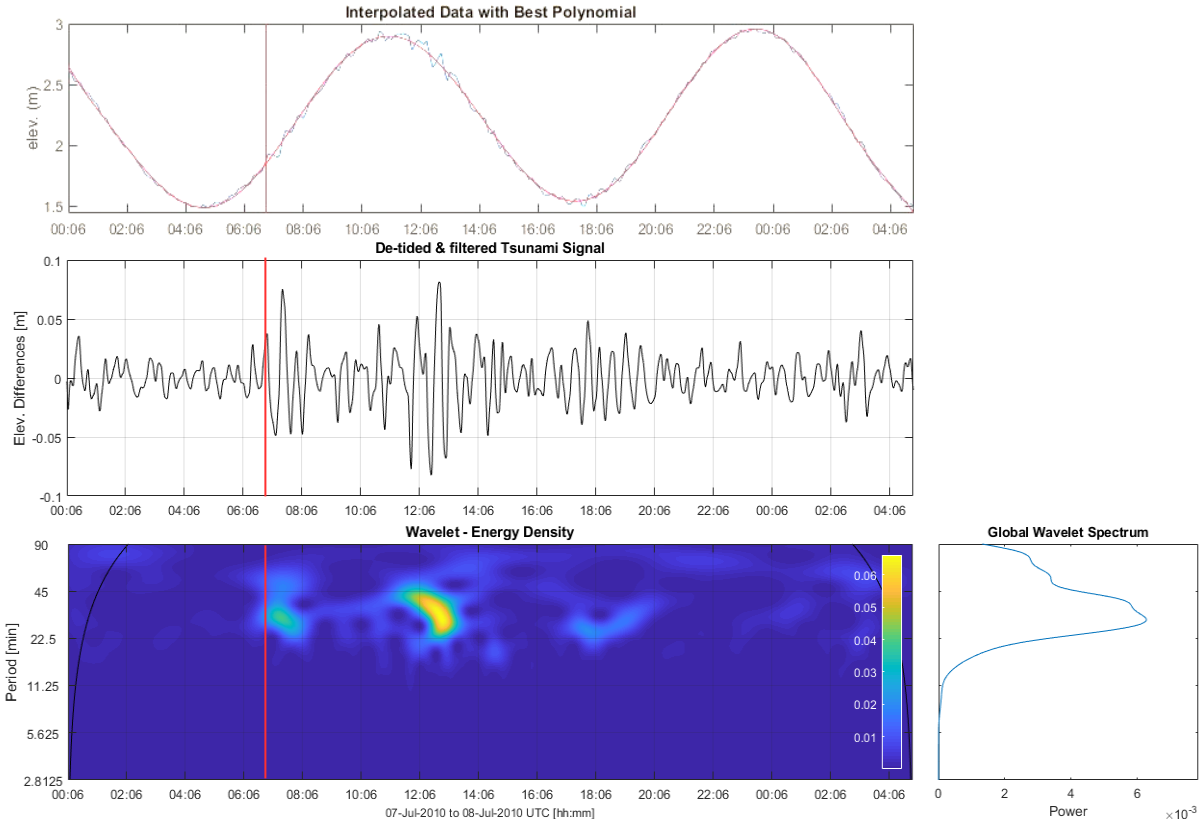

Figure III.8. Signal of meteotsunami in Viana do Castelo tide-gauge and spectral analysis of the sea level. The sample interval is 6 minutes.

b) Meteotsunami of 2011 on the Spanish coasts of the Iberian Peninsula and on the French Atlantic coast

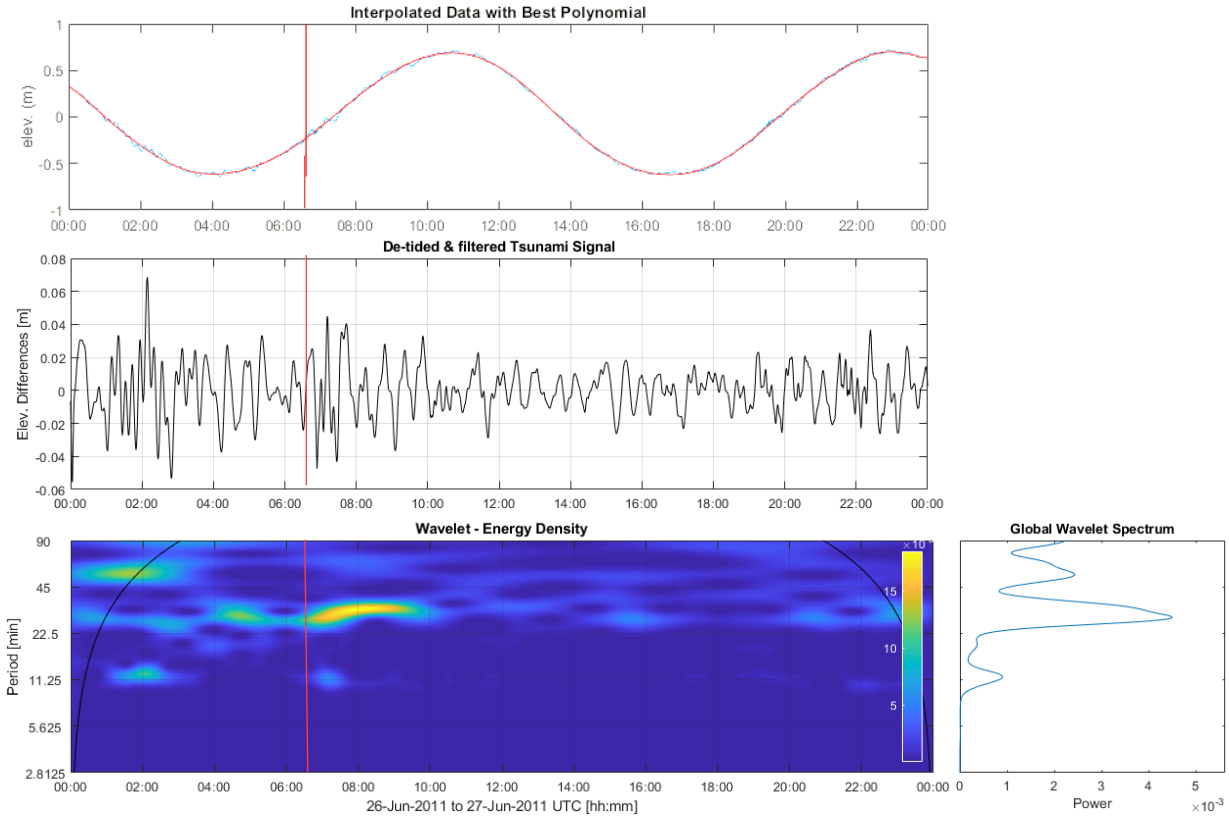

Figure III.9 Signal of meteotsunami in Huelva (Spain) tide-gauge and spectral analysis of the sea level. The sample interval is 1 minute.

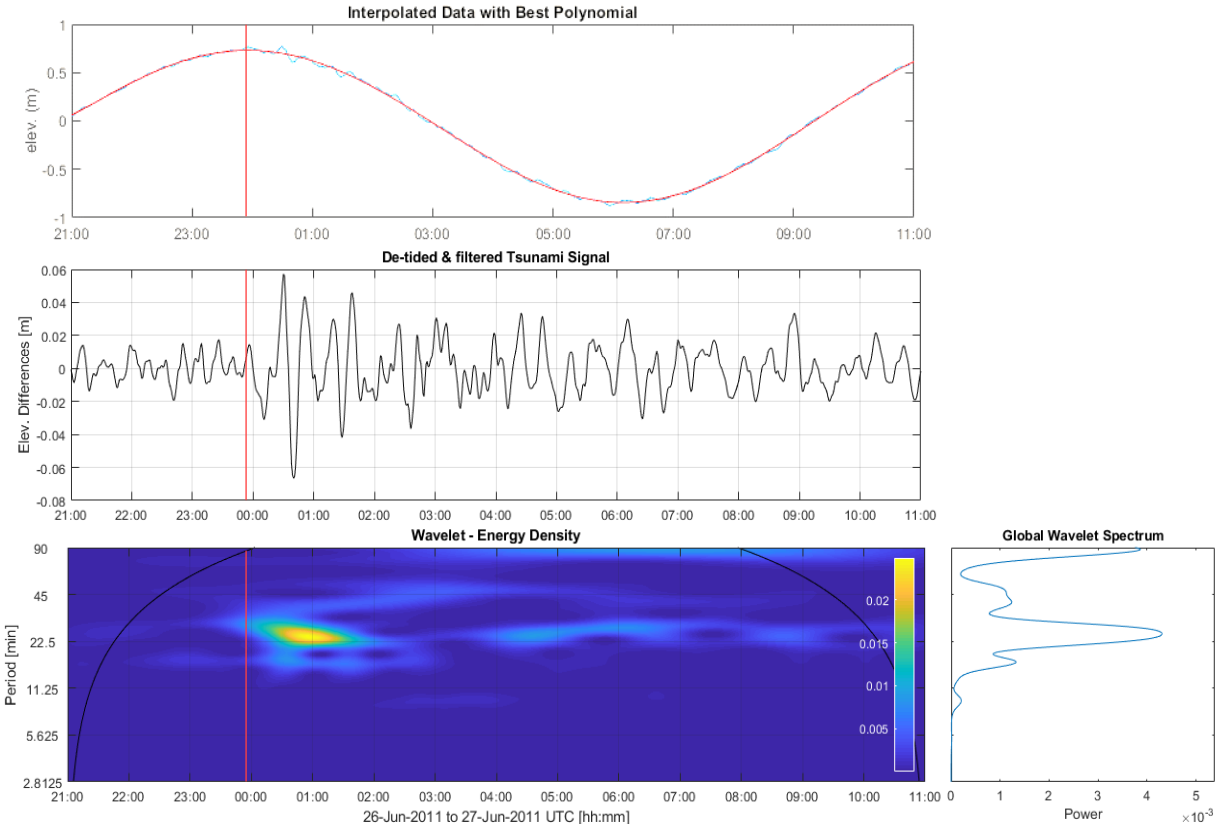

Figure III.10. Signal of meteotsunami in Ferrol (Spain) tide-gauge and spectral analysis of the sea level. The sample interval is 1 minute.

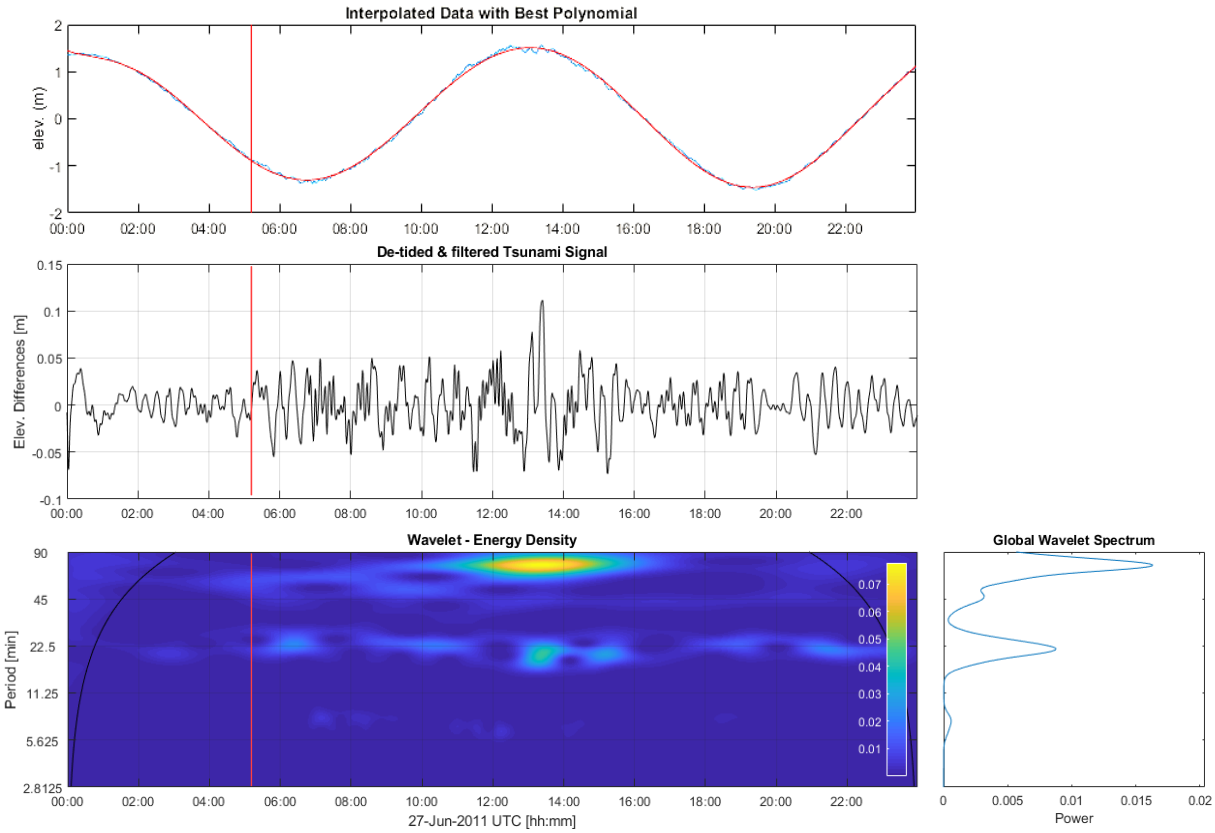

Figure III.11. Signal of meteotsunami in Brest (France) tide-gauge and spectral analysis of the sea level. The sample interval is 1 minute.

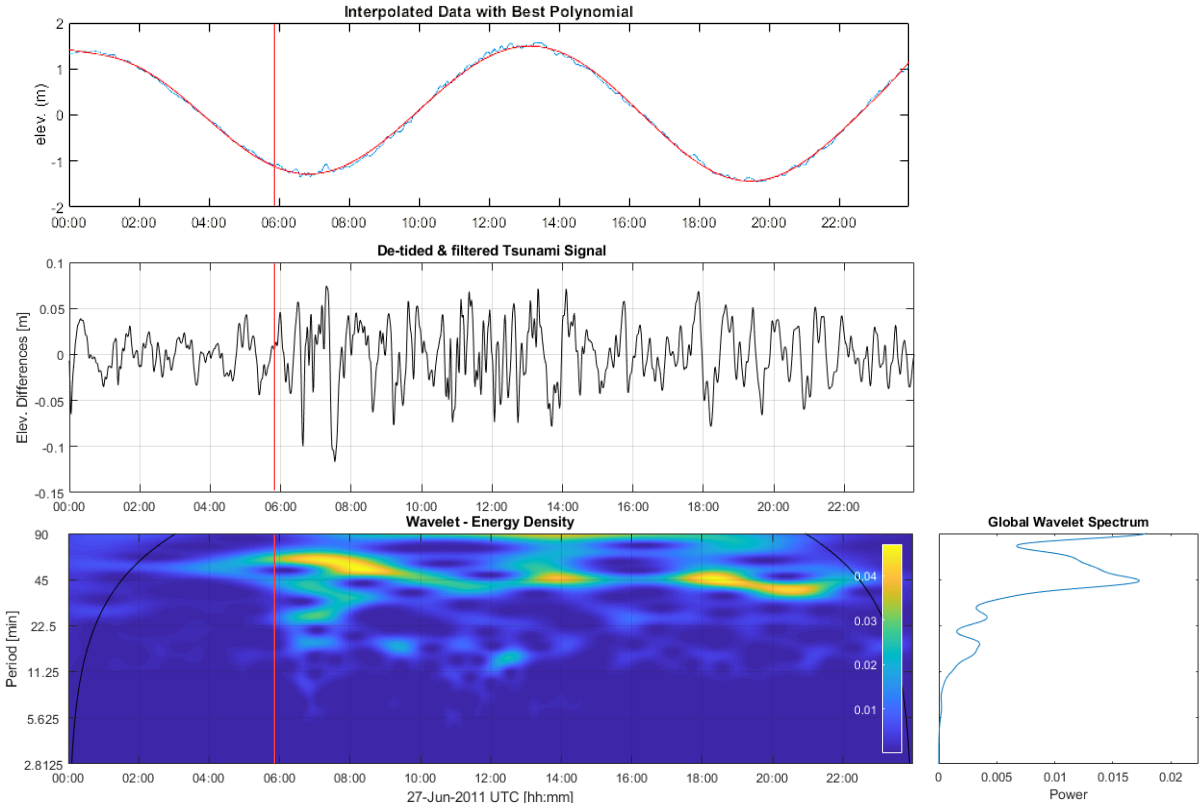

Figure III.12. Signal of meteotsunami in Le Conquet (France) tide-gauge and spectral analysis of the sea level. The sample interval is 1 minute.

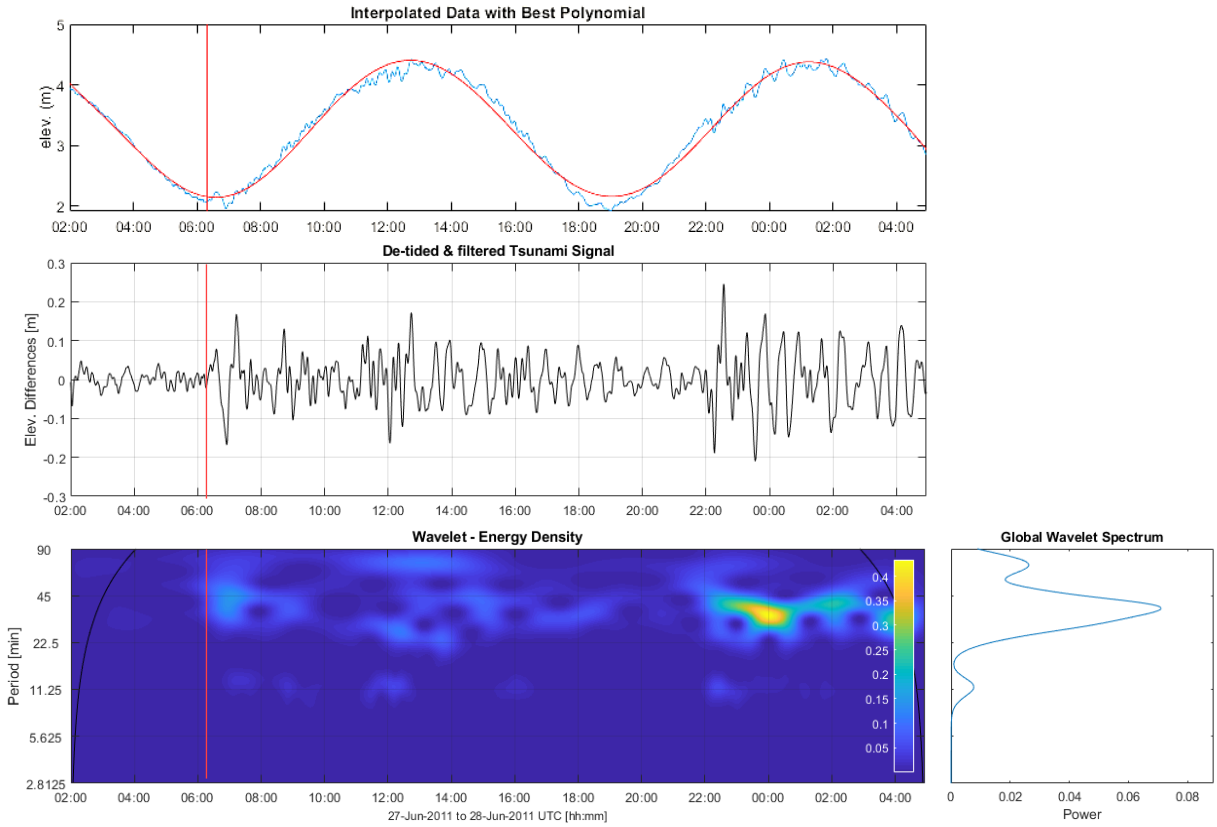

Figure III.13. Signal of meteotsunami in Les Sables d'Olonne (France) tide-gauge and spectral analysis of the sea level. The sample interval is 1 minute.

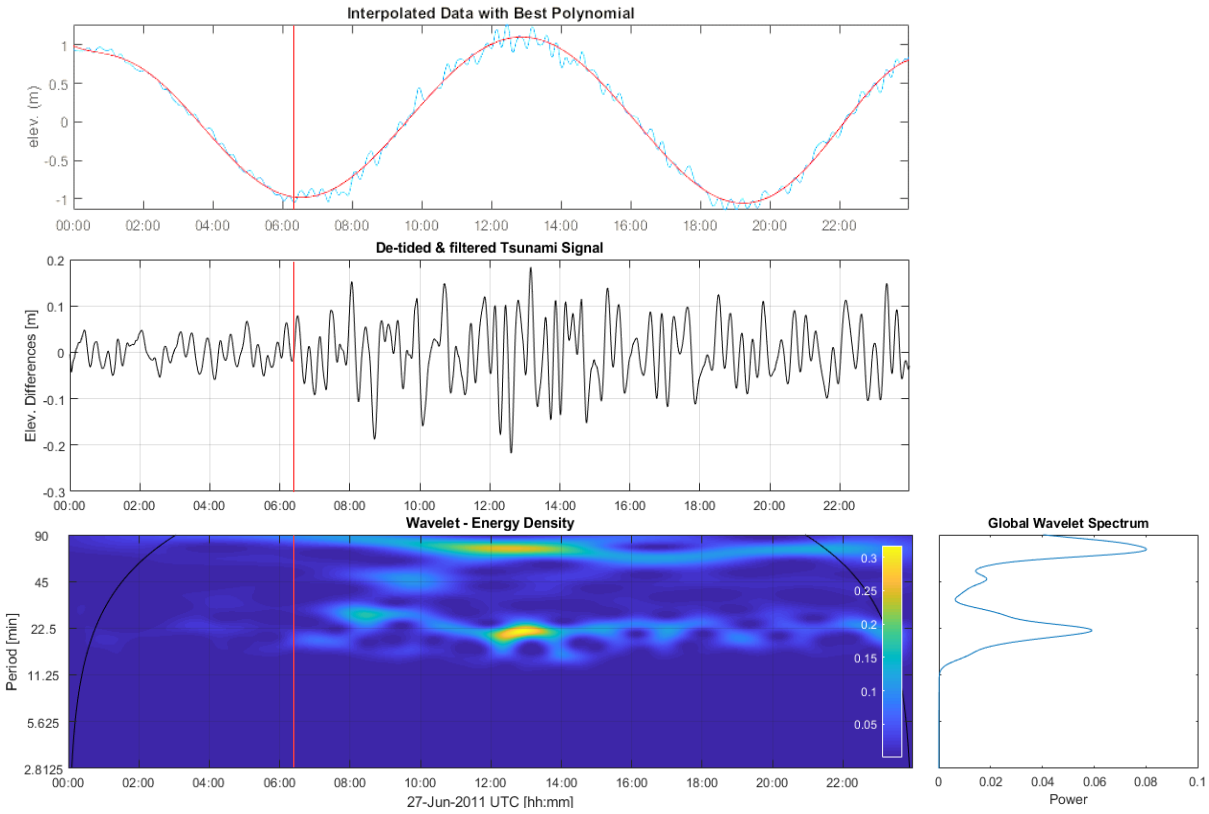

Figure III.14. Signal of meteotsunami in Concraneau (France) tide-gauge and spectral analysis of the sea level. The sample interval is 1 minute.

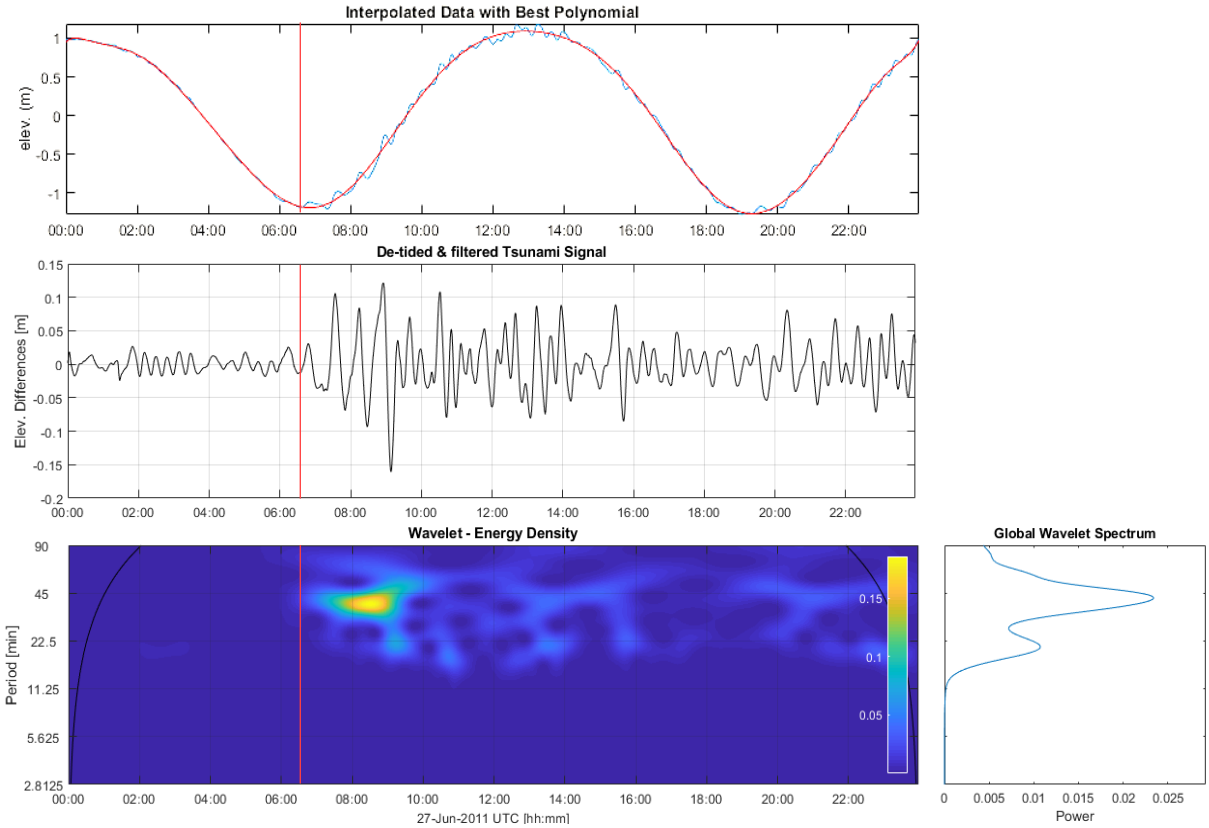

Figure III.15. Signal of meteotsunami in Le Crouesty (France) tide-gauge and spectral analysis of the sea level. The sample interval is 1 minute.

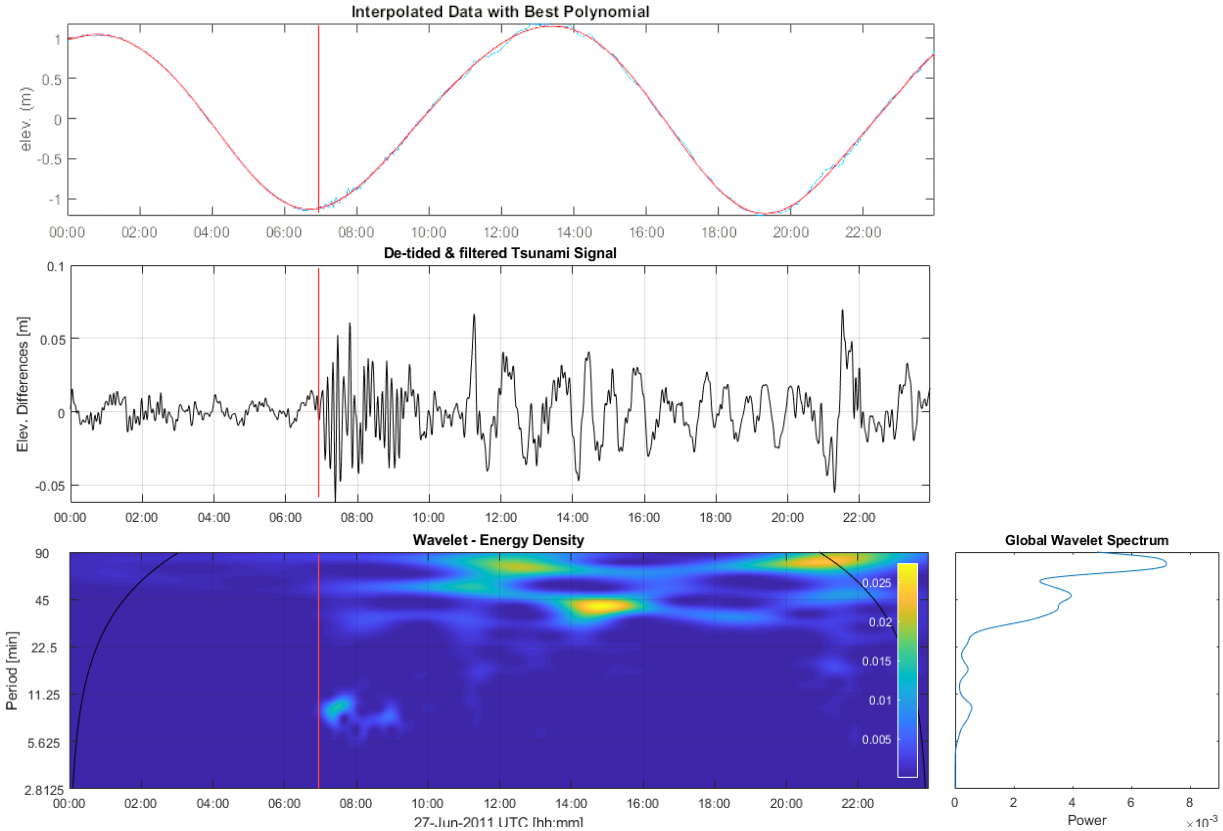

Figure III.16. Signal of meteotsunami in Port-Bloc (France) tide-gauge and spectral analysis of the sea level. The sample interval is 1 minute.

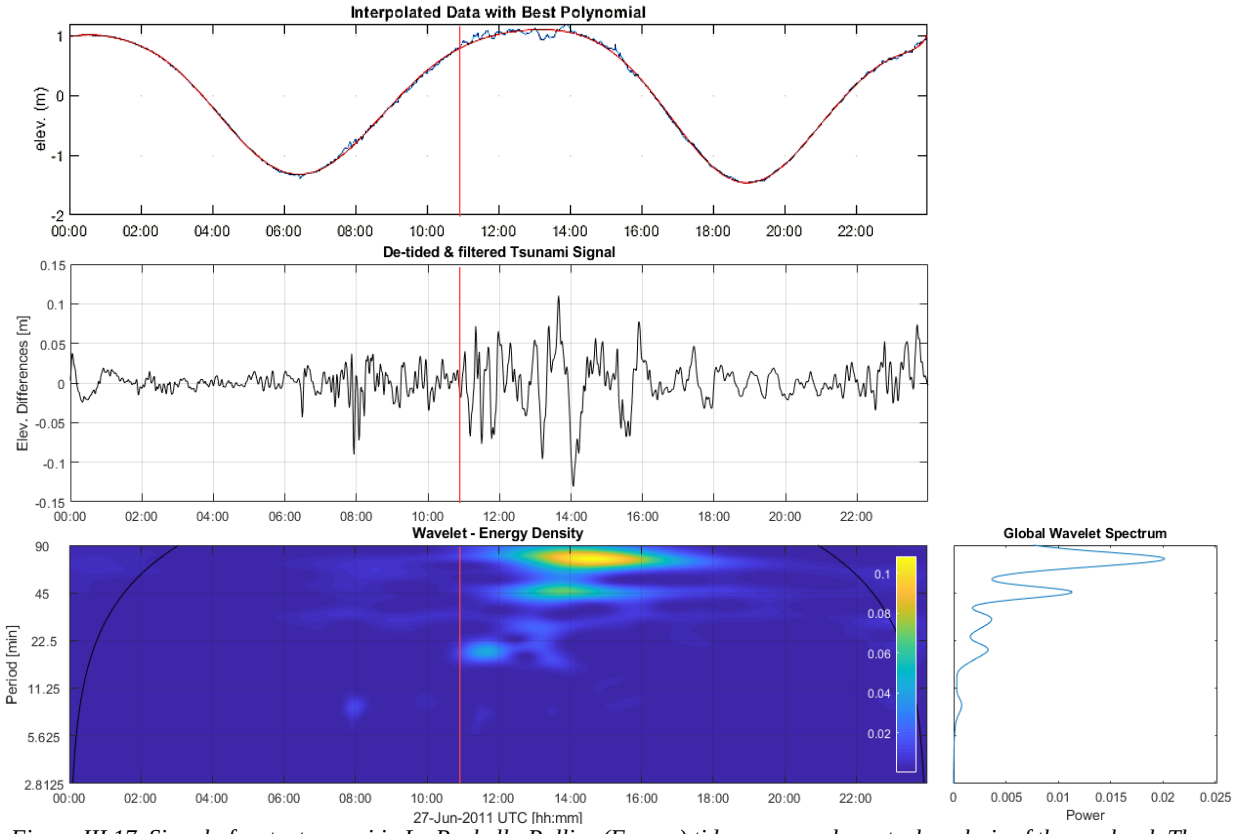

Figure III.17. Signal of meteotsunami in La Rochelle-Pallice (France) tide-gauge and spectral analysis of the sea level. The sample interval is 1 minute.

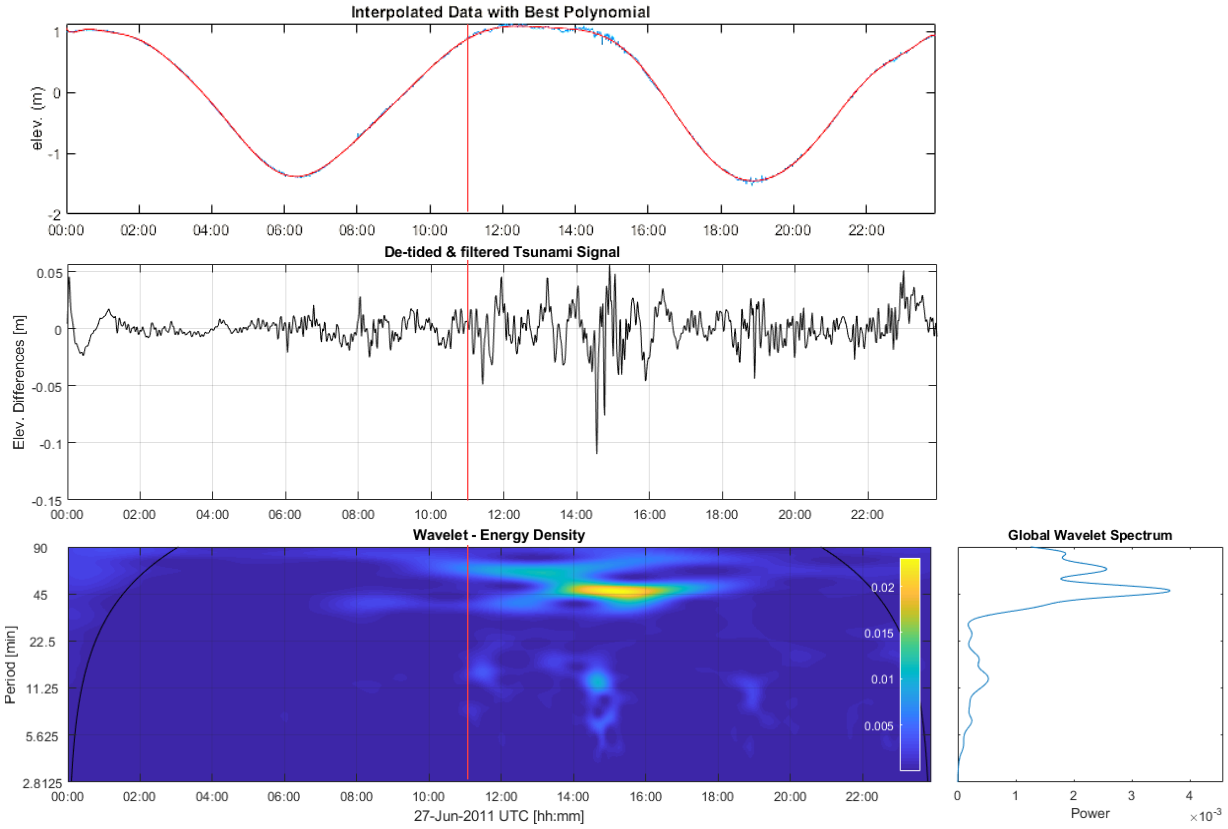

Figure III.18. Signal of meteotsunami in Ile d'Aix (France) tide-gauge and spectral analysis of the sea level. The sample interval is 1 minute.

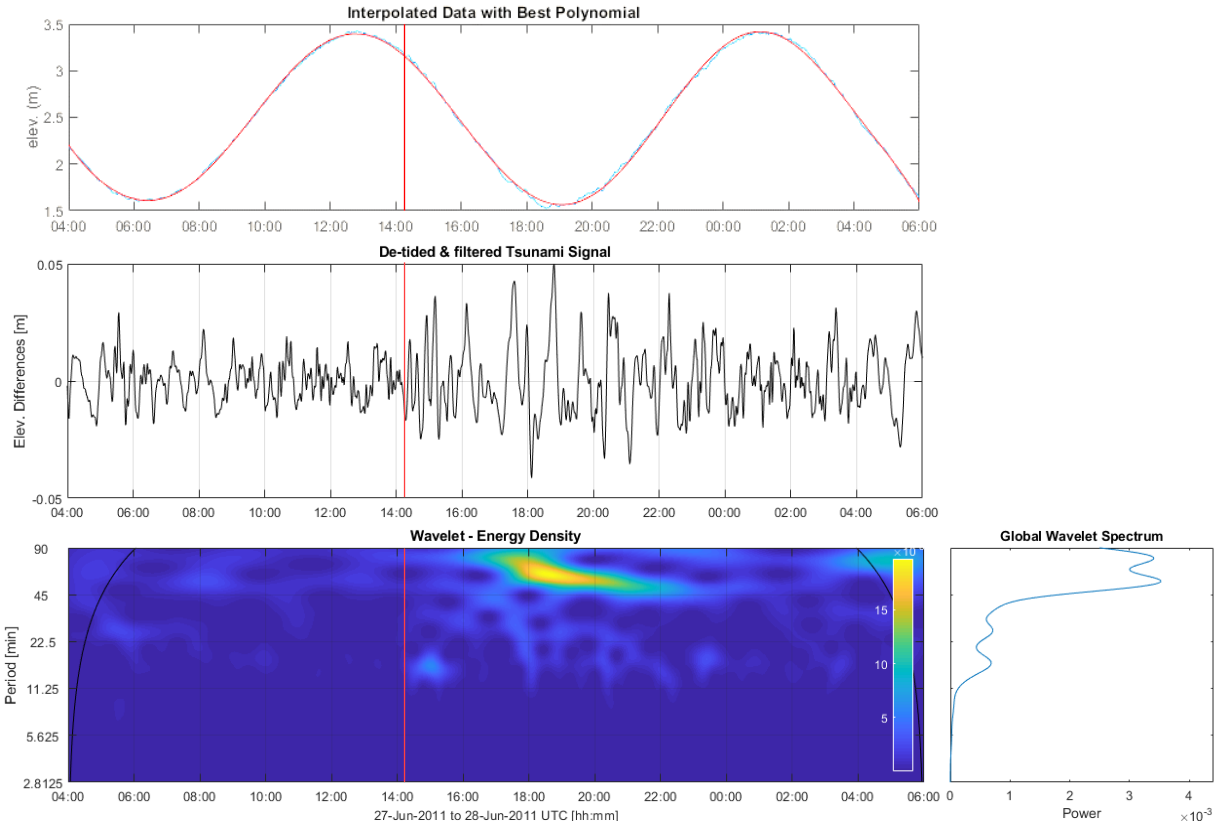

Figure III.19. Signal of meteotsunami in Boucau-Bayonne (France) tide-gauge and spectral analysis of the sea level. The sample interval is 1 minute.

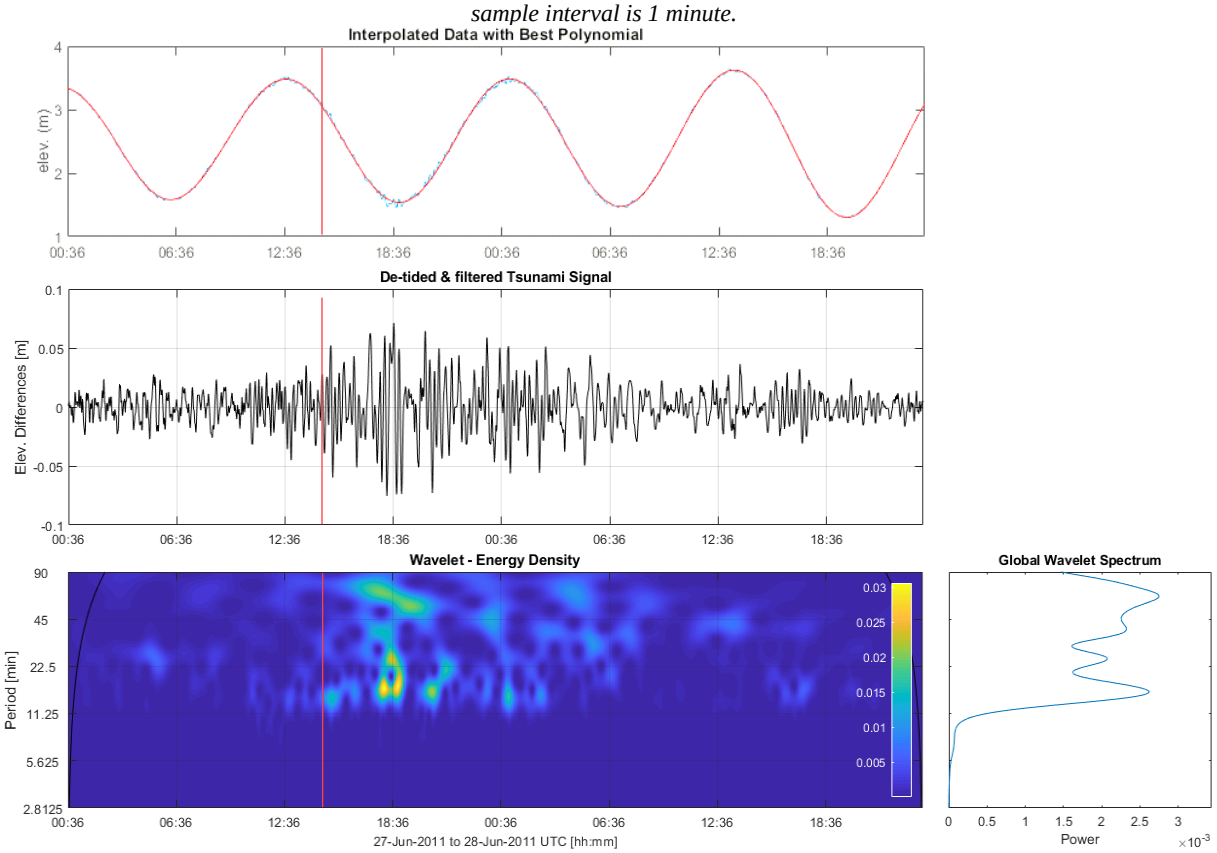

Figure III.20. Signal of meteotsunami in St. Jean de Luz (SOCOA) (France) tide-gauge and spectral analysis of the sea level. The sample interval is 1 minute.

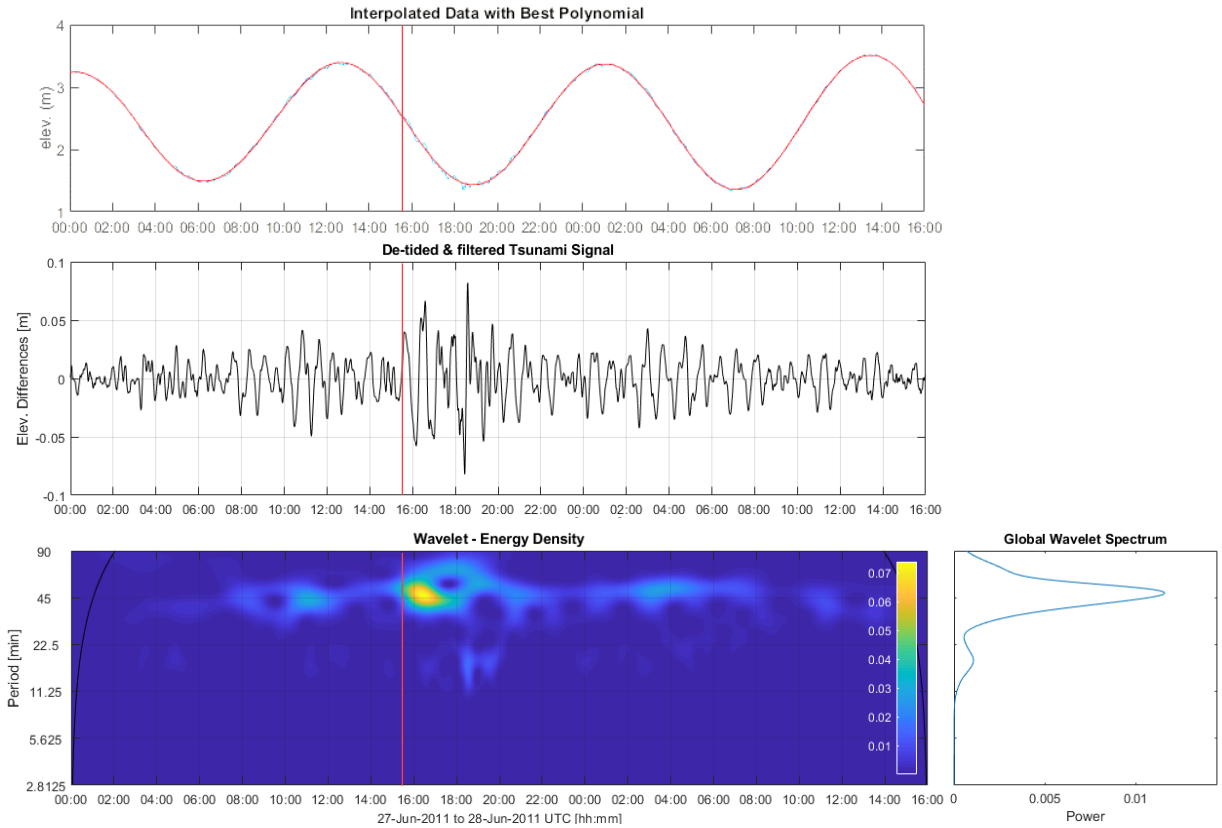

Figure III.21. Signal of meteotsunami in Bilbao (Spain) tide-gauge and spectral analysis of the sea level. The sample interval is 1 minute.